ISR WORKSHOP/2-9
February 1978

WORKSHOP ON FUTURE ISR PHYSICS
CERN, 14 - 21 September, 1977

$p\bar{p}$ AT THE ISR*

Compiled by P. Strolin with contributions from A. Donnachie, K. Hübner, G. Matthiae, M. Braccini, K. Hansen, F. Vannucci and U. Gastaldi

* Copies available upon request from Christine Redman, CERN/ISR

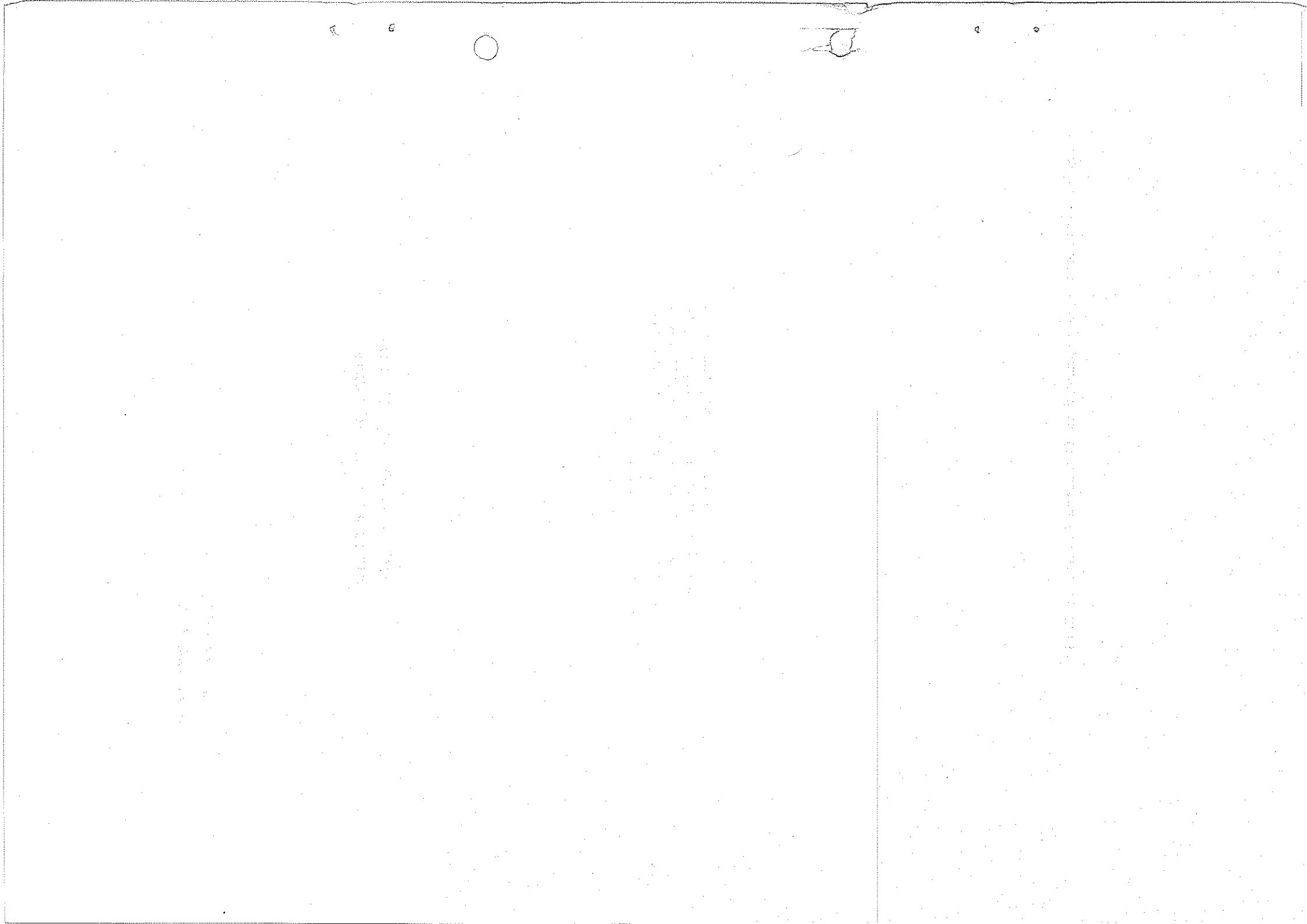

Table of Contents

1. Introduction

Considering the physics potential of the ISR over the coming five years, the possibility of studying $p\bar{p}$ interactions with luminosities of the order of 10^{29} cm^{-2} s^{-1}, is of very great interest. A full day plenary session of the Workshop was therefore devoted to assessments of what to expect along different lines of investigation, classical ones, such as very high energy collisions but also unorthodox ones such as low energy $p\bar{p}$ reactions. This session served as an introduction to the discussion sessions, chaired by C. Rubbia, and the conclusions of which were presented by P. Strolin at the end of the Workshop. P. Strolin's summary is separately available as document ISR WORKSHOP/2-16. The present report comes back in much greater detail on what was already discussed during the first session of the Workshop and summarized in "Physics with antiprotons, deuterons and heavy ions" by L. Bertocchi et al. It puts together the write-ups provided by the different speakers.

This report starts with a paper by A. Donnachie "$p\bar{p}$ at the ISR - Why?" which surveys the physics potential of $p\bar{p}$ interactions at ISR energies. Next is a report by K. Hübner which discusses what to expect from present techniques which include the construction of an intense source of $\bar{p}$, as obtainable from cooling and developed for use in the SPS.

Next follows a series of contributions which review different types of reactions and describe how experimentation with $\bar{p}$ can proceed and how far it can go, probing interesting kinematical ranges. In practically all cases, experimental equipment already available could be used to extend whatever was developed for pp reactions to the analysis of $p\bar{p}$ reactions. First comes a report by G. Matthiae, which discusses low multiplicity reactions. Next comes a report by P. Braccini which covers large cross-section reactions. In these two cases the further developments in $\ell n\ s$ physics at the ISR should much benefit from a comparison between pp and $p\bar{p}$ induced reactions, analyzed through the same detectors. This is emphasized in G. Bellettini's report ISR WORKSHOP/2-17.

One then considers low cross-section reactions of special topical interest in view of their relevance to hadron structure. In such cases a comparison between pp and $p\bar{p}$ induced reactions in the ISR energy range looks as particularly interesting. The question of large p_t phenomena is first reviewed by K. Hansen and the question of lepton pair production is then covered in the report by F. Vannucci.

This concludes the discussion of hadron physics at very high energy corresponding to what is typically expected at the ISR.

It is however conceivable to use the ISR in another way, having protons and anitprotons circulating in the same direction. This is referred to as an Ortho-ISR scheme. For practical reasons one would actually stack $\bar{p}$ and H^- in the two respective rings. Experimenting along such unorthodox lines one could study $p\bar{p}$ interactions at low energy (in the topical baryonium region) but get such a system at very large momentum, which makes available some very interesting laser techniques. This is discussed by U. Gastaldi who has given much attention to this very ingenious possibility.

From what is discussed here it can be concluded that a very rich physics programme can be expected from $p\bar{p}$ at the ISR, with the luminosities which are presently envisaged, and with the available detectors. It is hoped that this report will be of some use in generating new proposals for the few but interesting years of $p\bar{p}$ experimentation.

2. $p\bar{p}$ at the ISR - Why?

This section follows the presentation by A. Donnachie.

There are three main areas of interest in $p\bar{p}$ interactions at energies up to those obtainable at the ISR.

a) $\ell n\ s$ physics, i.e. primarily the study of the Regge aspects of high energy interactions.

b) Drell-Yan physics, both in the continuum and for the production of specific states (J/ψ, ψ', etc.).

c) Large p_t physics, both for single particle inclusive spectra and for the study of jets.

At the energies in question, the objective is to open a fresh door into existing physics via comparison with the corresponding pp interactions. It is unlikely that $p\bar{p}$ will provide any new physics at these energies.

For this comparison, the energy requirements are:

(i) to be sufficiently high for reasonably simple models to be applicable,

(ii) to be sufficiently low for pp-$p\bar{p}$ differences and/or ratios to be meaningful.

In practice this means ranging between top SPS energies and middle ISR energies, although one must always be aware of special cases, e.g. if there is sufficient luminosity to study Υ production, then this would require top ISR energies and it should be recalled that the Omega beam dump experiment has produced significant results on J/ψ production in $p\bar{p}$ interactions at 40 GeV/c.

In this talk we discuss these three main areas in turn, outlining briefly the present level of our understanding and illustrating some of the ways in which a comparison of $p\bar{p}$ with pp can be used to extend our knowledge. This also serves to give some indication of the quality of data required in $p\bar{p}$ physics to achieve a meaningful comparison.

2.1 Large p_t physics

The standard mechanism for large p_t phenomena is shown in Fig. 1, viz. the hard central hard scattering of partons. Power law scaling for single particle inclusive spectra arises naturally in this class of model, i.e.

$$E\frac{d\sigma}{d^3p} = \frac{1}{p_t^n} F(x_t, \theta_{cm})$$

where $x_t = 2p_t/\sqrt{s}$. This is consistent with existing data for $p_t \gtrsim 1.5$ GeV/c, $\sqrt{s} \gtrsim 10$ GeV. The observed jet structure of large p_t events is also a natural ingredient and the overall evidence for this class of model is strong.

However, there is considerable uncertainty as to the details of the model and in particular to the nature of the partons. The data point strongly in a definite direction, but do not provide an unambiguous solution.

1. Both π and K data have $n \approx 8$ over the measured x_t range ($0.05 \lesssim x_t \lesssim 0.6$) so that dimensional counting arguments imply that there are six elementary fields in the hard scatter.

2. The large ratio of jet to single particle cross-sections is essentially a consequence of trigger bias and is understandable in any model which explains the towards side correlation data. In particular, this includes models with meson jets, i.e. excited $q\bar{q}$ states.

3. The away side rapidity distributions provide strong constraints on the degree of peripherality of $d\sigma/d\hat{t}$, the parton-parton differential cross-section. It is consistent with simple one-particle exchange models in which the exchanged particle has spin ½, but not 0 or 1, i.e. it is natural to identify the partons with quarks.

These considerations lead naturally to the three models of Fig. 2.

a) Quark fusion (QF)

$q + \bar{q} \to M + M$

b) Constituent interchange model (CIM)

$q + M \to M + q$

$\bar{q} + M \to M + \bar{q}$

c) Diquark model (DQ)

$q + q \to M + qq$

$\bar{q} + \bar{q} \to M + \bar{q}\bar{q}$

The predictions of these three models have been discussed in detail recently by Chase and Stirling[1]. They show that each model by itself has difficulties with one or other aspect of the single particle inclusive data, but that the description is greatly improved by taking natural combinations of them, either QF and CIM or QF and DQ.

An alternative approach has been proposed by Field and Feynman[2], who prefer a quark scattering model,

$q + q \to q + q$

This has some quantitative problems with the 'meson jet' requirement, and obtains the necessary degree of peripherality of the parton-parton differential cross-section by specifying a suitable phenomenological form for $d\sigma/dt$. In general, the Field and Feynman (FF) model provides a good description of the data, but it it much more phenomenological than the other three models.

The basic ingredient of the models is knowledge of the parton distributions in the beam and target hadrons:

$$V_{qh}, S_{qh} \; ; \quad V_{mh}, S_{mh}, \; h = \pi, p, \; \ldots$$

The quark distributions V_{qh}, S_{qh} can be obtained (at least in principle) from deep inelastic scattering and lepton pair production. For the meson distributions it is normal to use the simplest forms consistent with Regge behaviour ($S_{mh} \to$ const, $V_{mh} \to \frac{1}{x^{1/2}}$ as $x \to 0$) and dimensional counting.

The single particle inclusive cross-sections are of the form

$$E\frac{d\sigma}{d^3p} = \frac{C}{p_T^q}\int_0^1 d\alpha_1\, d\alpha_2\, \delta(\alpha_1+\alpha_2-1)\, F_{ah_1}\left(\frac{x_1}{\alpha_1}\right) F_{bh_2}\left(\frac{x_2}{\alpha_2}\right) \alpha_1^{\ell}\alpha_2^{m}$$

where C is a constant, ℓ and m depend on the particular model and

$$x_1 = \frac{1}{2}x_T \cot\frac{\theta_{CM}}{2} \qquad x_2 = \frac{1}{2}x_T \tan\frac{\theta_H}{2}$$

Comparison with the available data show that QF is untenable by itself and that both CIM and DQ are in difficulty[1]. However, if CIM or DQ exist, then QF must also exist at some level, so it is natural to try mixtures of CIM and QF or DQ and QF. Typical consequences of doing this are shown in Figs. 3-5, which are taken from Chase and Stirling[1].

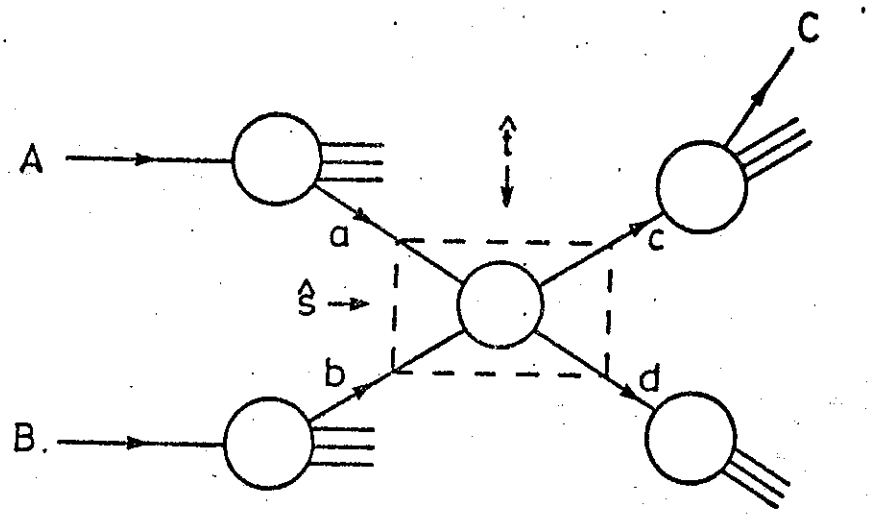

Figure 1 : The hard scattering model for the large transverse momentum process A + B → C + X

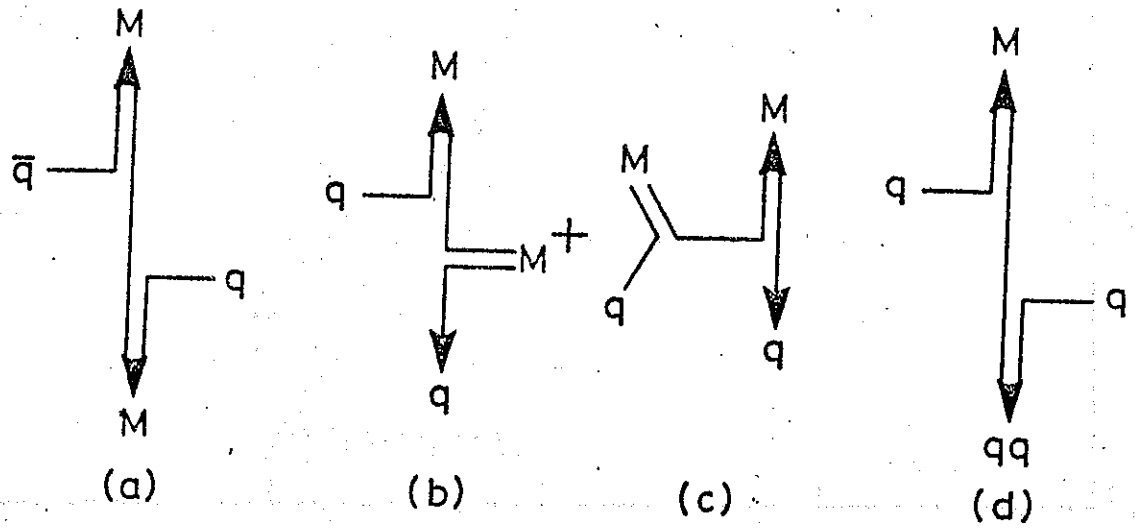

Figure 2 : The irreducible subprocesses for the models QF(a), CIM(b), (c) and DQ(d)

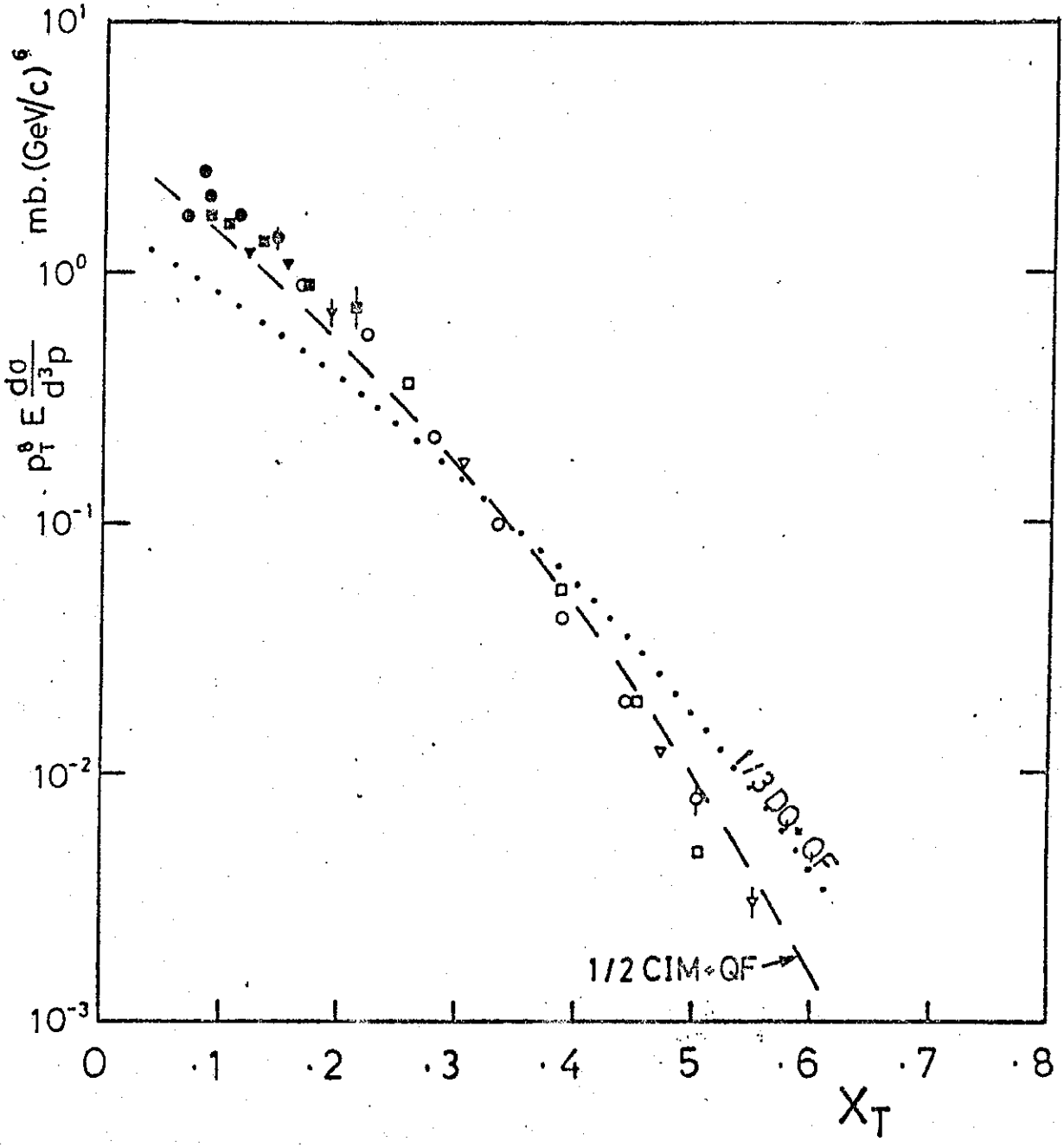

Figure 3 : The x_t dependence of p_t^8 E $d\sigma/d^3p$ for $pp \rightarrow \pi^+ X$ at $\theta_{cm} = 90^o$

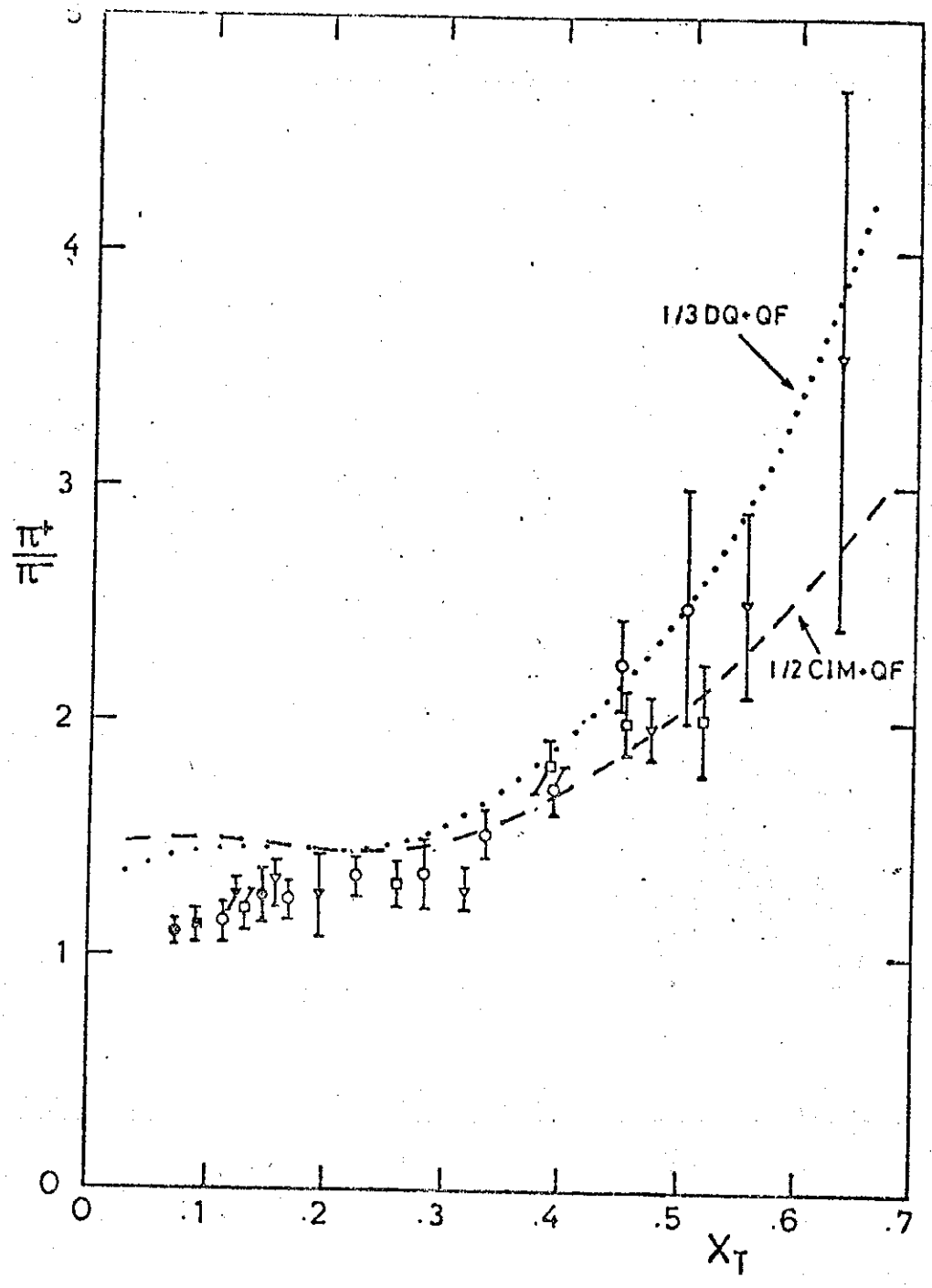

Figure 4 : The particle ratio $pp \to \pi^+X/pp \to \pi^-X$ at $\theta_{cm} = 90^o$

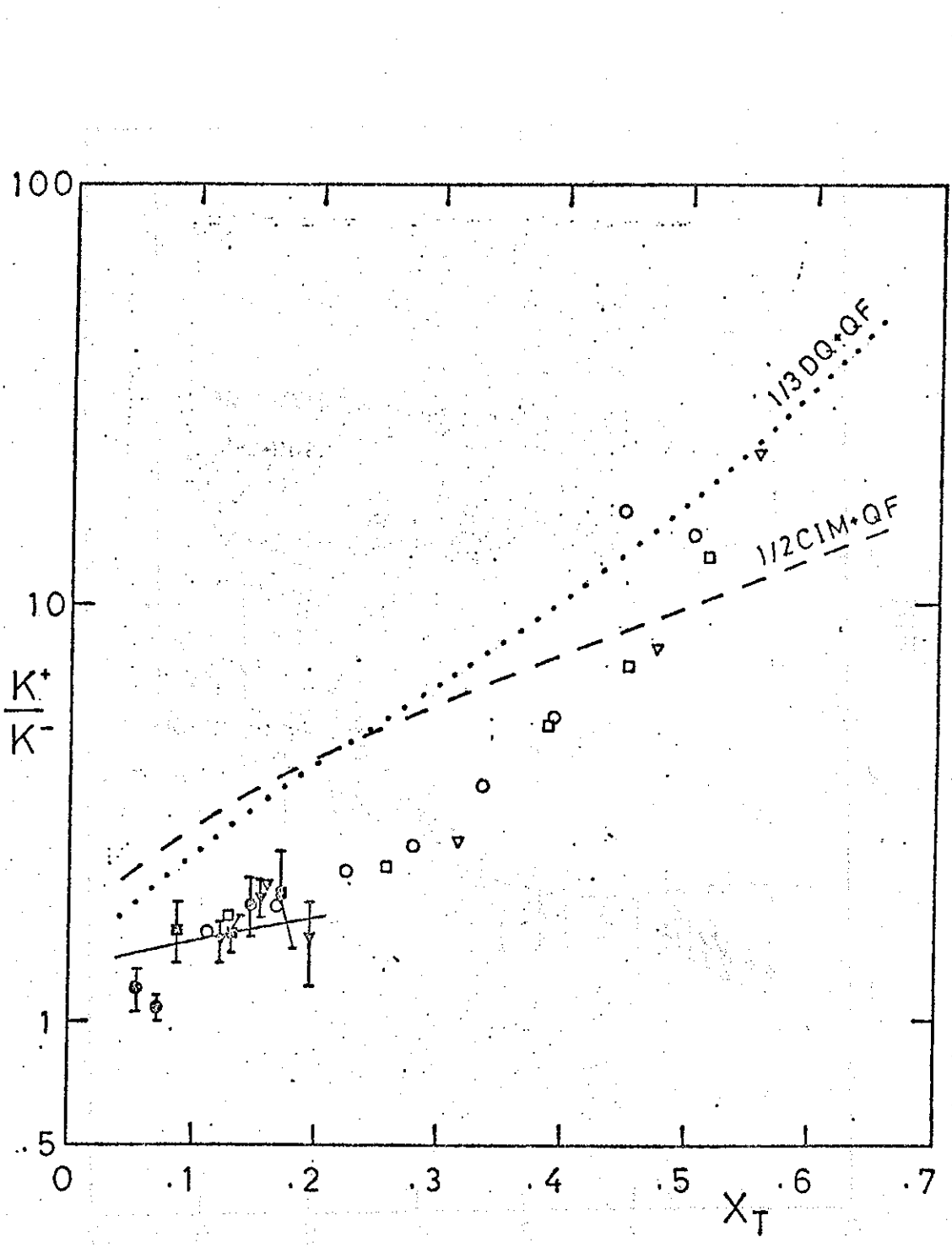

Figure 5 : The particle ratio $pp \to K^+X/pp \to K^-X$ at $\theta_{cm} = 90^o$

The situation is complicated. On the one hand, there is FF with pehnomenological parameters and on the other a mix of more specific models, but with the possibility of different quark distributions. It is clear that we require as great a variety of data as possible.

Can $p\bar{p}$ help? The answer obviously is yes, since in this context the $\bar{p}$ provides a beam of antiquarks. A typical example is shown in Fig. 6, which is the ratio $(p\bar{p} \to \pi^0 X)/(pp \to \pi^0 X)$ showing very large variations among the models (FF has this ratio identically 1). As a comparison, Fig. 7 shows the ration $(\pi^+ p \to \pi^0 X)/(\pi^- p \to \pi^0 X)$ which shows very little variation among the models.

Of course, $p\bar{p}$ is by no means the whole answer. Different data are sensitive to different models and/or to different aspects of the models, and no single set of data will solve the problem.

2.2 Drell-Yan (and hidden flavour)

For Drell-Yan the process (Fig. 8) and its interpretation are standard, viz. quark fusion to form a massive virtual photon. The basic ingredients are the quark distributions in the beam and target particles. The major uncertainties are an inadequate knowledge of the $\bar{q}$ distributions and the charm (and new flavour) component in the sea. Nonetheless, ignoring new flavours and assuming the sea to be SU(3) but not SU(4) symmetric (i.e. c content less than u,d,s content) yields satisfactory agreement with the data.

For $pp \to \ell^+\ell^- X$ contributions arise from VS and SS terms, and for $p\bar{p} \to \ell^+\ell^- X$ there is an additional contribution from the VV term. This latter dominates for $m/\sqrt{s}$ large (i.e. $\sim 0.1 - 0.15$) and so in most situations $\sigma(p\bar{p})$ will be significantly larger than $\sigma(pp)$. If we accept that the Drell-Yan continuum does not begin until $m_{\ell^+\ell^-} \gtrsim 4$ GeV, this statement will hold even at ISR energies, although at the top of the ISR range the VV term will no longer be dominant.

The comparison of $p\bar{p} \to \ell^+\ell^- X$ with $pp \to \ell^+\ell^- X$ is ideal for the study of the Drell-Yan mechanism, since the reactions involve the same quark and anti-quark distributions. The interpretation of the results is not necessarily straightforward, since it depends on the explanation of the breakdown of scaling in deep inelastic scattering. Whether this is due to new quarks and anti-quarks in the sea (i.e. threshold effects) or whether it is due to 'ordinary' quarks giving contributions varying with Q^2, the comparison of $p\bar{p}$ with pp Drell-Yan will certainly provide valuable and indeed essential information.

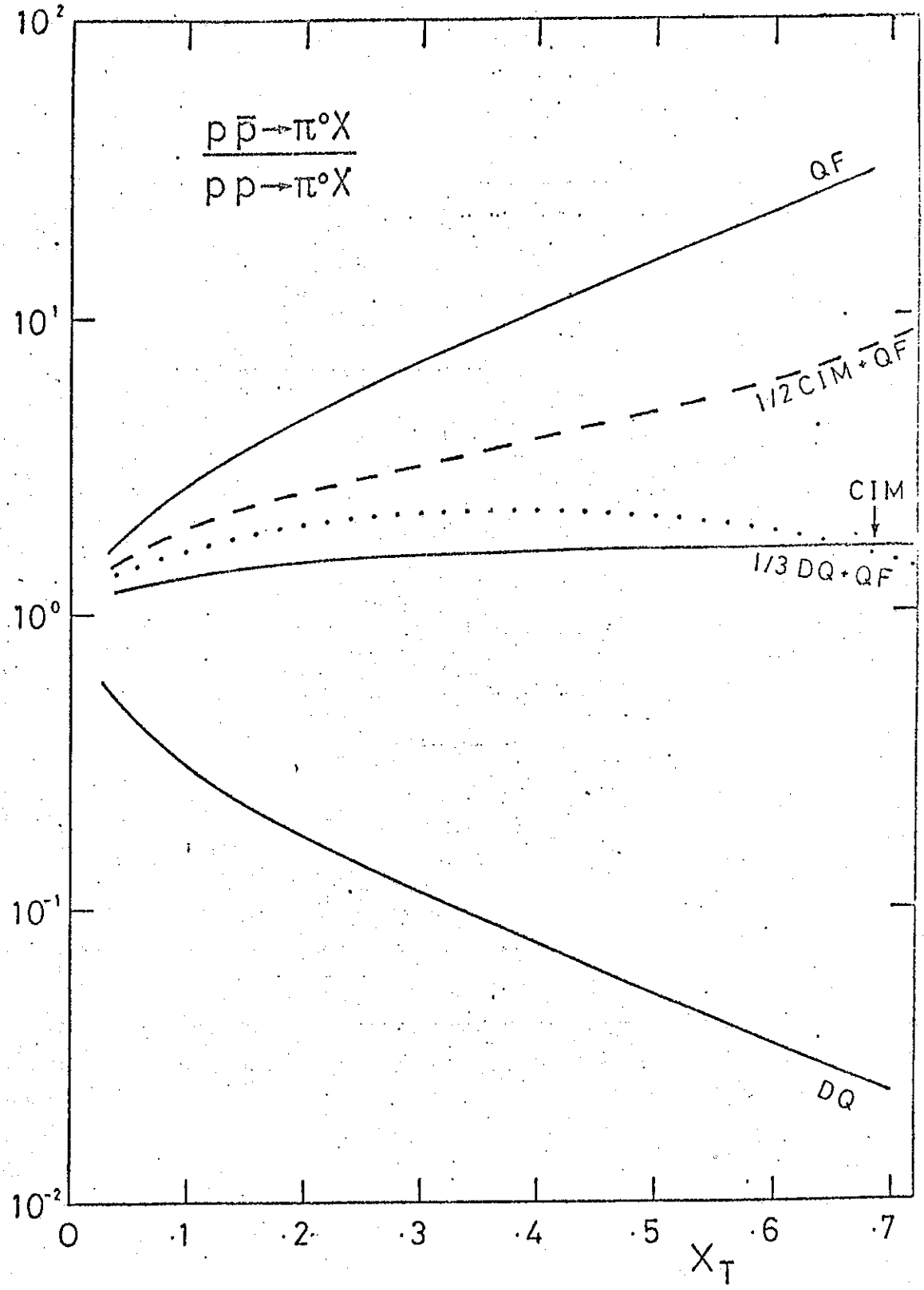

Figure 6 : Predictions for the beam ratio $p\bar{p} \to \pi^0X/pp \to \pi^0X$ at $\theta_{cm} = 90^o$

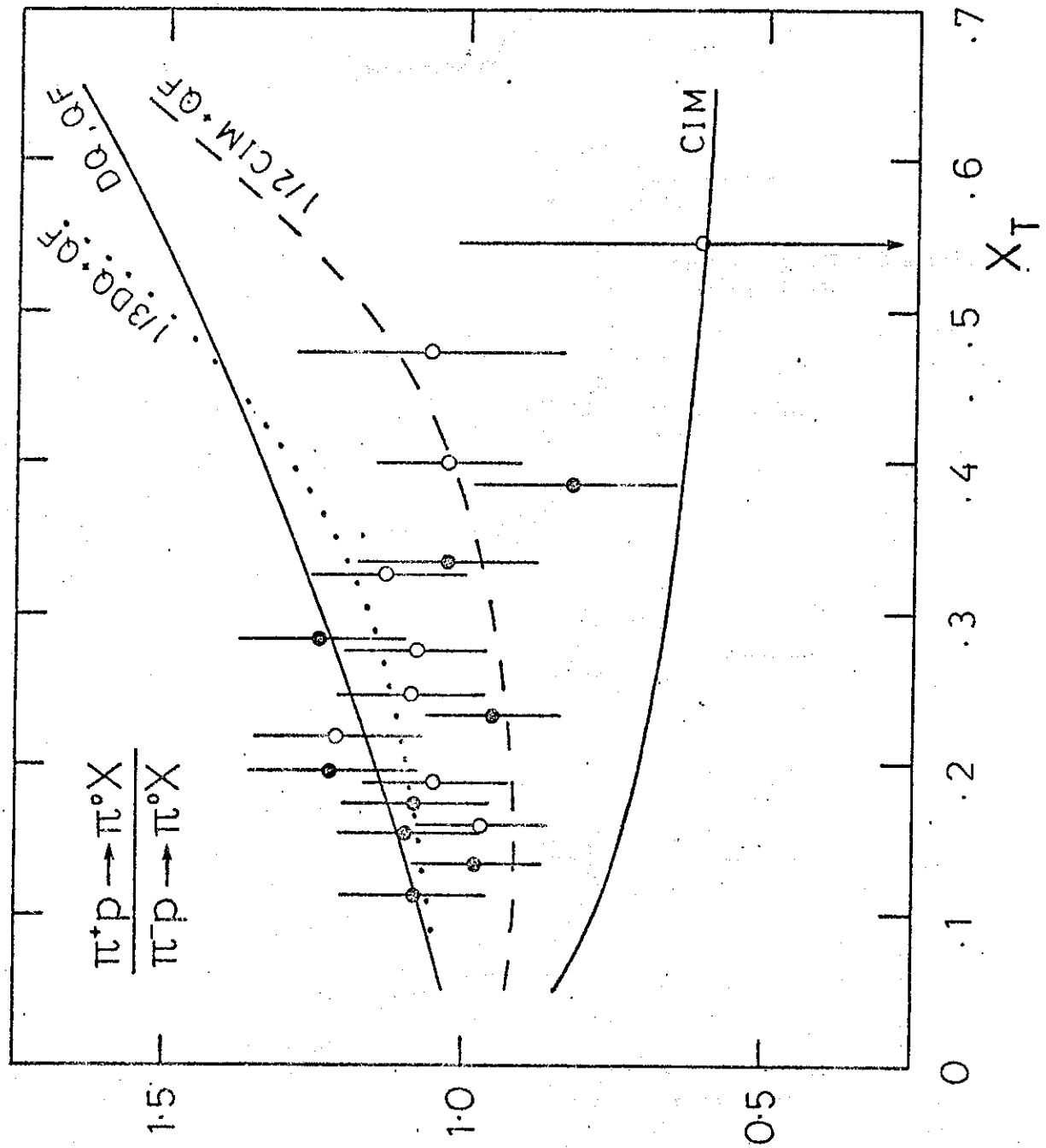

Figure 7 : The beam ratio $\pi^+ p \to \pi^0 X / \pi^- p \to \pi^0 X$ at $\theta_{cm} = 90^\circ$

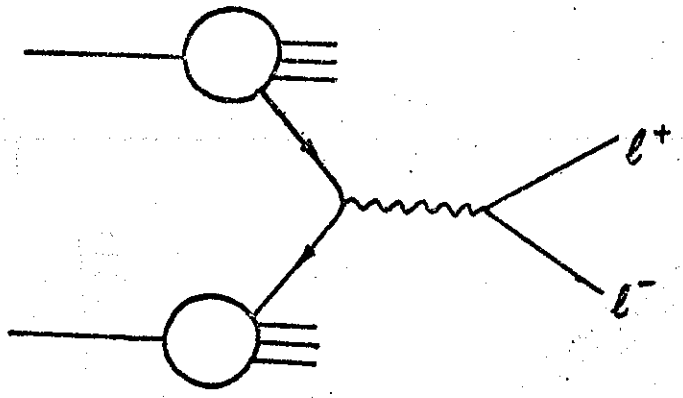

Figure 8 : The quark fusion model for the Drell-Yan production of massive lepton pairs

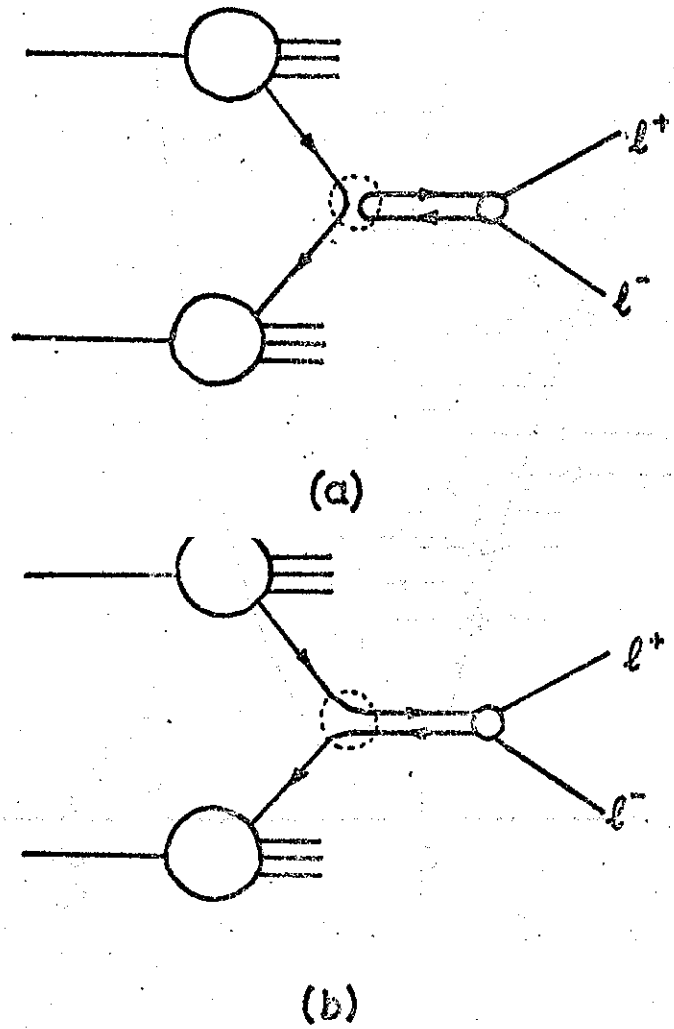

Figure 9 : The quark fusion model for J/ψ production, a) normal (u,d,s) quarks, b) charmed quarks

For J/ψ production, two basic mechanisms have been proposed. The first of these is quark fusion[3], either by a normal (u,d,s) quark-anti-quark pair converting to the J/ψ via an OZI violating coupling (Fig. 9(a)) or a charmed quark-anti-quark pair converting to the J/ψ via a normal hadronic coupling (Fig. 9(b)). For normal quark fusion, $pp \to J/\psi$ can have either VS or SS contributions, while $p\bar{p} \to J/\psi$ has additionally a VV term. If this were the only mechanism, then at low energies ($M/\sqrt{s}$ large) we would expect $\sigma(p\bar{p}) \gg \sigma(pp)$ and at high energies ($M/\sqrt{s}$ small) we would expect $\sigma(p\bar{p}) \gtrsim \sigma(pp)$. For charmed quark fusion, both $pp \to J/\psi$ and $p\bar{p} \to J/\psi$ can proceed only via an SS term, so we would expect $\sigma(p\bar{p}) = \sigma(pp)$ at all energies if this were the only mechanism.

The second basic mechanism is by cascade production from a χ state which has been produced by gluon exchange[4] (Fig. 10). In this case we expect $\sigma(p\bar{p}) = \sigma(pp)$. An important aspect of this mechanism is that a photon should be seen in coincidence with the J/ψ. Note, however, that while the absence of a photon excludes cascade decay from a χ state, the presence of a photon does not necessarily imply gluon exchange since a χ state can also be produced by quark fusion[5]. Experimentally, it is found that a fraction of the J/ψ's observed in pp collisions at the ISR do come from cascade decay[6], but this cannot be the sole mechanism.

A comparison of $p\bar{p}$ and pp production of J/ψ is available at 40 GeV/c[7] where it is found that $\sigma(p\bar{p})/\sigma(pp) = 7 \pm 3$. This clearly excludes charmed quark fusion (or gluon exchange) as the wole mechanism but is not sufficiently large to invoke only normal quark fusion, so at least two mechanisms must be operative. All existing data on J/ψ production are compatible with a mix of the two quark fusion mechanisms (e.g. Figs. 11, 12, 13), with normal quark exchange dominating at low energy (the VV term compensates for the small OZI violating coupling) and with charmed quark exchange dominating at high energy (the SS term is compensated by the large normal hadronic coupling).

In this model, the 'cross-over' in $pp \to J/\psi$ occurs at $\gtrsim$30 GeV and in $p\bar{p} \to J/\psi$ at $\gtrsim$100 GeV, and we would expect $\sigma(p\bar{p}) \to \sigma(pp)$ at ISR energies. There is no <u>need</u> for gluon exchange but it cannot be excluded: it can be added in addition to or in place of charmed quark fusion. It has been argued that the failure to observe explicit charm conjointly with the J/ψ, which is a natural consequence of normal quark fusion or gluon exchange, militates against charmed quark fusion in which <u>some</u> associated charm would be expected. However, there are possible strong suppression mechanisms, and the current experimental limits are above what would be expected on this basis.

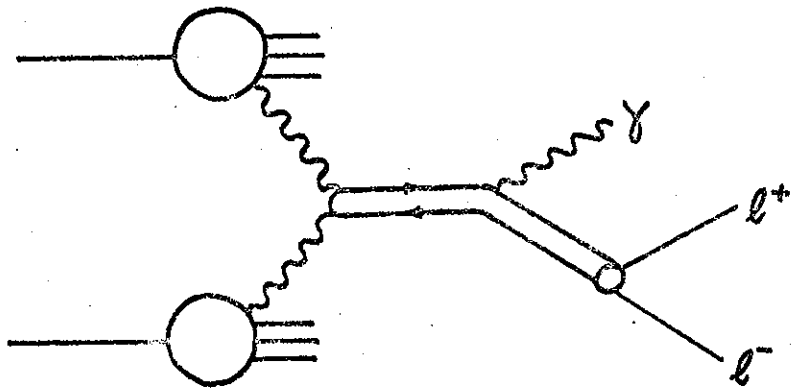

Figure 10 : The gluon exchange model for J/ψ production

For the present, the choice of model is largely a matter of personal prejudice. The study of the variation of $\sigma(p\bar{p} \rightarrow J/\psi)/\sigma(pp \rightarrow J/\psi)$ with energy will be of considerable interest, especially if information can be obtained on the cascade contribution. The extent of the experimental problem is clear from Fig. 13, and it must also be remembered that the Drell-Yan background in $p\bar{p}$ is much larger than that in pp.

It may be that ψ' production will provide a better test, despite its smaller cross-section, since there are no narrow χ states from which it can be produced by cascade decay.

The T will also prove of considerable importance. It is interesting to note that $M/\sqrt{s}$ for J/ψ at the Ω beam dump experiment (40 GeV/c) is the same as $m/\sqrt{s}$ for T at ISR energies, so naively we would expect $\sigma(p\bar{p})/\sigma(pp)$ to be the same. However, with the multiplicity of mechanisms available it is dangerous to make any statement other than that comparison of J/ψ with T for p and $\bar{p}$ interactions will clearly be important.

2.3 ℓn s Physics

Differences between particle and antiparticle interactions often show structures and/or regularities which are not obvious in interaction cross-sections themselves, e.g. the power behaviour of total cross-section differences, and the cross-over in elastic scattering.

The main aspects of the study of differences are:

a) the behaviour of amplitudes odd under cross-channel charge conjugation, i.e. no Pomeron to confuse the issue.

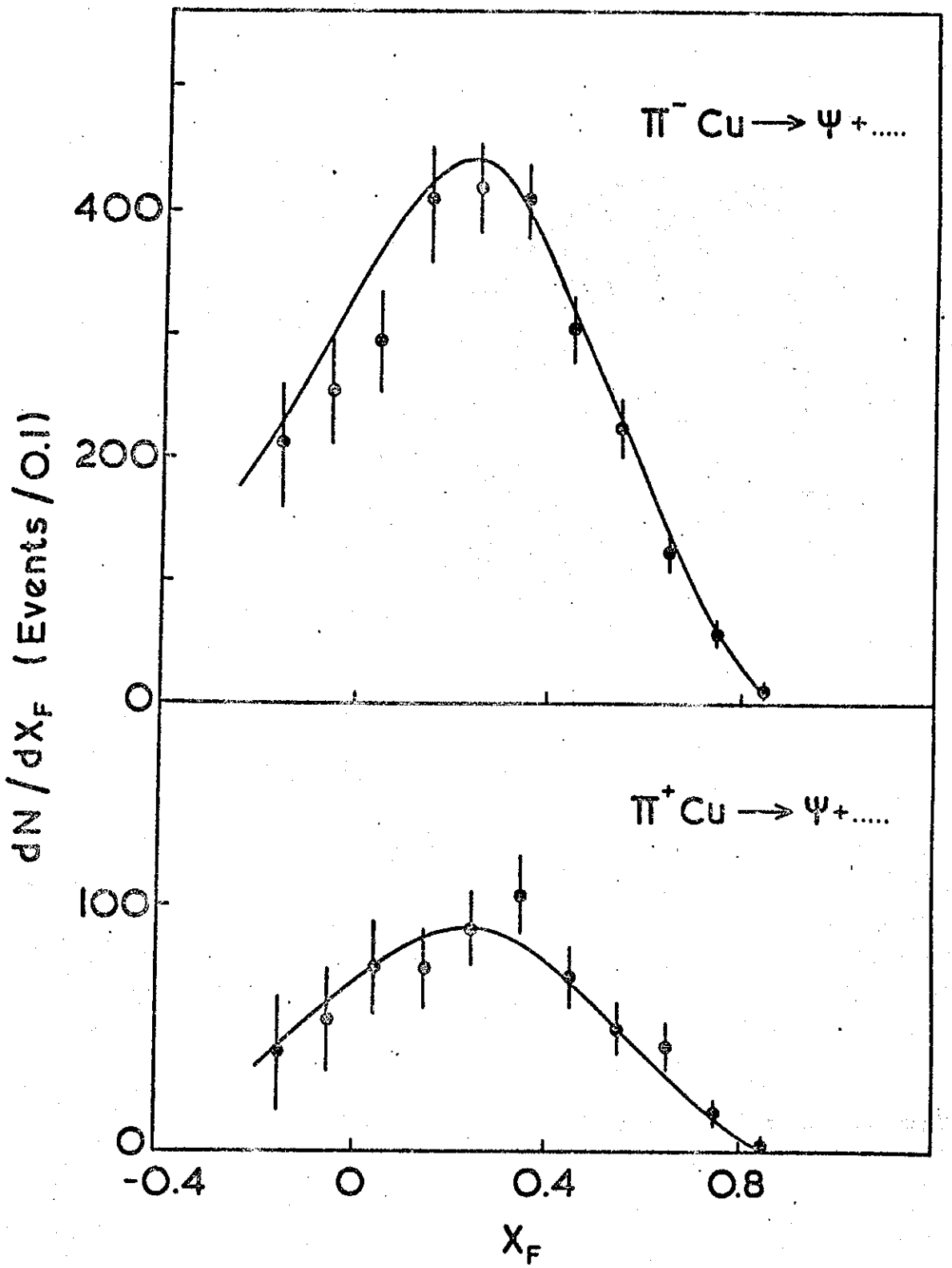

Figure 11 : $d\sigma/dx_F$ for π^+ and $\pi^- \rightarrow J/\psi$ at 40 GeV/c

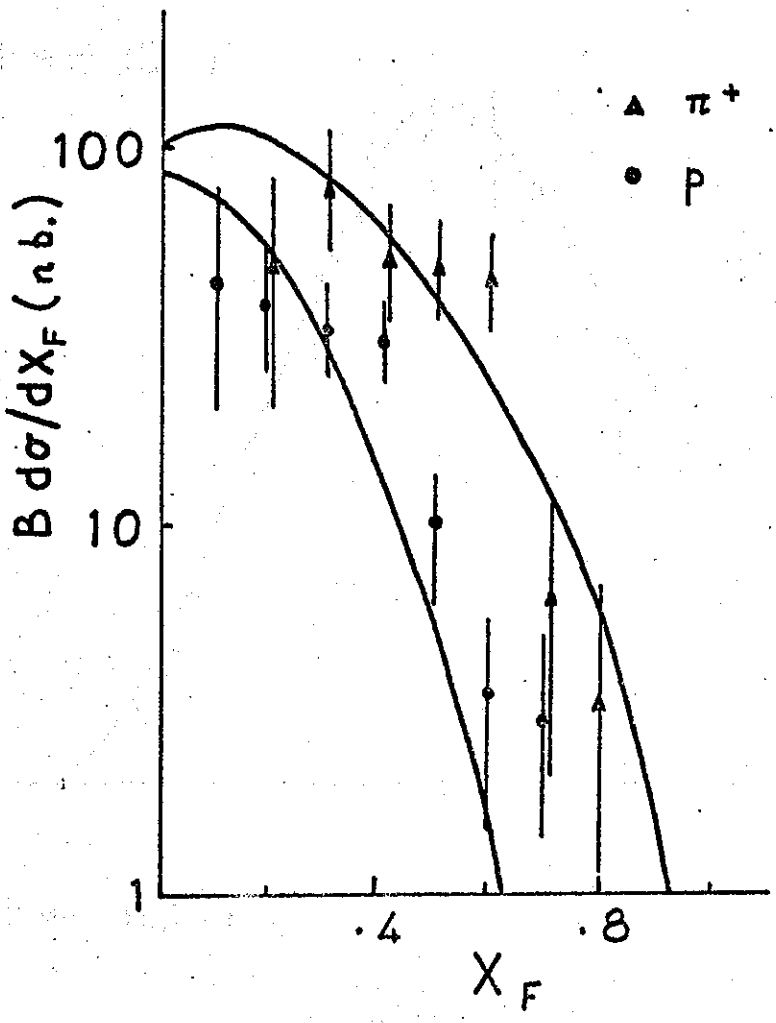

Figure 12 : $d\sigma/dx_F$ for $\pi^+ \rightarrow J/\psi$ and $p \rightarrow J/\psi$ at 240 GeV/c

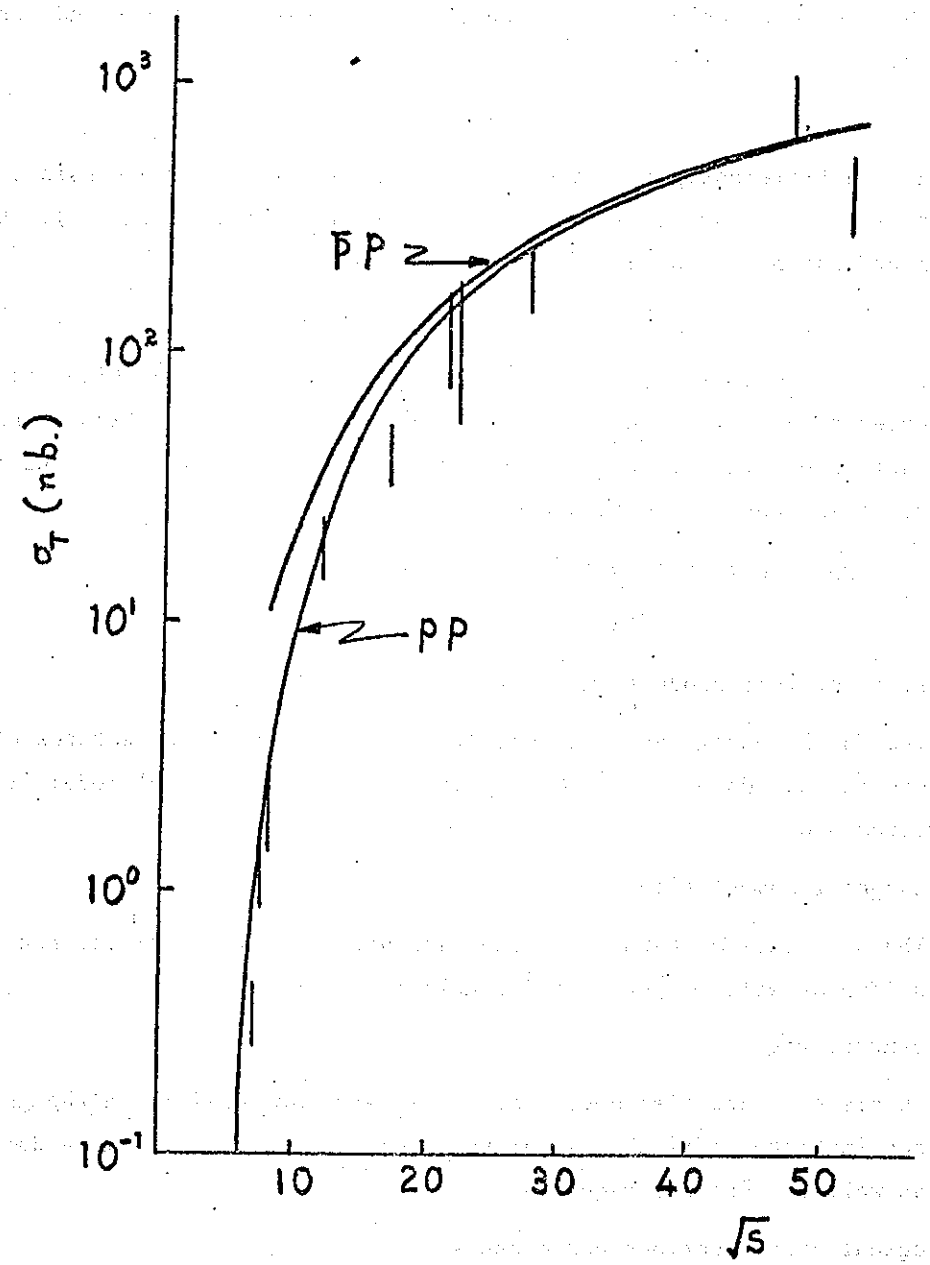

Figure 13 : σ_T for $\bar{p} \to J/\psi$ and $p \to J/\psi$

b) is the simple Regge pole/Regge-Mueller picture successful for differences?

c) to what extent do differences depend on specific mechanisms, e.g. does annihilation play any rôle in $p\bar{p}$ vs. pp?

This subject has been comprehensively reviewed recently[8] and here we simply list the relevant features.

1. σ_{Tot}

All particle-antiparticle cross-section differences are consistent with a power decrease, $\Delta\sigma = \gamma s^{\alpha-1}$, implying a simple Regge picture (Fig. 14). Does this behaviour continue through the ISR energy range?

2. $d\sigma/dt$

The cross-over ($\pi^{\pm}p$, $K^{\pm}p$, $p^{\pm}p$) at $|t| \approx -0.1 \rightarrow -0.2$ (e.g. Fig. 15) has no dynamical understanding in a pure Regge pole picture, the explanation being in terms of absorption. If the absorptive correction is proportional to the convolution of elastic and Regge pole exchanges, then

$$pp : Kp : \pi p \quad 10\ \sigma_T(pp) : 4\ \sigma_T(Kp) : 2\ \sigma_T(\pi p)$$

$$15 : 4 : 2$$

3. Inclusive particle production

The Mueller-Regge approach has difficulties with some features of inclusive cross-sections. However, it does appear to provide a useful model if Pomeron effects are removed.

a) target fragmentation

The qualitative features of the data are readily explained, but we need better data ($K^{\pm}p$ as well as $p^{\pm}p$) for a conclusive test.

c) central region

At present, detailed checks of models are not possible, although qualitative analyses indicate difficulties for the theory. Considerably more data ($\pi^{\pm}p$, $K^{\pm}p$ as well as $p^{\pm}p$) are required.

4. Topological cross-sections and moments

For $\pi^{\pm}p$, $K^{\pm}p$ $\Delta\sigma_n$ is small and the difference is mainly in the low multiplicities. For $p^{\pm}p$, $\Delta\sigma_n$ is significant, even for large multiplicities (Fig. 16). For example, at 100 GeV/c,

$$n_{ch} = 9.06 \pm 0.56 \text{ for } p\bar{p}$$
$$= 6.32 \pm 0.07 \text{ for } pp$$

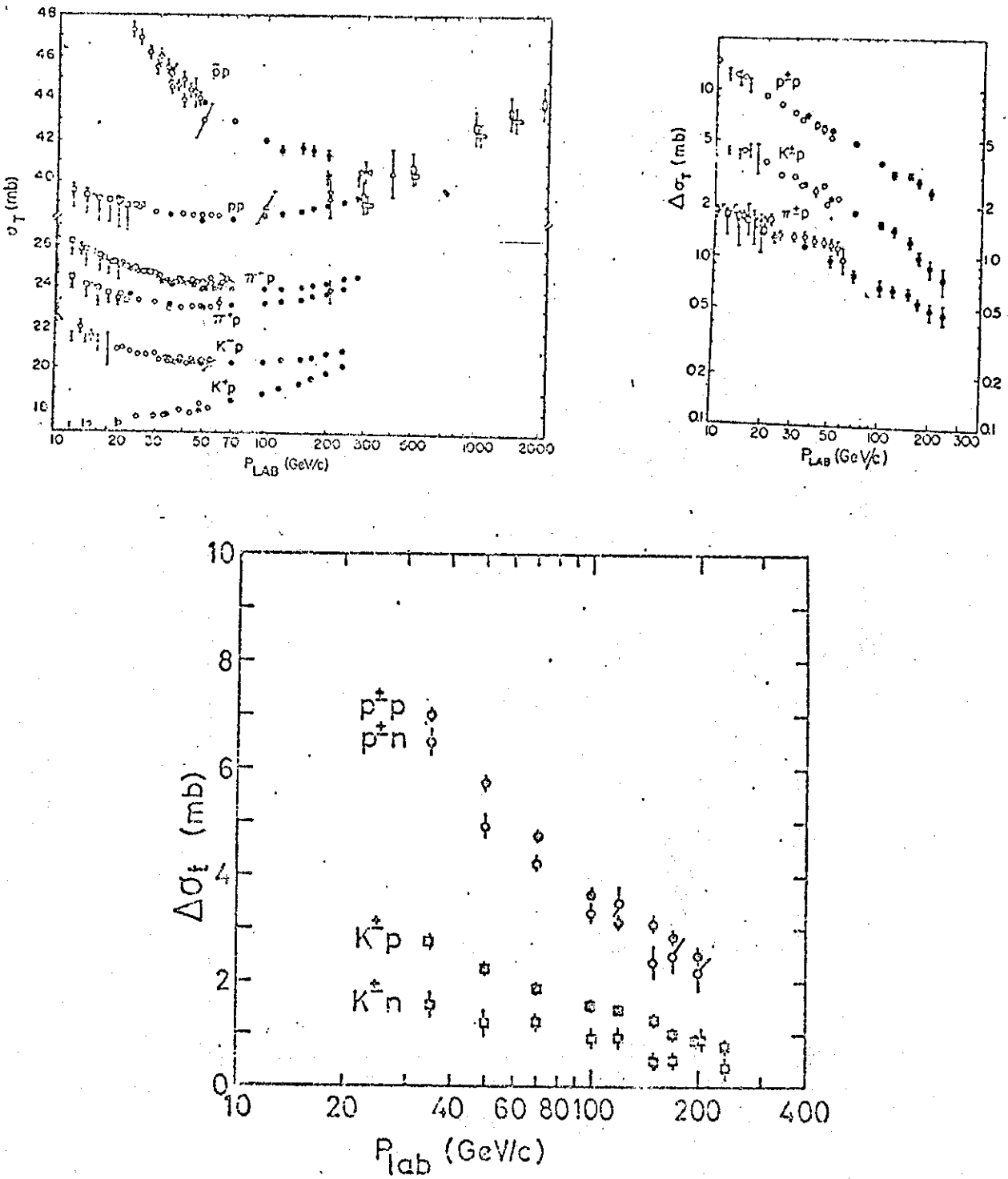

Figure 14 : Total cross-sections and total cross-section differences, showing power law dependence

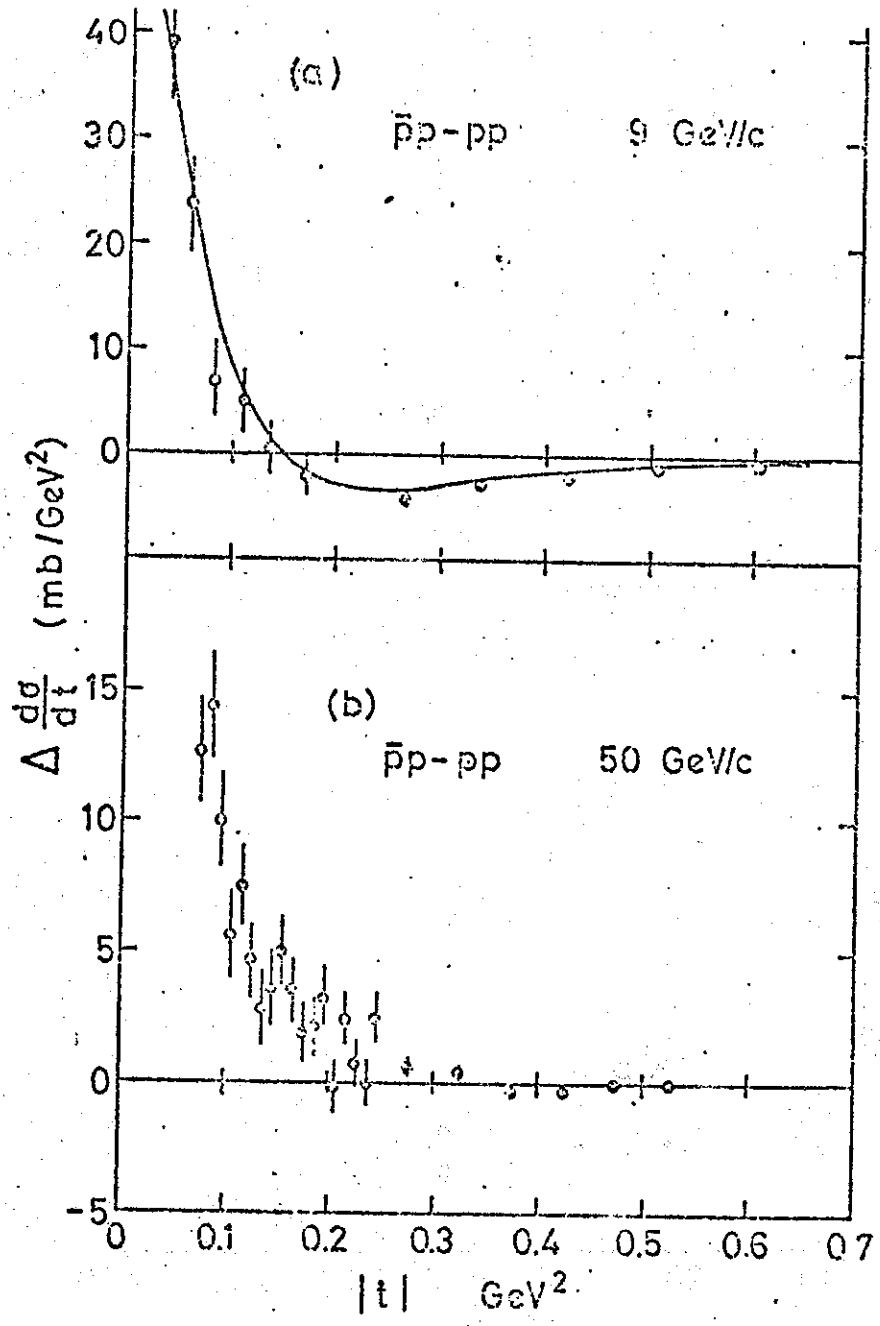

Figure 15 : $p\bar{p}$ - pp elastic differential cross-section, showing cross-over

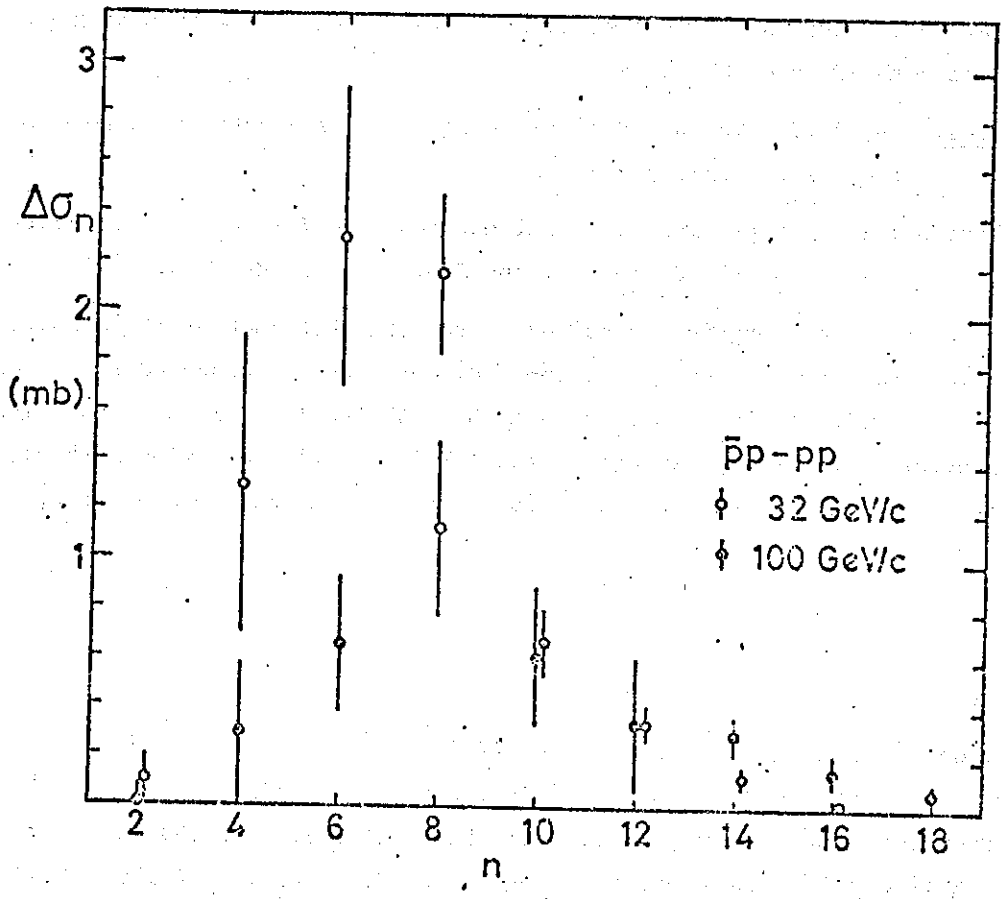

Figure 16 : Differences between $p\bar{p}$ and pp inelastic topological cross-sections at 32 GeV/c and 100 GeV/c

With the usual assumption of ℓn s dependence, pp will not reach this $p\bar{p}$ value of $\langle n_{ch} \rangle$ until $\sim$ 1000 GeV.

2.4 Summary

Even on the basis of this brief look at the gross features of $p\bar{p}$ vs. pp it is clear that there is an interesting programme of physics with $\bar{p}$ at high energies, in both SPS and ISR ranges.

ℓn s physics: σ_T, $d\sigma/dt$, inclusive single particle cross-sections, topological cross-sections and moments.

parton physics : $\bar{p}$ vs. p provides an excellent test-bed for reaction mechanisms in large p_t, Drell-Yan, and J/ψ, ψ', Υ production.

Not all the $\bar{p}$ physics is suited to the ISR, but much of it is and could form a valid programme. However, the $p\bar{p}$-pp differences are expected to be small, in many cases smaller than the errors on much of the earlier ISR pp data. The present generation of pp experiments on the ISR is clearly improving markedly on earlier results, and the important question to ask is whether $p\bar{p}$ experiments could match this?

References

1) M.K. Chase and W.J. Stirling, DAMTP 77/15
2) R.D. Field and R.P. Feynman, Phys. Rev. D15 (1977), 2590
3) A. Donnachie and P.V. Landshoff, Nucl. Phys. B112 (1976), 233
4) S.D. Ellis, M.B. Einhorn and C. Quigg, Phys. Rev. Lett. 36 (1976), 1263
5) A. Donnachie and P.V. Landshoff, unpublished
6) J.H. Cobb et al., CERN prepring, Nov. 1977
7) Corden et al., Phys. Lett. 68B (1977), 96
8) J.G. Rushbrooke and B.R. Webber, Cavendish Laboratory prepring, HEP 77/7

3. ISR Performance with Antiprotons

This section follows the presentation by K. Hübner.

3.1 History

Table I

Earlier estimates (normalized to normal $\beta_v^* = 14$ m, $I_p = 40$ A)

Date	Author	L cm^{-2} s^{-1}	$\bar{p}$ collection time	Method
1970	vdM[1]	4.10^{25} - 4.10^{26}	24 h	SPS → antihyperons → $\bar{p}$
1973	H[2]	10^{25} - 6.10^{25}	3 h	SPS → $\bar{p}$
1975	HJK[3]	7.10^{24}	2 h	SPS → $\bar{p}$
1976	BDMSST[4]	2.10^{26}	24 h	PS → $\bar{p}$ accu. + e-cooling
1976	MST[5]	$3.5.10^{26}$	24 h	PS → $\bar{p}$ accu. + stoch. cool.
1976	HMST[6]	2.10^{28}	24 h	PS → $\bar{p}$ accu. + stoch. cool.

3.2 Upper limit of $L_{p\bar{p}}$

Assume $N_{\bar{p}} = 0.5 \cdot 10^{12}$ at 3.5 GeV/c from shuttle-ring[7];

Accelerate in ISR to $\leqslant$ 31 GeV;

Scale from the design value of $L_{pp} = 4 \cdot 10^{30}$ using $L \sim I_1 I_2 / h_{eff}$

$$L_{p\bar{p}}^{max} = 4 \cdot 10^{30} \cdot \left(\frac{40}{20}\right) \cdot \left(\frac{0.02}{20}\right) \left(\frac{10}{5}\right) \cdot 1.4 \cdot 7$$

A proton current of 40 A and an antiproton current of 20 mA is assumed. The effective height h_{eff} is nowadays 5 mm instead of 10 mm and a perfectly cool $\bar{p}$ beam reduces h_{eff} by another factor 1.4; if the superconducting low β is used, h_{eff} diminishes by a further factor 7. Hence

$$L_{p\bar{p}}^{max} = \underline{2.10^{28} \cdot 7}$$

Table II

Reasonable Expectation for $L_{p\bar{p}}$	
Normal $\beta_v^* = 14$ m	Low $\beta_v^* = 0.31$ m
10^{28}	10^{29}

3.3 Items examined

a) $\bar{p}$-source

Momentum of 3.5 GeV/c is low. We plead for a higher energy, if possible above ISR-transition ($\approx$8.3 GeV/c). We expect that the antiprotons come in 5 bunches created by a 9.5 MHz system in the shuttle-ring.

b) Transfer

$\bar{p}$'s remain in TT2a until they are past the pulsed part of TT2. They will be transferred to TT2 by two slow switching magnets. Fig. 1 shows the lay-out.

c) Injection and trapping

Has been tried with protons at 3.8 GeV/c. We injected 18 mA in 4 bunches; they were trapped and accelerated to 4.06 GeV/c[8].

$\Gamma = 0$ $\quad U = 16$ kV $\quad A_{bucket} = 0.038$ $\quad f_s = 360$ Hz

the RF accepts a bunch area of $A_b = 0.032 \equiv 2$ times the usual proton bunch area. the lifetime was 80 minutes when the kicker was withdrawn. A proton beam was injected at 3.5 GeV/c and accelerated to 8.3 GeV/c in a recent experiment (A. Hofmann et al.).

d) Acceleration

According to S. Oliver $\dot{p}/p = 3.10^{-4}$ s^{-1} is used for accelerating stacks from 26 to 31 GeV. Single pulses have been accelerated with 4.10^{-3} s^{-1} with a following accuracy of 5.10^{-4} in the power supplies. Since one wants to be very careful with the $\bar{p}$-pulse the rate should be limited to

$$\dot{p}/p = 6.10^{-4}\ s^{-1}$$

where the following accuracy is 10^{-4}.

Attenuation of the magnetic field by the copper heat-shields sets in only at $\dot{p}/p < 1$ s^{-1} [9], and is therefore of no importance.

The present tuning system of the ISR-RF system provides $\dot{f}$ = 40 kHz/min but can be speeded up easily, if required, according to H. Frischholz. The finite voltage of the RF ($\simeq$16 kV) and the required bucket area set another limit to acceleration. If one assumes a bucket area of 15 mrad, about the usual proton bunch area, one gets the rate shown in Table III which gives a summary of these limits.

Table III

Limits of Acceleration Rate

P GeV/c	$\dot{p}_{max}$ in (MeV/c)/s limited by			Comments
	RF-tuning	RF voltage	Power supplies	
3.5	205	2300 (Γ=0.45)	2.2	injection
8.8	3260	-	5.3	$\gamma = \gamma_{tr}$
14.3	14000	4300 (Γ=0.84)	8.9	$\gamma = \gamma_{tr} \cdot \sqrt{3}$
31	14200	4400 (Γ=0.87)	19	top energy

However, it is believed that neither of these limits will determine the total acceleration time, but rather continuous control of Q and orbit, which is known to be very tedious.

e) Transition.

A. Hofmann proposed to cross transition by displacing the bunch across the aperture. Let us assume that the magnetic field is constant. Fig. 2 shows γ and γ_{tr} versus x for the FP-line. The pulse sits at - 40 mm prior to crossing occupying for $\varepsilon_x = 20\pi$ mrad mm a width of

$$\delta\times\beta = \pm \frac{\varepsilon_x/\pi \quad \max}{\beta\gamma} \beta_H = \pm 9.6 \text{ mm}$$

$$\delta\times_p = \pm 1 \text{ mm} \ll \delta\times\beta$$

Accelerating the bunch (15 mrad) in a three times bigger bucket with $\hat{U}$ = 16 kV, Γ = 0.5, p = 2.6 GeV/c/s brings it within 67 ms to transition. The change in parameters is very non-adiabatic since the particles will have made only 1/30 of a phase-oscillation during this time. Thus transition can be passed easily in this way in the limit of vanishing space charge forces.

However, it is known from the PS that space charge and negative mass instability play a rôle at 10^{11} particles per bunch. A preliminary estimate by W. Hardt with our parameters indicates that these effects are indeed serious. By how much this will blow up the bunch and cause concurrent beam loss due to limited RF-acceptance is not known at present; only a detailed study would reveal it. This study could also examine the beneficial effect of a γ_{tr}-jump as used in the PS[10]. The table below gives a comparison between available speeds; the ISR values were taken from Fig. 2 taking into account $\dot{\gamma}$ = 2.6 s^{-1} from before.

Table IV

Comparison

	ISR s^{-1}	PS (γ_{tr}-jump) s^{-1}
$\dot{\gamma}$	2.6	50
$\dot{\gamma}_{tr}$	- 7.9	- 120·50

Debunching the $\bar{p}$-beam at injection and trapping it in 30 buckets might also be helpful since it reduces the intensity per bunch by a factor 6.

f) Cooling and beam blow-up at 26.6 GeV

In order to gain ≈ 1.4 in luminosity the height of the antiproton beam must be reduced from, say, 5 mm to 1 mm by a stochastic cooling system which has also to maintain this small height of the beam over many hours.

The results of the cooling experiments indicate, according to W. Schnell, that one may hope for an initial rate of

$$\frac{1}{\tau_c} = -\ 2\%\ \text{per min}$$

and a compression factor 5 within two hours from the 1 - 2 GHz system without undue extrapolation. As a matter of fact, L. Faltin has achieved this compression factor with 500 μA and H. Henke has shown that the initial cooling rate of a 5 mA beam is identical to the one measured with 500 μA.

g) Experimental magnets

SFM

According to K. Brand the crossing point will be displaced by 27 cm (cf. Fig. 3) in the longitudinal direction; hence a new vacuum chamber is required. On top of it an aperture restriction for the $\bar{p}$'s will be generated in the shielding channels of the SFM because they are adjusted for operation with protons. However, L. Resegotti suggested that this limitation could be overcome by making the channels moveable. The SFM field would be reduced by p_{inj}/p_{final} during $\bar{p}$ injection and acceleration, then ramped to the desired value. Only then would one inject the protons.

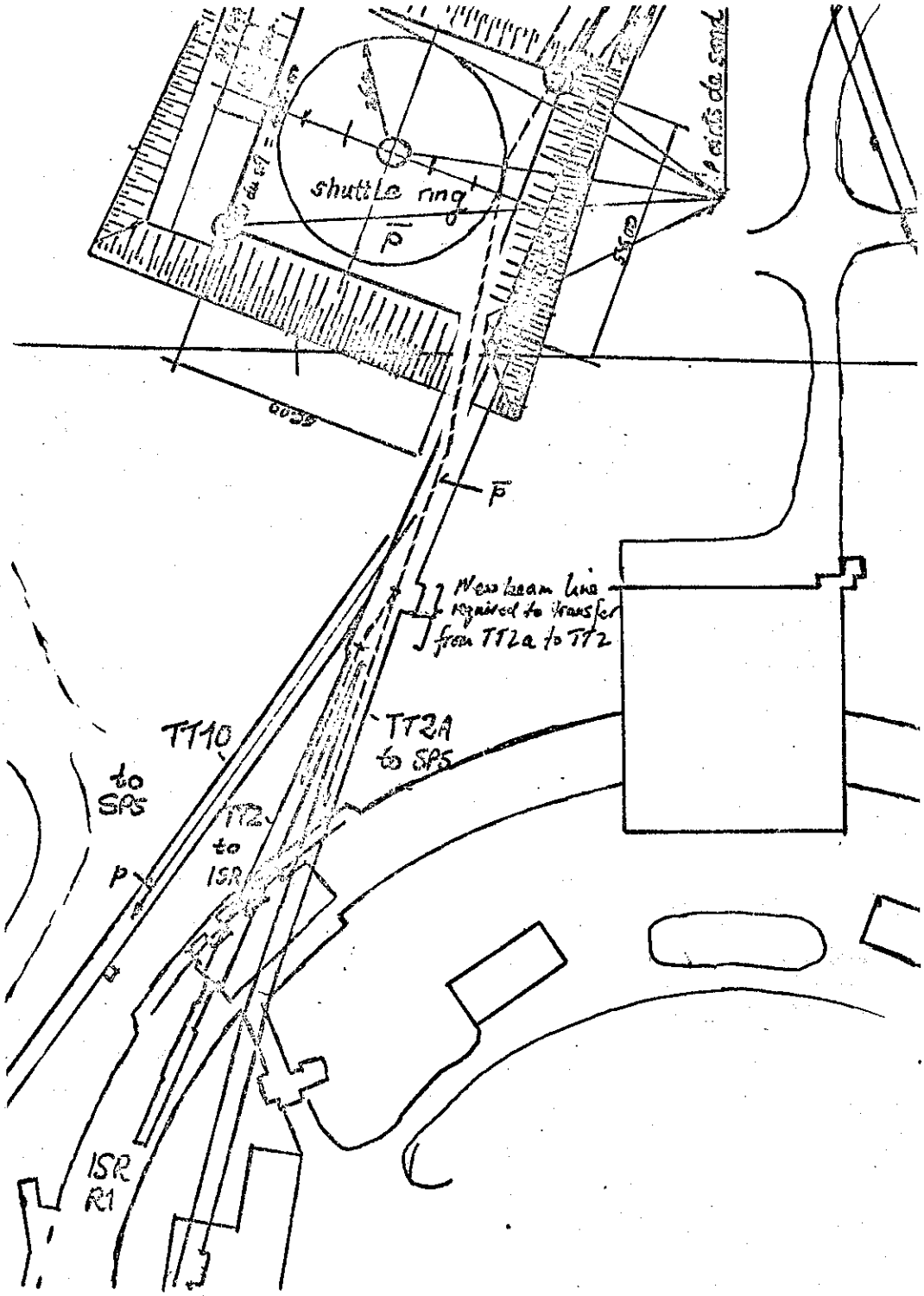
shuttle ring
$\bar{p}$
$\bar{p}$
New beam line required to transfer from TT2a to TT2
TT10
to SPS
TT2A to SPS
TT2 to ISR
p
ISR R1

Figure 1

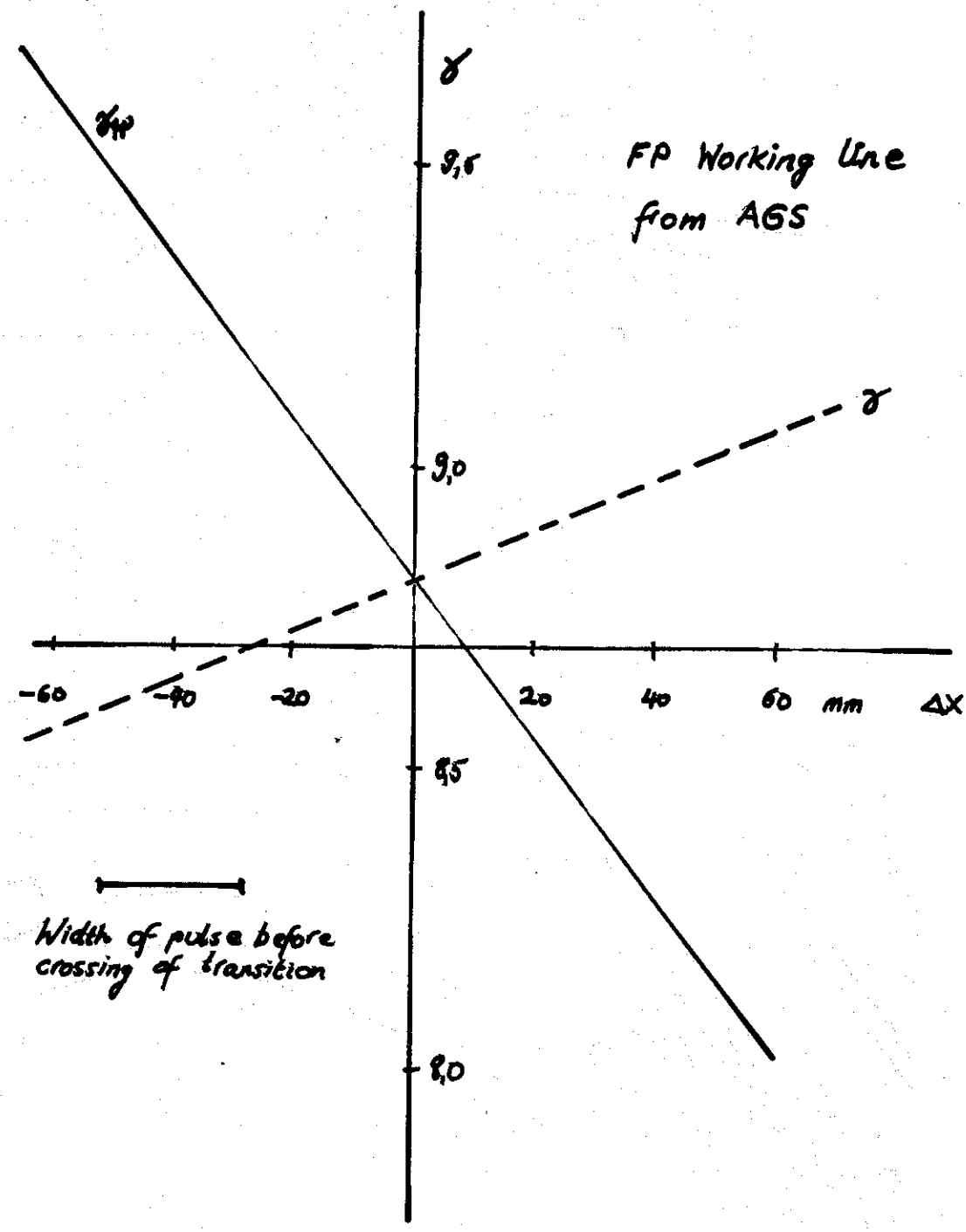

γ and γ_{FP} in ISR versus ΔX

Figure 2

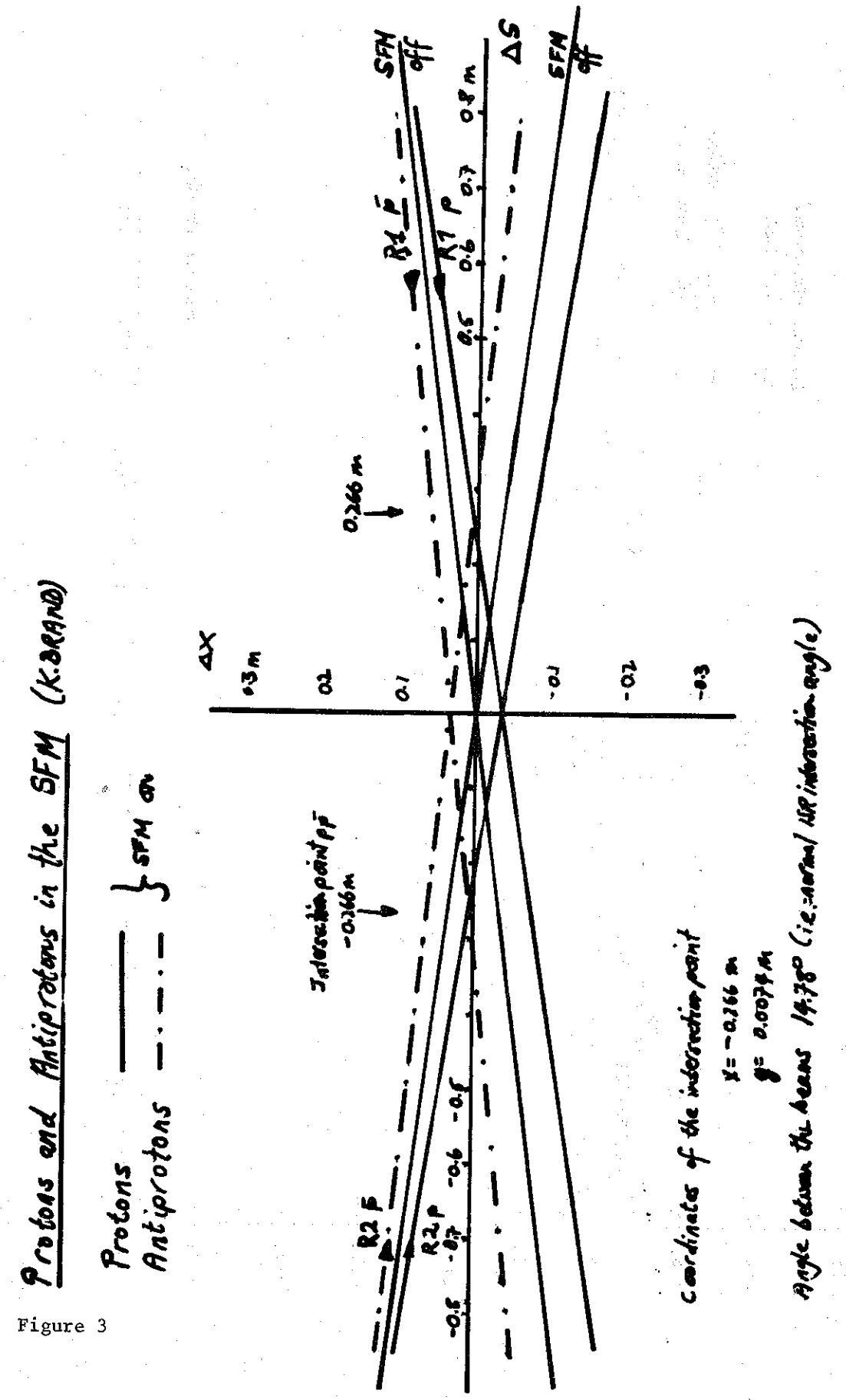
Protons and Antiprotons in the SFM (K.BRAND)
Protons
Antiprotons
SFM on
SFM off
ΔX
ΔS
+3m
0.2
0.1
-0.1
-0.2
-0.3
0.5
0.6
0.7
0.8m
0.266 m
Intersection point F̄
-0.36m
R2 F̄
R2 P
R1 F̄
R1 P
-0.5
-0.4
-0.6
-0.5
Coordinates of the intersection point
x = -0.166 m
y = 0.0078 m
Angle between the beams 14.78° (i.e. arms/IIR interaction reg(e.)

Figure 3

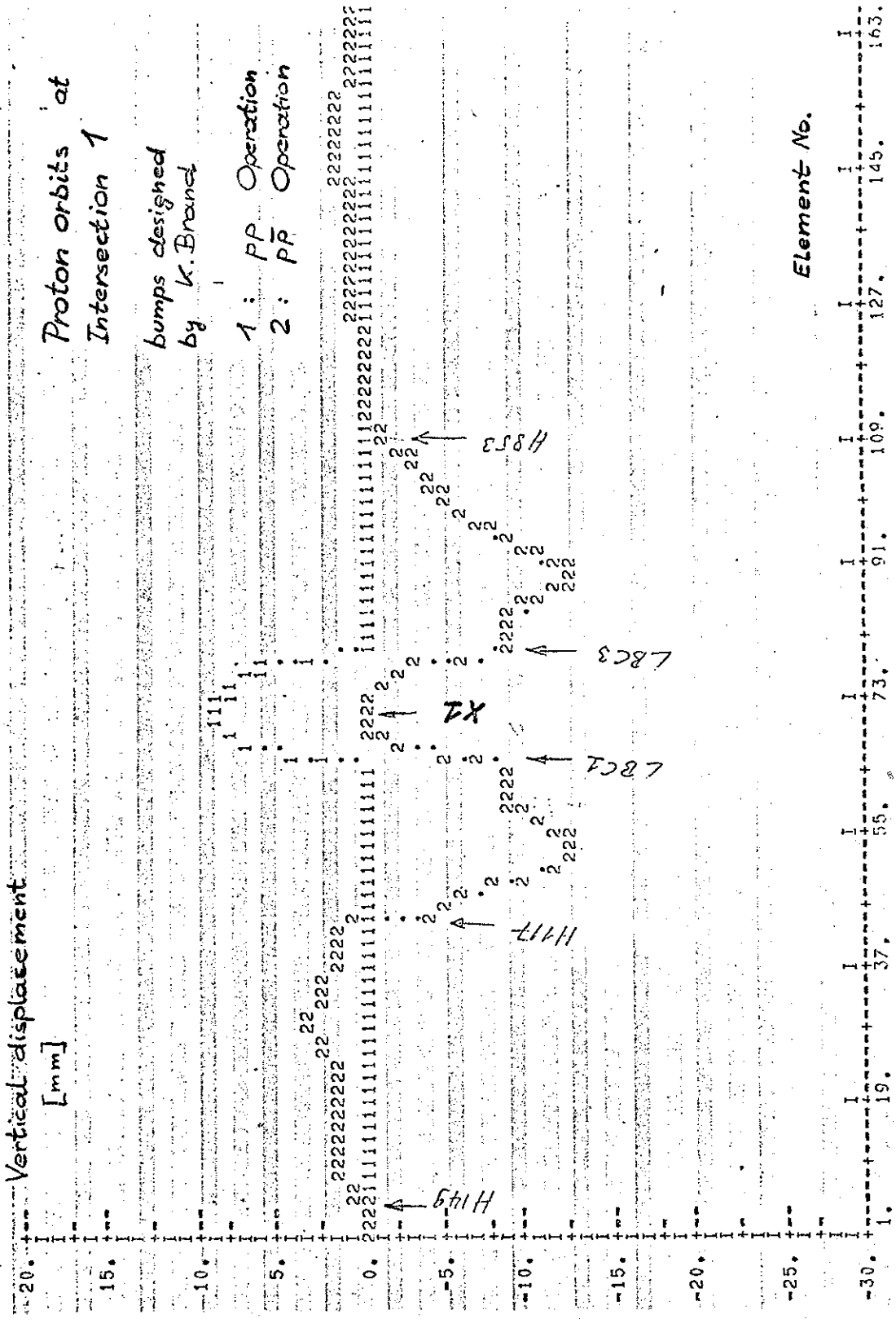
Vertical displacement
[mm]
Proton orbits at
Intersection 1
bumps designed
by K. Brand
1 : pp Operation
2 : pp̄ Operation
Element No.
HV19
XZ
LBC1
LBC3
HS53
20.
15.
10.
5.
0.
-5.
-10.
-15.
-20.
-25.
-30.
1.
19.
37.
55.
73.
91.
109.
127.
145.
163.

Figure 4

Solenoid

The proton beams are displaced by 9 mm in the centre of the solenoid, the antiprotons by - 9 mm if the present correction scheme is applied, K. Brand has designed special bumps to make the displacement zero in both rings. Fig. 4 shows these bumps for the p-ring; the bumps in the $\bar{p}$-ring are the same except of opposite sign. Obviously, these bumps will reduce the vertical aperture up- and downstream of the intersection for p's and $\bar{p}$'s. The bumps should be re-examined for the superconducting low β insertion.

Axial Field Magnet

The same considerations as for the solenoid apply. According to T. Taylor the displacement is only 4 mm which eases the correction.

h) New hardware

* Transfer of $\bar{p}$ from TT2a → TT2
* Polarity reversing switches for main magnets
* Lenses and power supplies for a γ_{tr}-jump?

i) Operational problems

Low intensity beams which are very rare.

3.4 Conclusions

* A luminosity between 10^{28} to 10^{29} cm^{-2} s^{-1} seems to be possible.
* Crossing of transition needs attention. Two lines of attack are recommended: i) theoretical study
  ii) try it with protons injected close to transition to avoid painful ramping.
* A cooling experiment with a 20 μA beam should be performed to demonstrate that our extrapolations are justified.
* A higher injection energy would be extremely useful, especially if one could avoid crossing transition!
* All experimental magnets can be used if adequate provisions are made.

C. Rubbia suggested to consider whether the luminosity could not be increased by using low intensity but well cooled beams.

3.5 Acknowledgements

This compilation is based on the discussions between K. Hübner and many of the colleagues in the ISR. They are all thanked for their interest.

References

1) S. van der Meer, CERN-ISR-PO/70-5 (1970)

2) K. Hübner, CERN-ISR-TH/73-19 (1973)

3) K. Hübner, K. Johnsen, G. Kantardjian, CERN-ISR-LTD/75-45 (1975)

4) D. Möhl, L. Thorndahl, P. Strolin, G.I. Budker, N. Dikansky, A.N. Skrinsky, CERN-EP/76-03 (1976)

5) D. Möhl, L. Thorndahl, P. Strolin, CERN-EP/76-05 (1976)

6) K. Hübner, D. Möhl, L. Thorndahl, P. Strolin, CERN-PS-DL/76-27 (1976)

7) S. van der Meer et al., CERN-SPS-DI-PP/77-9 (1977)

8) A. Hofmann et al., ISR Performance Report, 12.9.77

9) J-P. Gourber and K. Hübner, ISR Performance report 2.12.73

10) W. Hardt, IXth Int. Conf. on High Energy Acc., Stanford (1974) 434.

4. Low Multiplicity Reactions with Antiprotons in the ISR

This section follows the presentation by G. Matthiae.

4.1 Introduction

The success of present cooling techniques allows one to expect sizeable values for the luminosity of antiproton-proton collisions at the ISR. Actual estimates lead to the value $L \simeq 2 \times 10^{28}$ cm^{-2} s^{-1} in a normal straight section while in a low-β section the luminosity will be about 7 times larger. As shown in Fig. 1, the expected value of the $p\bar{p}$ luminosity at the ISR compares rather well to that obtained with secondary beams and fixed target experiments at conventional accelerators.

The luminosity of 10^{28} cm^{-2} s^{-1}, which is about a factor of one thousand less than the present luminosity of the ISR for pp collisions, will be obtained with a proton current of 30 to 40 A and an antiproton current of about 30 mA. The signal over background ratio will therefore be about one thousand times less for $p\bar{p}$ collisions than it is at present for pp collisions. This may cause difficulties in experiments at low counting rate and in those which are especially sensitive to background. On the other hand, for elastic scattering experiments there should be no problem. In fact, tests made with proton currents of a few Amps in one ring only using the small angle elastic scattering set-up (CERN-Rome) and the elastic trigger at the SFM of the CHOV group, demonstrated that elastic scattering measurements would be feasible even for a luminosity of $\sim 10^{26}$ cm^{-2} s^{-1} (Amaldi et al. CERN 76/12, page 152).

4.2 Total Cross-section

By extrapolating the power law trend of the total cross-section difference $(p\bar{p})-(pp)$, one finds at ISR energies values of 1 - 2 mb (Fig. 2.a)). This conclusion is supported by the high-energy extrapolation of $p\bar{p}$ and pp total cross-sections as obtained by inserting into dispersion relations the recent ISR results on the real part of the pp forward elastic amplitude (Fig. 2.b)).

At the ISR, by measuring the total interaction rate and the small angle elastic scattering rate at the same time, both the total cross-section and the machine luminosity were determined (PSB + CR, 1975). The value of the luminosity given by this method, agreed with that obtained from the standard Van der Meer method within ±0.9%. Once it is known that the Van der Meer method provides the absolute calibration of the machine luminosity to better than ±1%, the simplest method for measuring σ_t is that based on small angle scattering. This method is also less sensitive to background than that based on the measurement of the interaction rate.

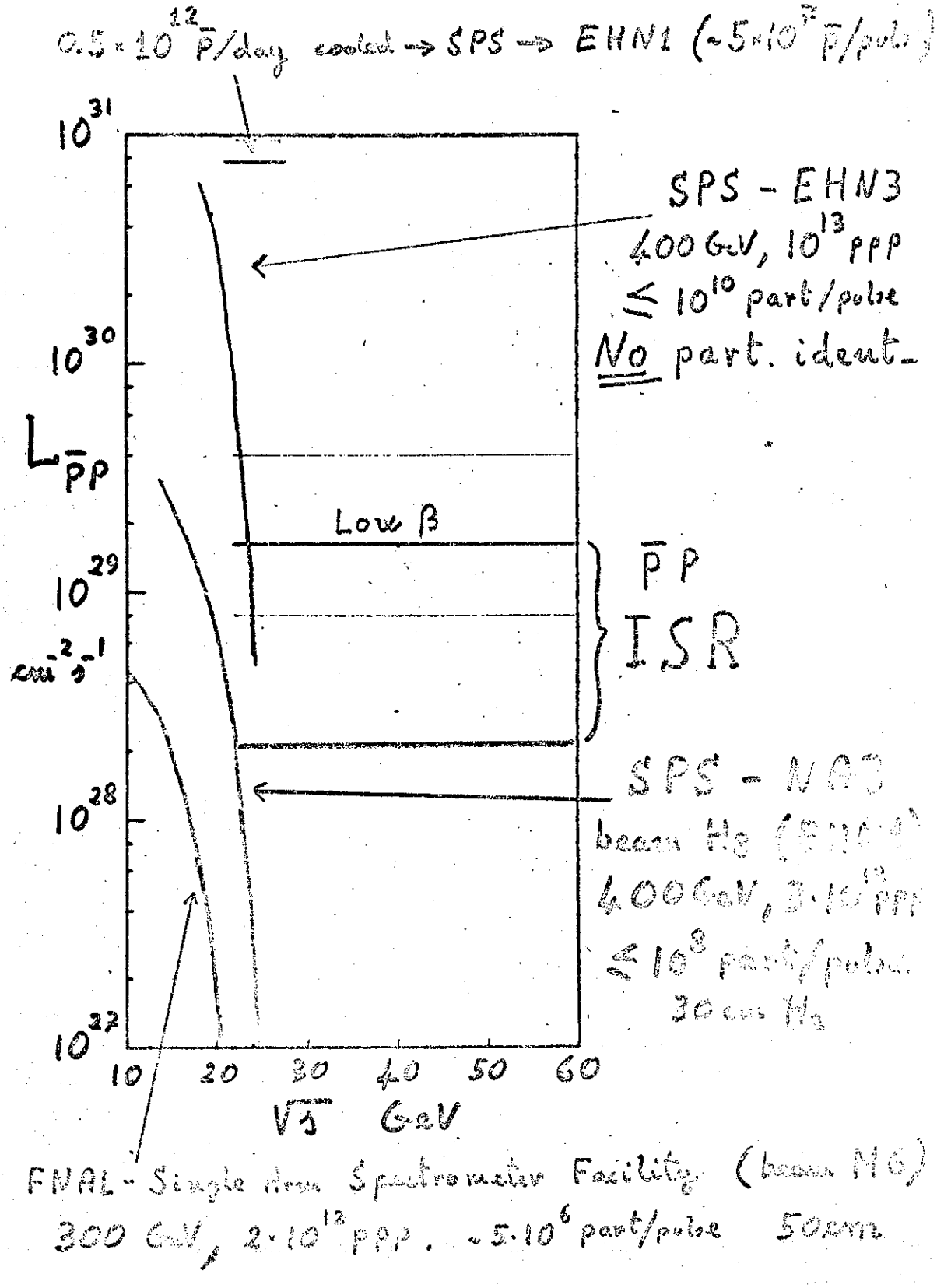
0.5 × 10^12 p̄/day cooled → SPS → EHN1 (~5×10^7 p̄/pulse)
10^31
10^30
10^29
10^28
10^27
L p̄p
cm^-2 s^-1
SPS - EHN3
400 GeV, 10^13 ppp
≤ 10^10 part/pulse
No part. ident.
Low β
p̄p
ISR
SPS - M 03
beam He
400 GeV, 3·10^13 ppp
≤ 10^8 part/pulse
30 cm H2
10
20
30
40
50
60
√s GeV
FNAL - Single Arm Spectrometer Facility (beam M6)
300 GeV, 2·10^12 ppp. ~5·10^6 part/pulse 50cm

Figure 1

$$\Delta\sigma_t \sim p_L^{\alpha_0 - 1}$$

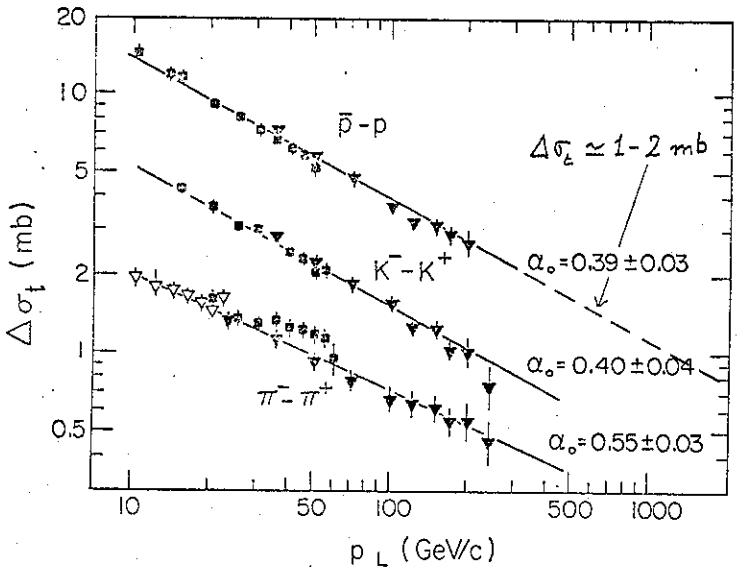

Figure 2.a)

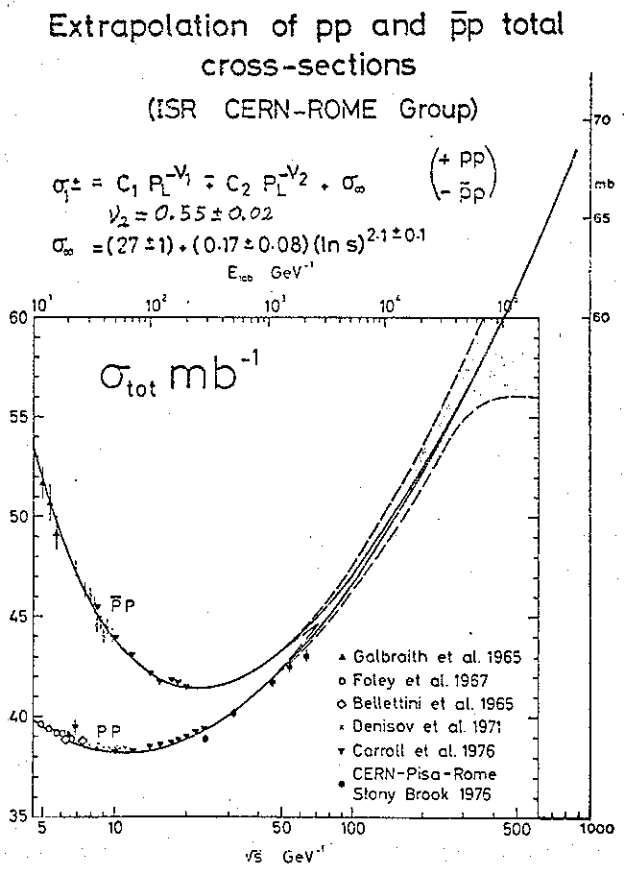

Figure 2.b)

The accuracy on σ_t, reached for pp collisions was of ±0.3 to 0.4 mb. For $p\bar{p}$, the forward slope being larger, one may guess an error of about 0.5 mb. Consequently the total cross-section difference $(p\bar{p})-(pp)$ would be measured with an error of about 0.6 to 0.7 mb.

4.3 Elastic Scattering

The measurement of elastic scattering in the Coulomb interference region is feasible. However, the requirement of narrow and clear beams, which implies a proton current of only a few Amps, together with the need for a large statistical sample, makes the determination of the real part, with the same accuracy which may be reached in pp collisions, rather problematic. The knowledge of the real part is, however, quite important in view of the fact that it complements the measurements of the total cross-section and, through dispersion relations analysis, allows to estimate the behaviour of the total cross-section at higher energies.

A compilation of data on the ratio ρ of the real to the imaginary part of the forward amplitude for pp and $p\bar{p}$ scattering is shown in Fig. 3.

Data on the slope of the forward elastic peak are shown in Fig. 4 for pp and $p\bar{p}$ scattering. In the very small t region, around 0.05 GeV^2, data are available only for pp scattering. They came from gas jet experiments and from the ISR.

Results on pp and $p\bar{p}$ elastic scattering from 50 up to 175 GeV/c and for $-t \lesssim 0.8$ GeV^2 as measured by the Single Arm Spectrometer group at FNAL are shown in Fig. 5. From the comparison of the $p\bar{p}$ and pp data, the position of the cross-over point, t_c, is obtained, which seems to show some energy dependence.

For $p\bar{p}$ scattering, large $|t|$ data above a few GeV/c incident momentum are missing (Fig. 6).

It should be stressed that detailed studies of the shape of $p\bar{p}$ and pp angular distributions in the diffraction peak region can easily be made at the ISR even with a luminosity of the order of 10^{28} cm^{-2} s^{-1}. In fact a sample of data (~ one million events) similar to that collected in 1971 by the ACGHT collaboration (Fig. 7) could be obtained in $p\bar{p}$ collisions with $L = 10^{28}$ cm^{-2} s^{-1} in about 2 days of running time.

In Fig. 7 the most recent ISR data on large t elastic scattering from the CHHOV group are also shown. These data were obtained with the SFM using the elastic trigger which has a large acceptance (30 - 40%). The same experiment, if repeated for $p\bar{p}$ with a luminosity of $\sim 10^{28}$ cm^{-2} s^{-1} would lead to explore elastic scattering up to a cross-section value of about 5×10^{-6} mb/GeV^2, corresponding for the pp case to a maximum $|t|$ of about 4 GeV^2. The displacement of the crossing

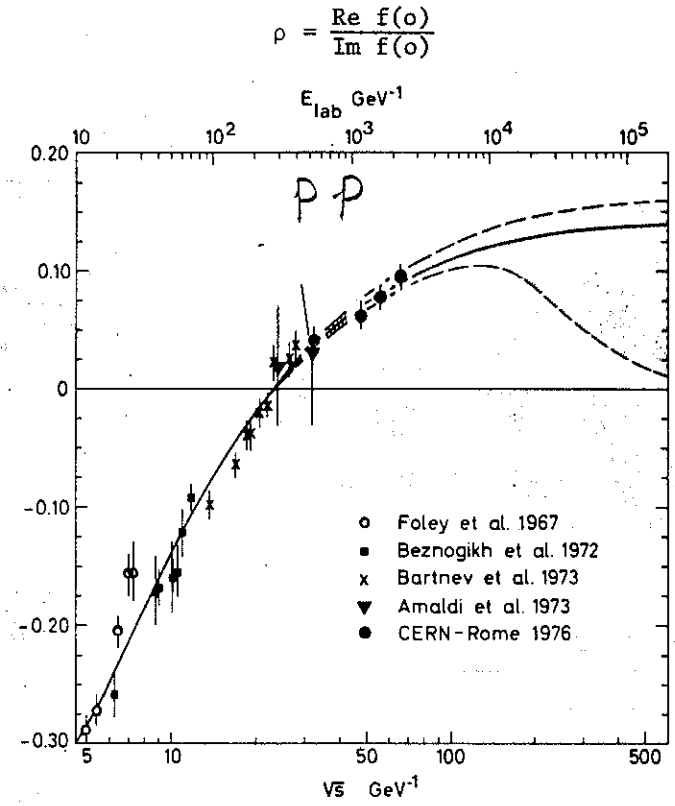
ρ = Re f(o) / Im f(o)
E_lab GeV⁻¹
10
10²
10³
10⁴
10⁵
0.20
0.10
0
-0.10
-0.20
-0.30
p p
ρ
Foley et al. 1967
Beznogikh et al. 1972
Bartnev et al. 1973
Amaldi et al. 1973
CERN-Rome 1976
5
10
50
100
500
√s GeV⁻¹

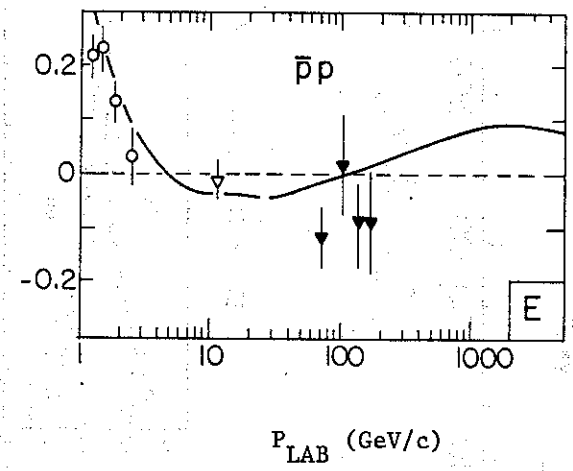
0.2
0
-0.2
p̄p
ρ
E
10
100
1000
P_LAB (GeV/c)

Figure 3

FORWARD SLOPE

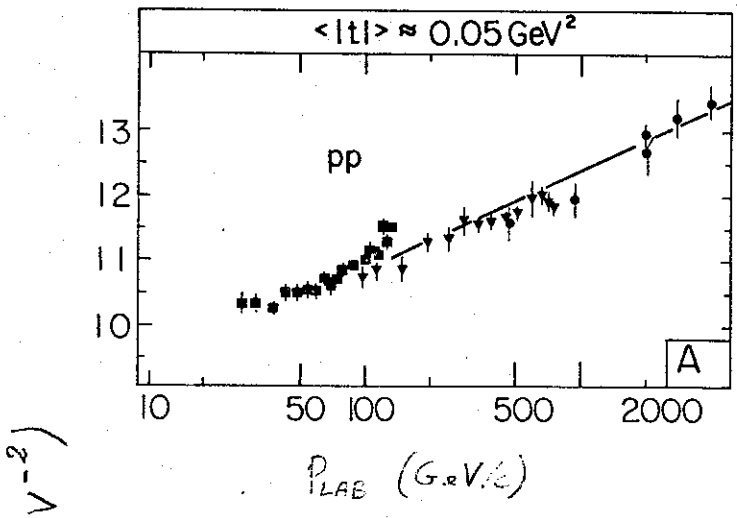

<|t|> ≈ 0.2 GeV²

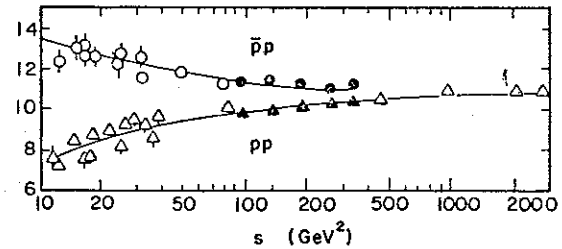

Figure 4

p̄p - pp CROSS-OVER

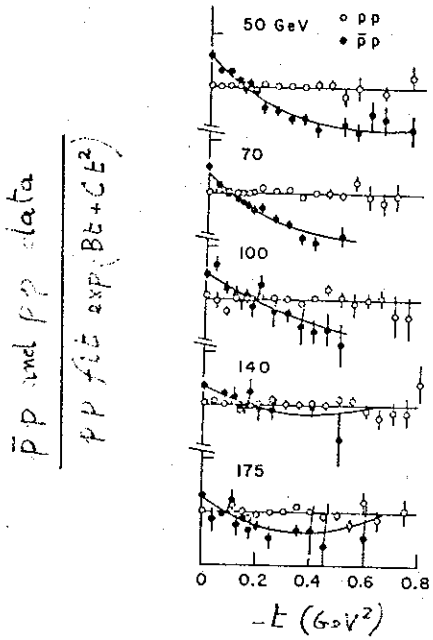

FNAL

Single Arm Spectrometer Group

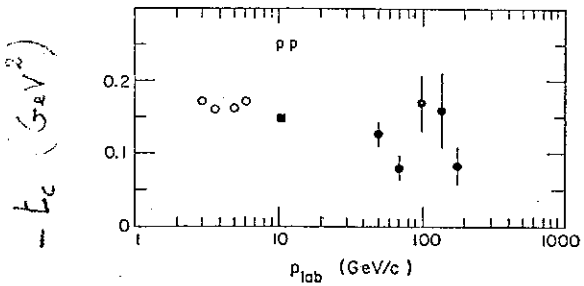

Figure 5

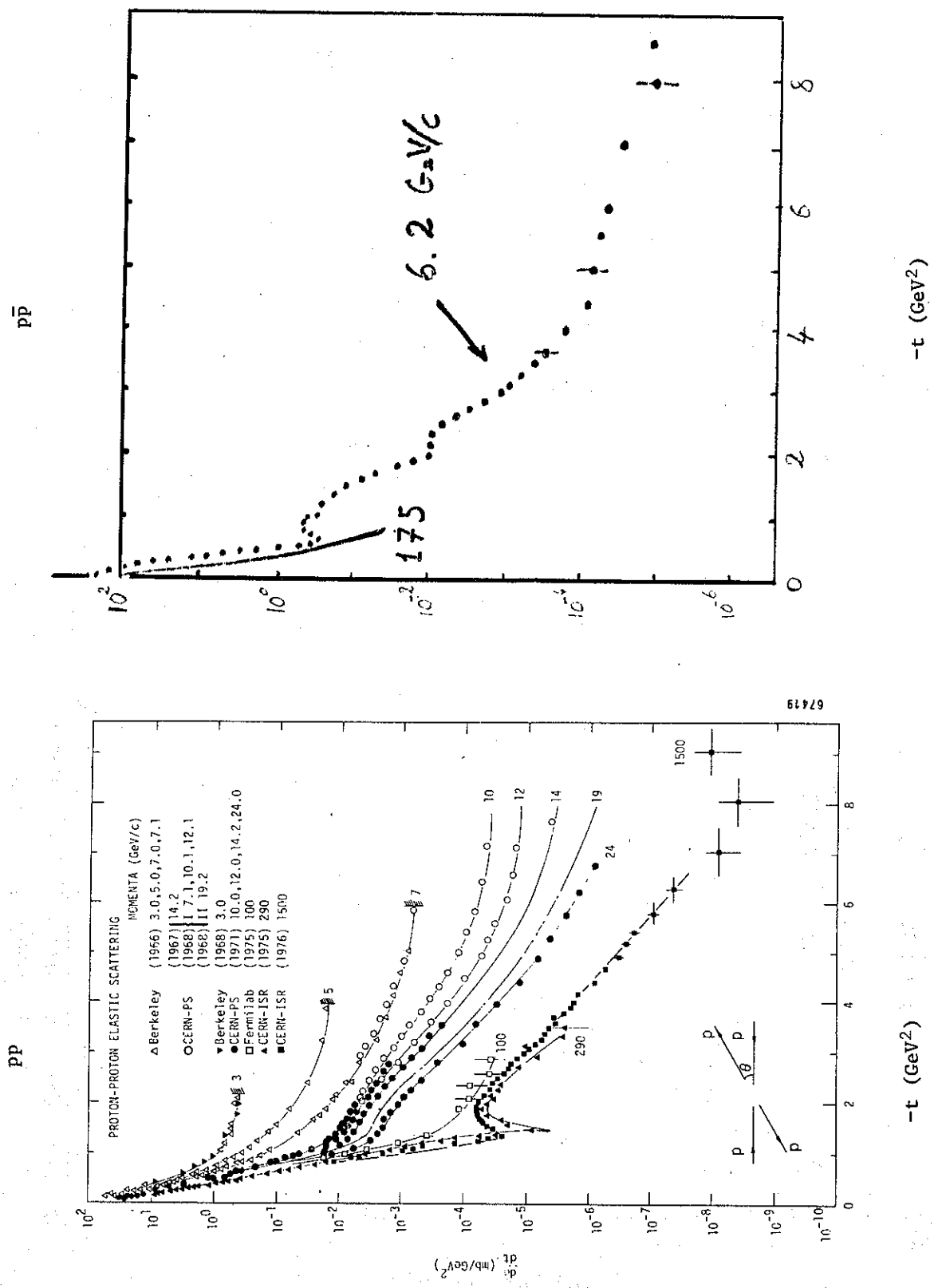
p̄p
5.2 GeV/c
175
-t (GeV²)
pp
PROTON-PROTON ELASTIC SCATTERING
MOMENTA (GeV/c)
Berkeley (1966) 3.0,5.0,7.0,7.1
CERN-PS (1967) 14.2
(1968) 7.1,10.1,12.1
(1968) 19.2
Berkeley (1968) 3.0
CERN-PS (1971) 10.0,12.0,14.2,24.0
Fermilab (1975) 100
CERN-ISR (1975) 290
CERN-ISR (1976) 1500
-t (GeV²)
67419

Figure 6

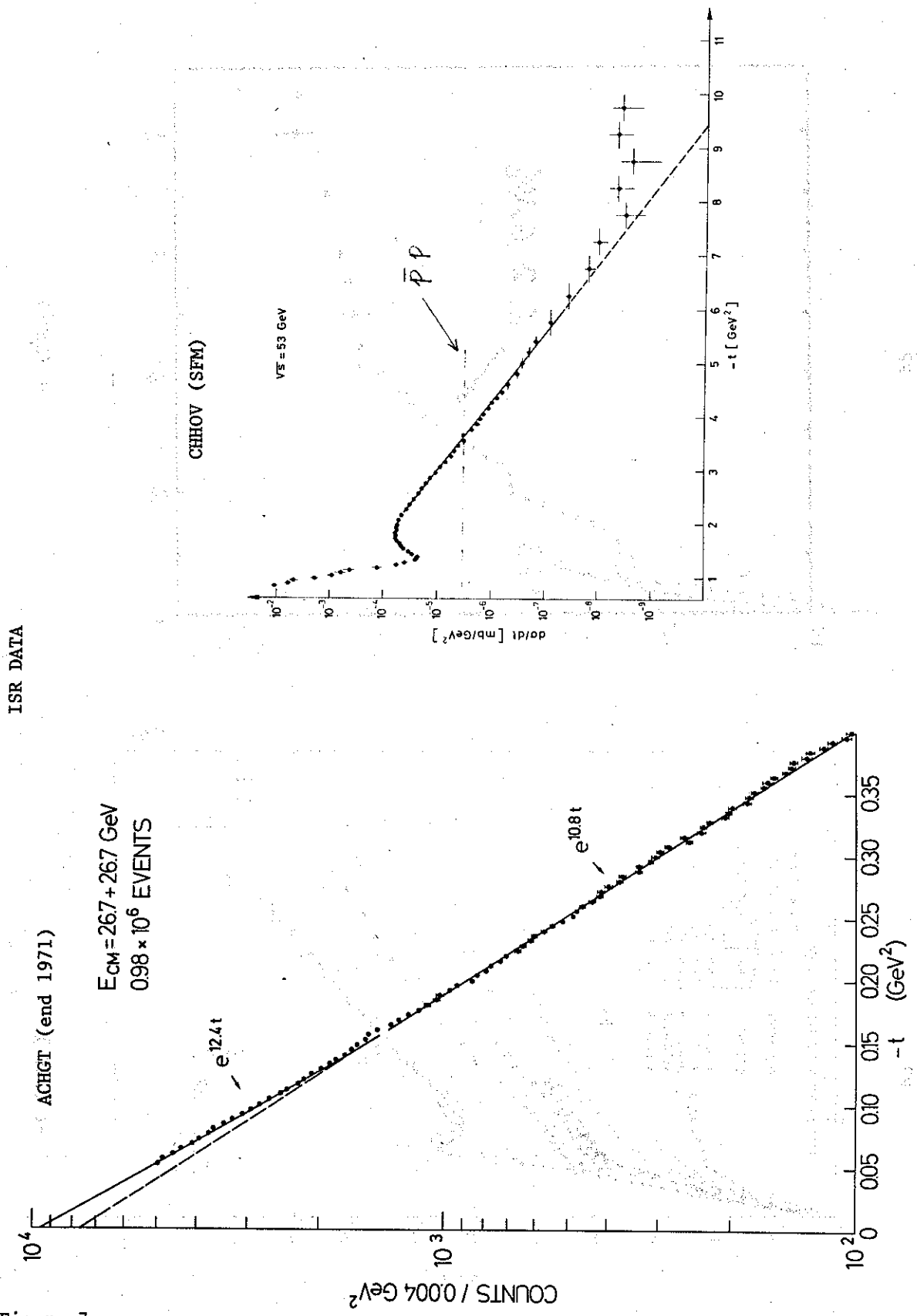
ISR DATA
ACHGT (end 1971)
$E_{CM} = 26.7 + 26.7$ GeV
0.98×10^6 EVENTS
$e^{12.4t}$
$e^{10.8t}$
COUNTS / 0.004 GeV^2
10^4
10^3
10^2
0 0.05 0.10 0.15 0.20 0.25 0.30 0.35
$-t$ (GeV^2)
CHHOV (SFM)
$\sqrt{s} = 53$ GeV
$\bar{p}p$
$d\sigma/dt$ [mb/GeV^2]
$-t$ [GeV^2]

Figure 7

point in the SFM for $p\bar{p}$ collisions, which was calculated to be of about 30 cm (see K. Hübner's report), should not cause any serious complications.

The simplest and intuitive way to understand differences between the $p\bar{p}$ and the pp systems is provided by the impact parameter representation. A summary of results on the values of the inelastic function $G_{in}(b, s)$ at $b = 0$ as a function of s for $p\bar{p}$ and pp, on the difference of the two profile functions $\Gamma_{p\bar{p}}(b)$ and $\Gamma_{pp}(b)$ and on the energy dependence of $G_{in}(b)$ for pp collisions is shown in Fig. 8.

The picture that emerges from these data concerning the validity of geometrical scaling and the increasing peripherality of the collisions at higher energies would clearly benefit from studies of $p\bar{p}$ scattering at ISR energies.

4.4 Two-body Inelastic Reactions

Quite a lot of work has gone into single and double diffractive dissociation at the ISR. Limiting ourselves to the reactions where the excited system is identified, i.e. its quantum number is known, a summary of results is shown in Fig. 9. The excitation of systems with $I = \frac{1}{2}$ shows a very weak energy dependence. On the contrary, the charge exchange reaction $pp \to n\Delta^{++}$ shows at low energy ($P_{LAB} \lesssim 25$ GeV/c) the well known behaviour $\sigma \sim P_{LAB}^{-2}$ which is usually interpreted as due to π exchange. However, recent data from the CHHOV collaboration show that, just in the energy range of the ISR, the energy dependence of the cross-section becomes more gentle ($\sigma \sim P_{LAB}^{-1}$). This result indicates that at high energy the exchange of trajectories with higher intercepts (ρ, A_2) becomes the dominant contribution.

For $p\bar{p}$ collisions a compilation of reactions with charge exchange ($p\bar{p} \to n\bar{n}$), strange meson exchange ($p\bar{p} \to \Lambda\bar{\Lambda}$) and baryon exchange ($p\bar{p} \to \pi^-\pi^+$) is shown in Fig. 10. For the first two reactions the expected cross-section in the ISR range is of $0.1 \sim 1$ μb which, for $L \approx 10^{28}$ cm^{-2} s^{-1}, leads to expect a few hundred events per day.

4.5 Conclusions

Even with the rather low luminosity of 10^{28} cm^{-2} s^{-1} there is room for important measurements on the $p\bar{p}$ system. The $p\bar{p}$ total cross-section can and should be measured. Elastic scattering could be measured up to $-t \approx 4$ GeV^2, well beyond the dip of pp scattering, using existing equipment (SFM). The accurate comparison of the shape of the angular distribution of pp and $p\bar{p}$ elastic scattering is perhaps the most interesting topic.

IMPACT PARAMETER REPRESENTATION

PROFILE FUNCTION $\Gamma(b) \propto i \int f(q)\, J_0(qb)\, b\, db$

INELASTIC OVERLAP FUNCTION $G_{in}(b) = 2\,Re\,\Gamma(b) - |\Gamma(b)|^2$

$G_{in}(b) \leq 1$

$G_{in}(b=0, s)$ $\bar{p}p$ pp

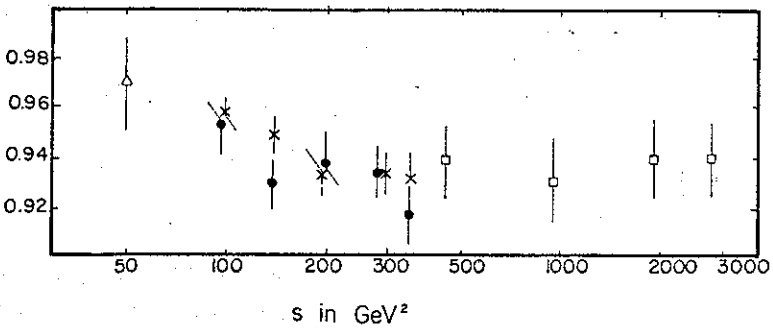

$\Gamma_{\bar{p}p}(b) - \Gamma_{pp}(b)$

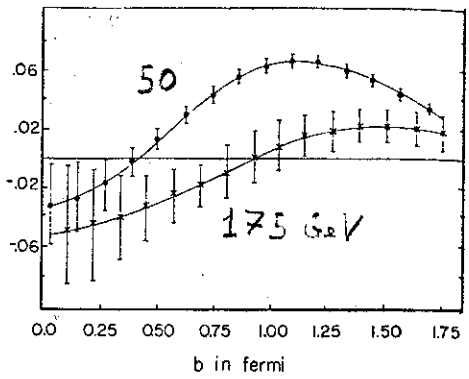

Energy dependence of $G_{in}(b)$ for pp

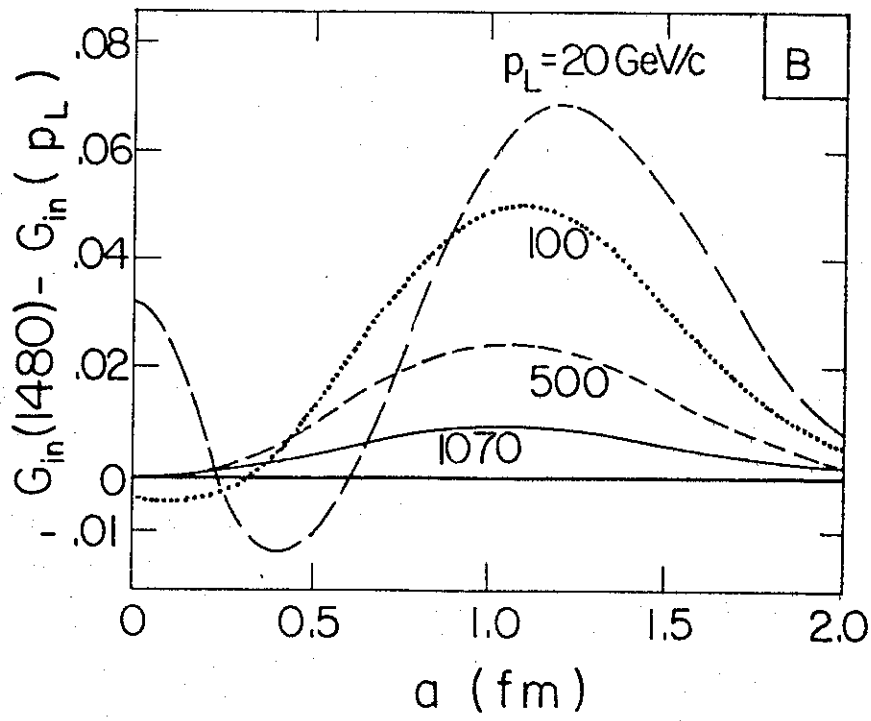

Figure 8

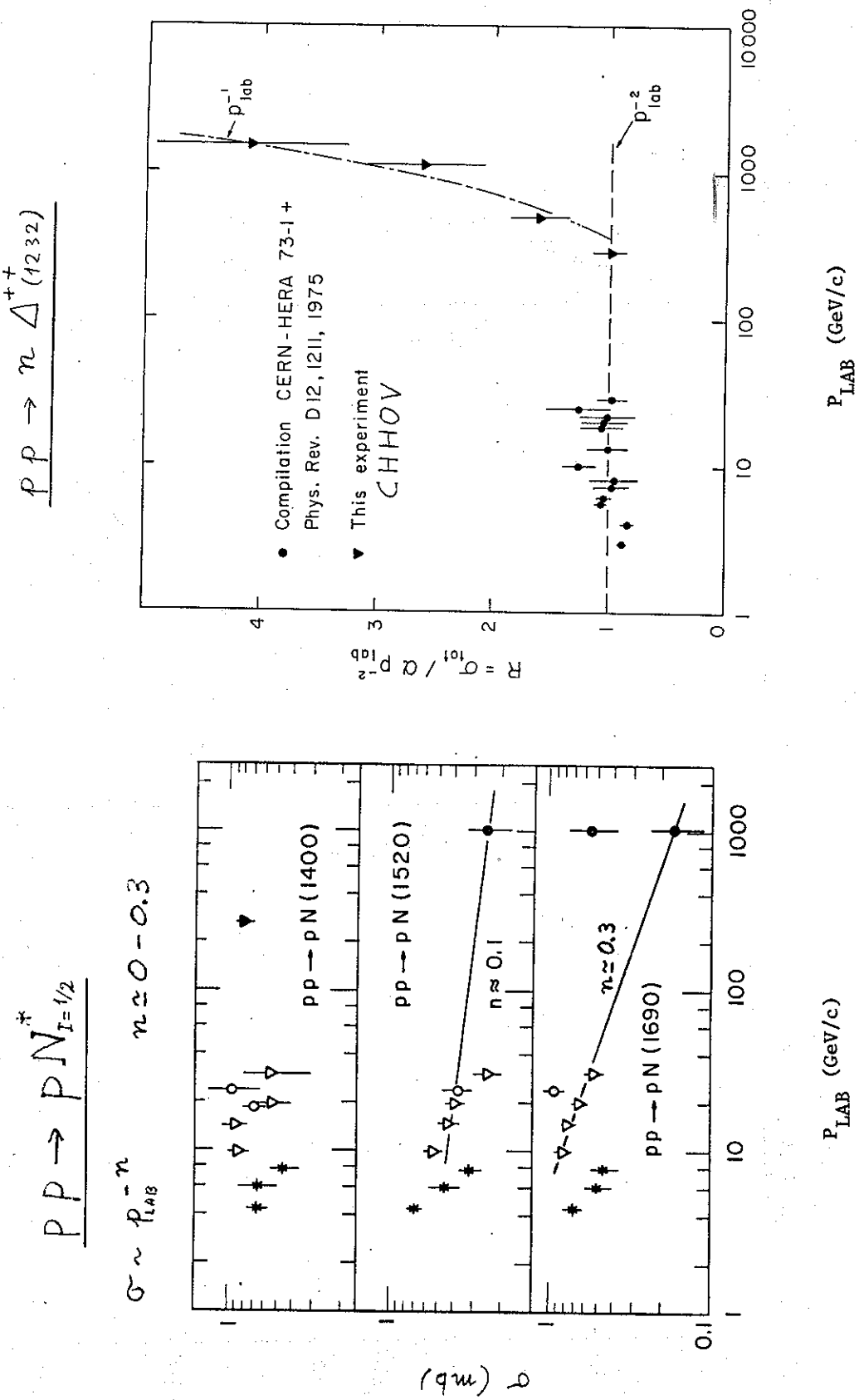
p p → n Δ++(1232)
R = σ101 / α p1lab-2
Compilation CERN-HERA 73-1 + Phys. Rev. D12, 1211, 1975
This experiment CHHOV
p1lab
p2lab
PLAB (GeV/c)
p p → p N*I=1/2
σ ~ p-nLAB
n ≈ 0 - 0.3
pp → pN(1400)
pp → pN(1520)
n ≈ 0.1
n ≈ 0.3
pp → pN(1690)
σ (mb)
PLAB (GeV/c)

Figure 9

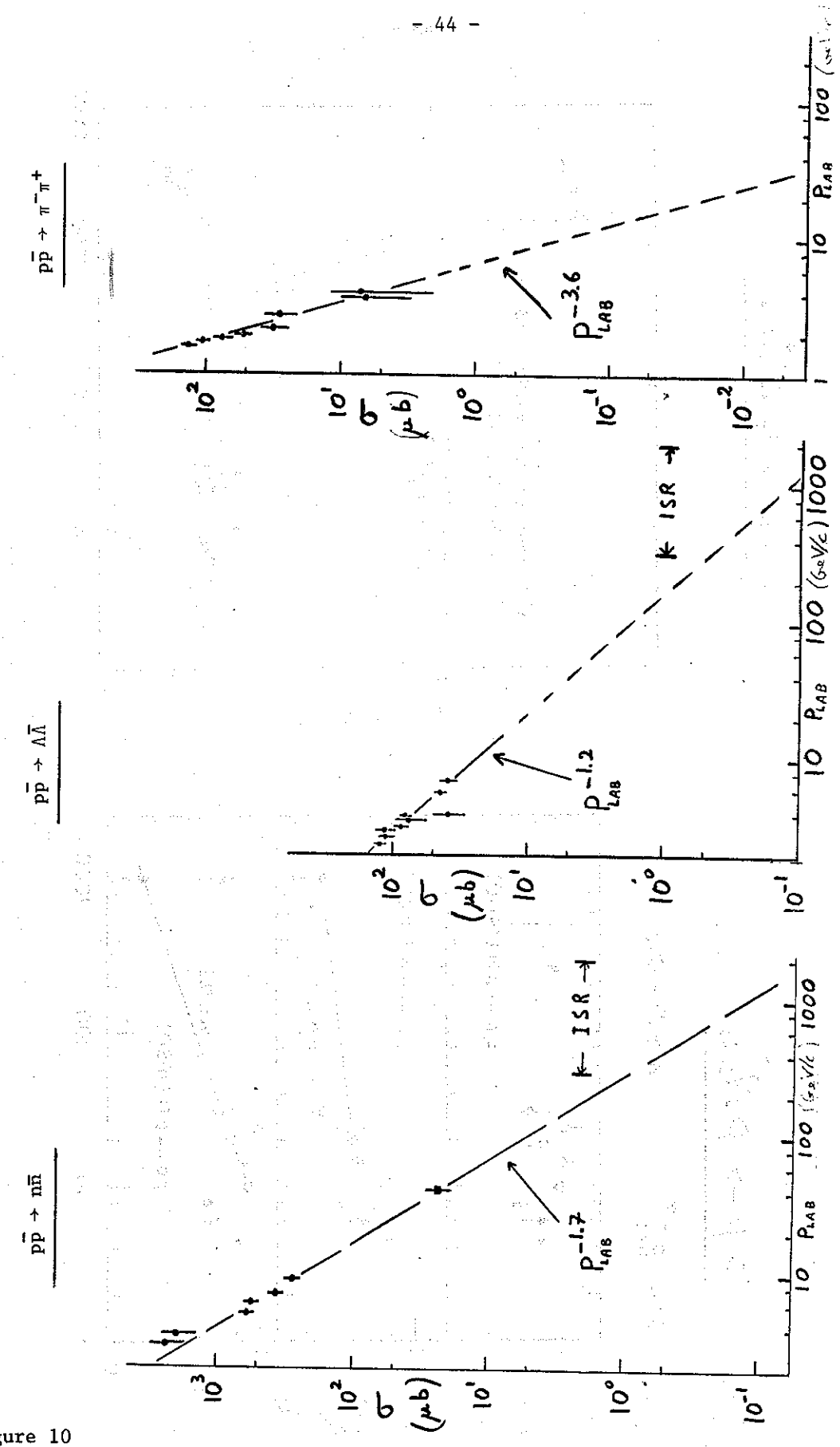
$\bar{p}p \to n\bar{n}$
$\bar{p}p \to \Lambda\bar{\Lambda}$
$\bar{p}p \to \pi^-\pi^+$
σ (μb)
P_{LAB} (GeV/c)
$P_{LAB}^{-1.7}$
$P_{LAB}^{-1.2}$
$P_{LAB}^{-3.6}$
← ISR →
← ISR →
10
100
1000

Figure 10

5. Large Cross-sections

This section follows the presentation by P.L. Braccini.

According to prevailing theoretical ideas, $p\bar{p}$ and pp induced reactions are expected to converge to a common behaviour with increasing energy. This is most generally expressed in terms of Pomeron dominance. The Pomeron now appears as a complicated object when analyzed in terms of J plane singularities. Nevertheless it remains even under charge conjugation with identical contributions to pp and $p\bar{p}$ reaction amplitudes.

5.1 Total cross-section

According to the Pomeranchuck theorem the ratio of the $p\bar{p}$ and pp total cross-sections is expected to become unity at asymptotic energies. According to prevailing theoretical models the $p\bar{p}$ and pp cross-sections are expected to quickly and monotonically become equal, their difference decreasing according to an inverse power (Regge) behaviour. This is compatible with present data (Fig. 1) and calculations of ρ, which meet so well the CERN-Rome data, take into account the rising pp cross-section but also its merging with the $p\bar{p}$ cross-section. As is well known, this implies that the $p\bar{p}$ total cross-section should rise over the ISR energy range (Fig. 1) a property which should be tested.

If one may check that the $p\bar{p}$ total cross-section reaches indeed the expected values, one may however not hope for a very precise measurement. This is illustrated by Figs. 2 and 3. Fig. 2 shows how total cross-section measurements at the ISR have improved with time. One has arrived at a precision which is well below the mb. Nevertheless, the difference between the $p\bar{p}$ and pp total cross-sections is also expected to be of that order of magnitude. This is shown explicitely in Fig. 3 which gives the extrapolated (Regge) behaviour expected to hold through the ISR energy range, together with the type of precision which could be reasonably hoped for. One should be able to reach the precision of present pp measurements. However, one cannot expect to go beyond.

One may then conclude that the aim is either to verify that the $p\bar{p}$ total cross-section behaves as predicted (Figs. 1 and 3), or to fish for a violent disagreement, which we have however no reason to anticipate from the present knowledge of ρ. If a check of the expected behaviour results one should say that nothing very precise could be expected as to how exactly the two cross-sections approach their common behaviour (Fig. 3).

5.2 Particle production

At low energy the annihilation channels, proper to $p\bar{p}$, provide important and specific effects. Their relative importance is expected to disappear as one goes to higher and higher energies. This can be first verified with mean multi-

plicities and multiplicity distributions. Experimentation of the ISR can be conducted in such a way that pp and $p\bar{p}$ induced reactions can be studied in turn with the same detector. Many systematic errors can thus be eliminated. Fig. 4 shows the mean charged multiplicities in pp and $p\bar{p}$ reactions, together with the (Werbensky) parameter $\langle n \rangle / D$.

At lower (Serpukhov and Fermilab) energies one knows that $p\bar{p}$ and pp induced reactions differ mainly through their rather low multiplicity components. This is shown in Fig. 5. This is readily associated with the annihilation cross-section and, as shown in Figs. 5 and 6, the corresponding contribution decreases rapidly with energy. It would however be very interesting to follow this trend through the ISR energy range. Similarities and differences in large multiplicity configurations, the analysis of which has recently made much progress (see ISR WORKSHOP/2-17), should also provide important information about hitherto poorly known production mechanisms.

The difference in topological cross-sections shifts to higher and higher multiplicities as it falls in magnitude. This is an expected behaviour for a contribution associated with annihilation. Yields in particle production in $p\bar{p}$ and pp reactions are expected to converge toward each other to the extent that their respective increases are associated with the contribution from the central region. This is shown in Fig. 7. Rapidity distributions still show important differences at Fermilab energy. Whereas proton fragmentation into π^- appears (as expected) to be the same whether bombarding the target proton with proton or antiproton, the low center of mass energy particles are still in excess in $p\bar{p}$ induced reactions. This again is most generally expected from the contribution of annihilation reactions (Fig. 8). One then expects however the difference in pion yields at wide angle to decrease with energy. As shown by Fig. 9, the ISR range is such that this difference should still be non-vanishingly small.

Conclusions are then similar to those arrived at in the case of the total cross-section. There are differences in yields which are expected to gradually disappear with energy. They should still be sizeable over the ISR energy range to allow for checks of the expected behaviour. One should find that yields converge as they are expected to (within errors) or meet an unexpected behaviour with large differential cross-section differences.

The energy behaviour of the annihilation cross-section can certainly be followed through the ISR range. Specific triggers could be implemented. This is a very interesting topic.

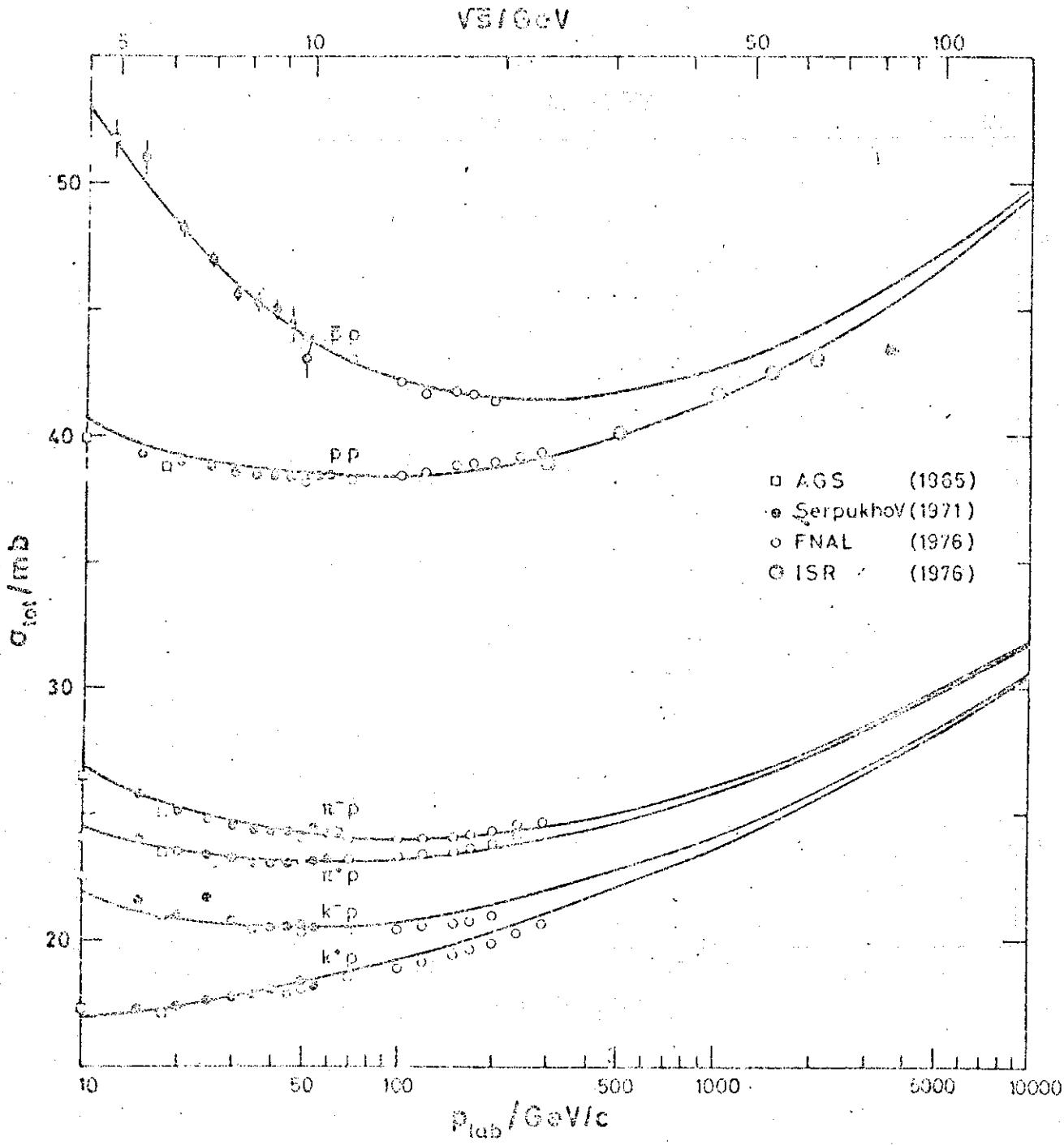

Figure 1 : The particle-particle and antiparticle - particle total cross-sections - with in particular measured and expected values for $p\bar{p}$

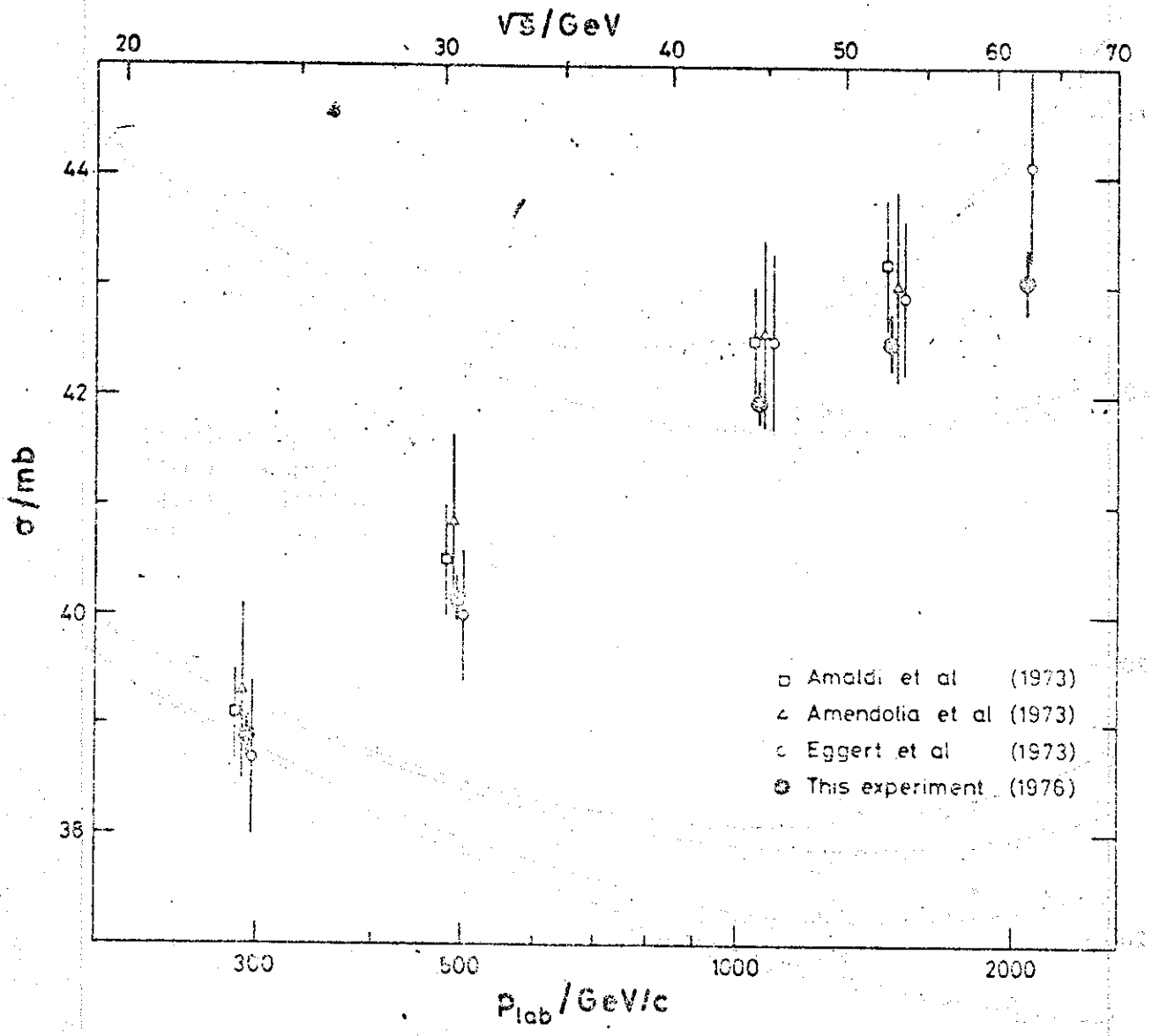

Figure 2 : Increase in precision for the measurement of the pp total cross-section at the ISR. What is achieved sets a limit for what to expect in $p\bar{p}$ measurements

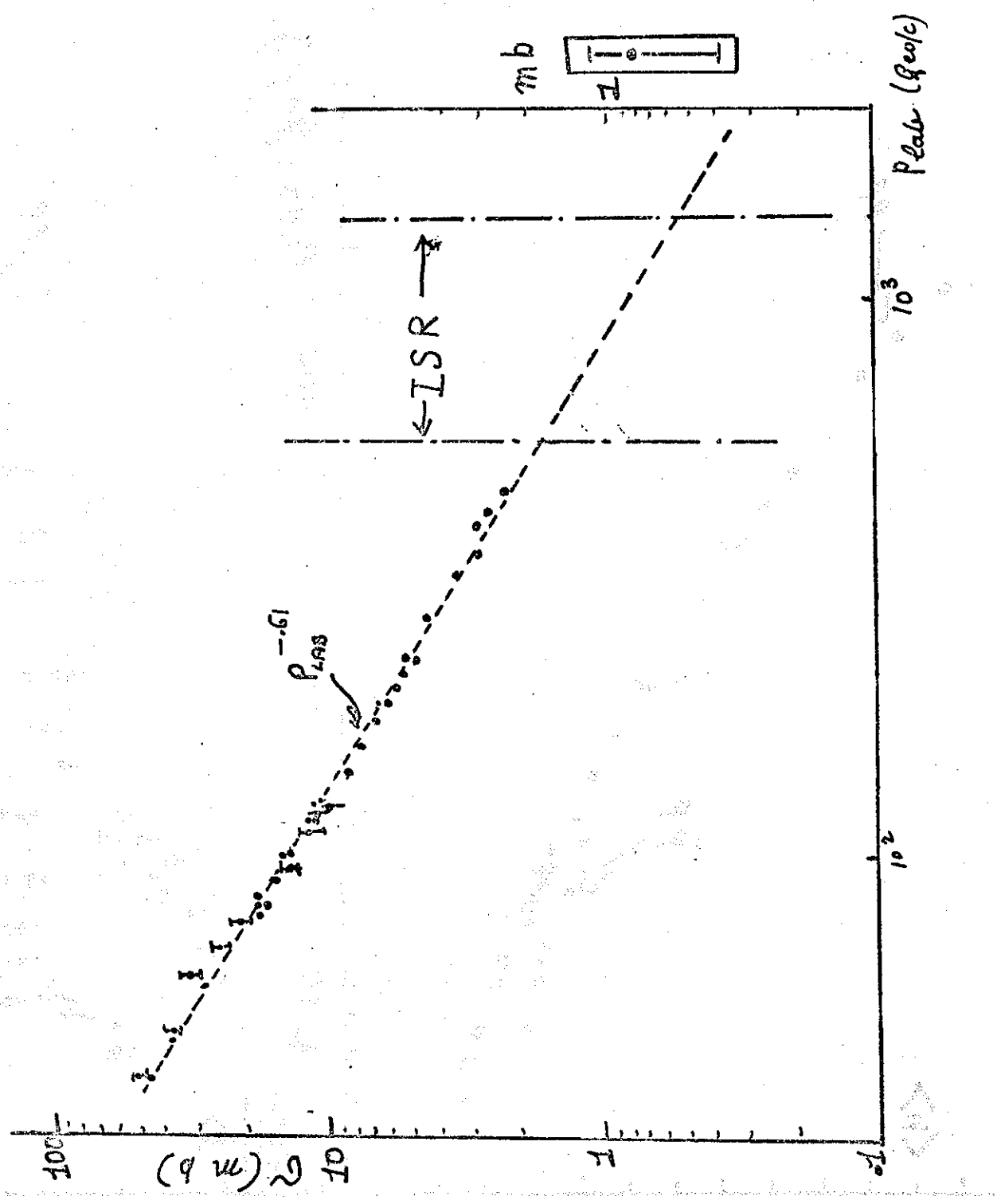

Figure 3 : The difference between the $p\bar{p}$ and pp total cross-section as compared to the precision which could be reached at the ISR

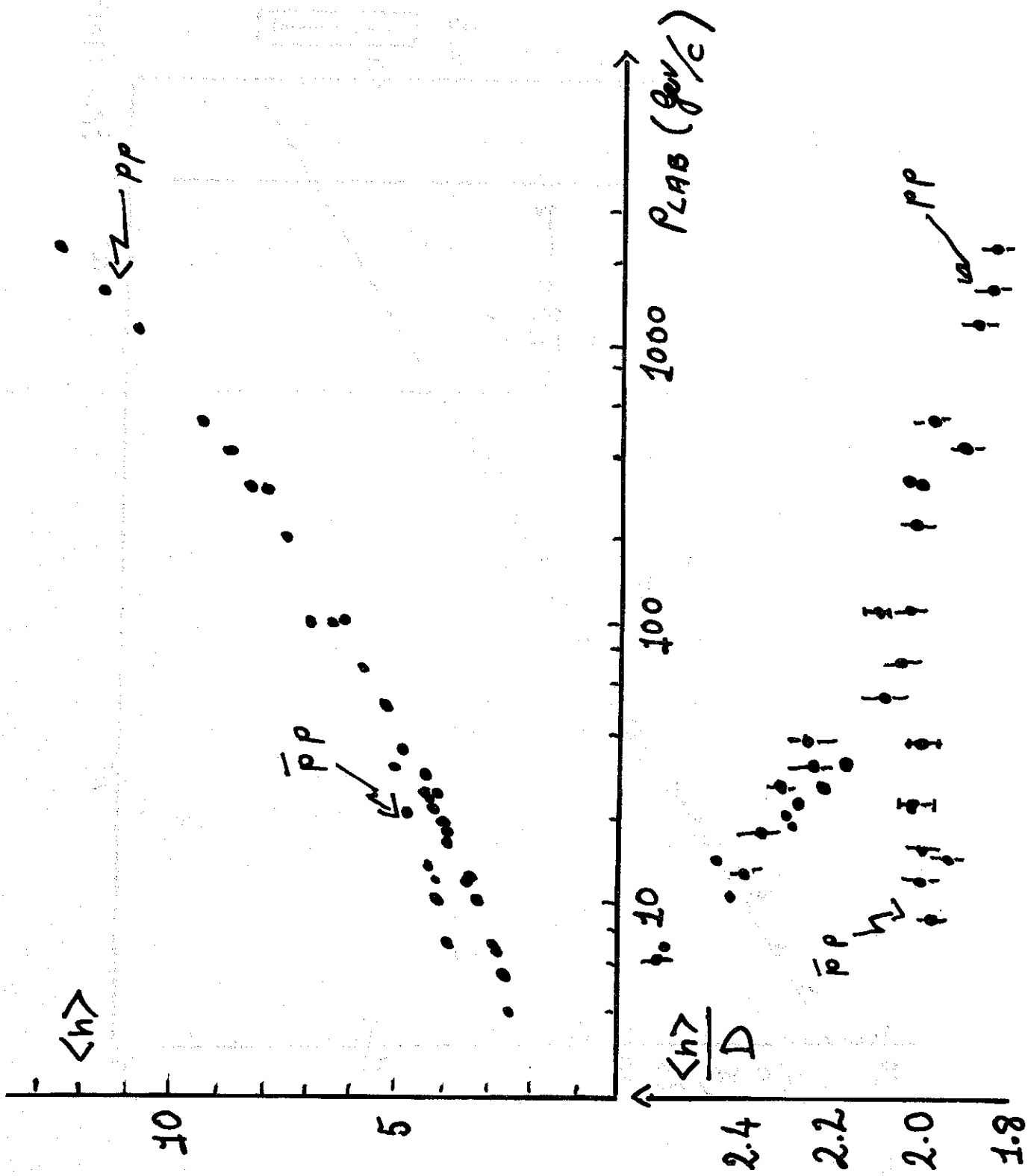

Figure 4 : Mean multiplicity and dispersion in $p\bar{p}$ and pp induced reactions

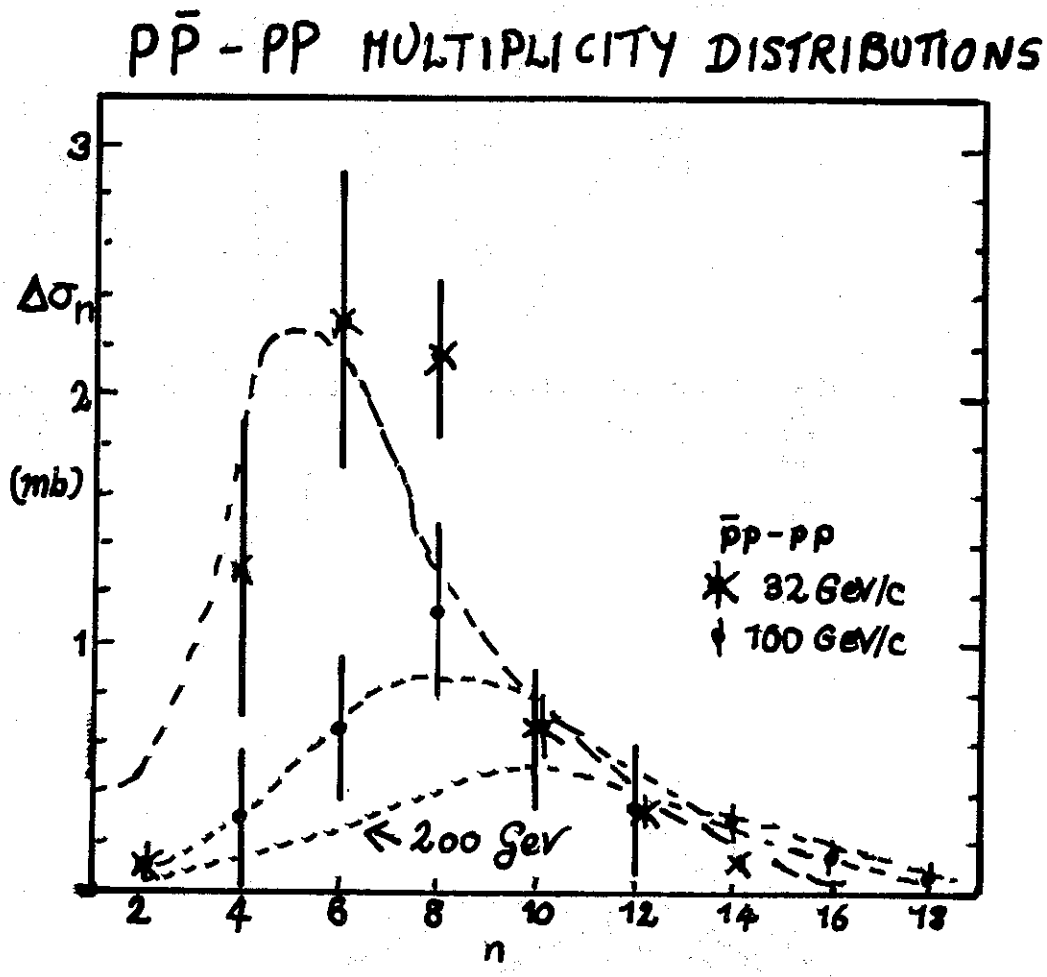

Figure 5 : Multiplicity distributions in pp and $p\bar{p}$ induced reactions at Serpukhov and Fermilab energies. Important differences are clearly associated with annihilations

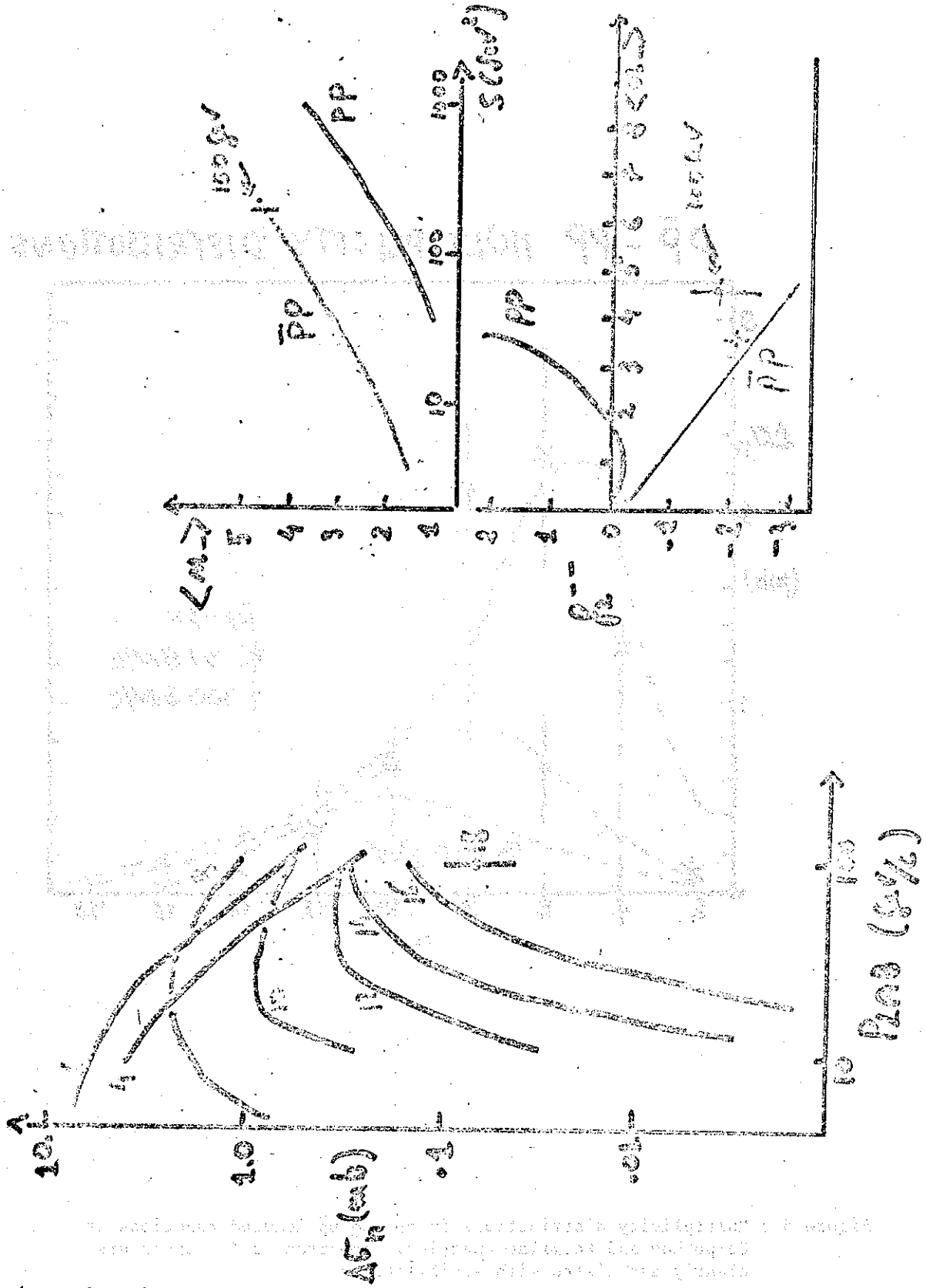

Figure 6 : Differences between topological cross-sections and different moments

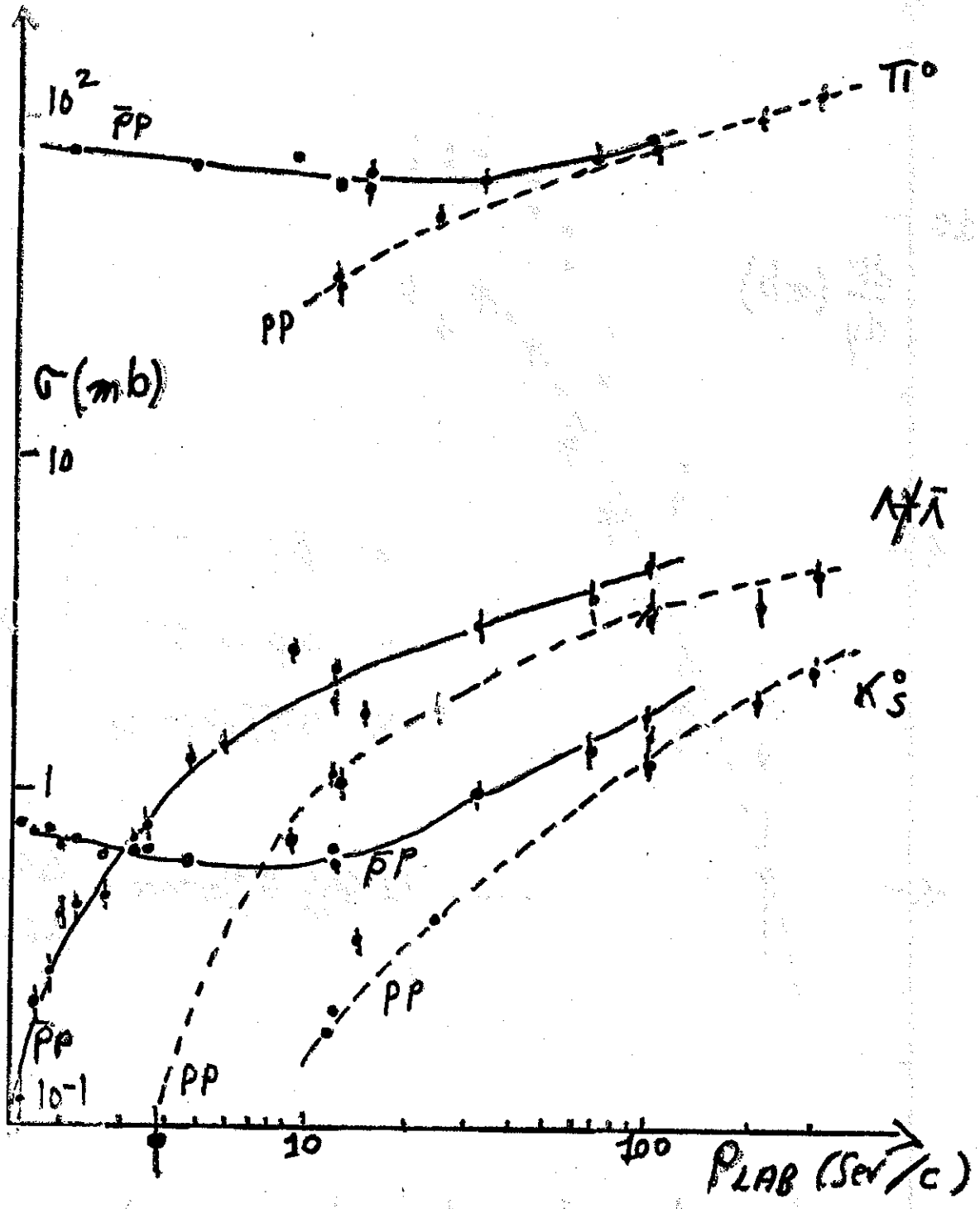

Figure 7 : Particle yields in pp and $p\bar{p}$ reactions

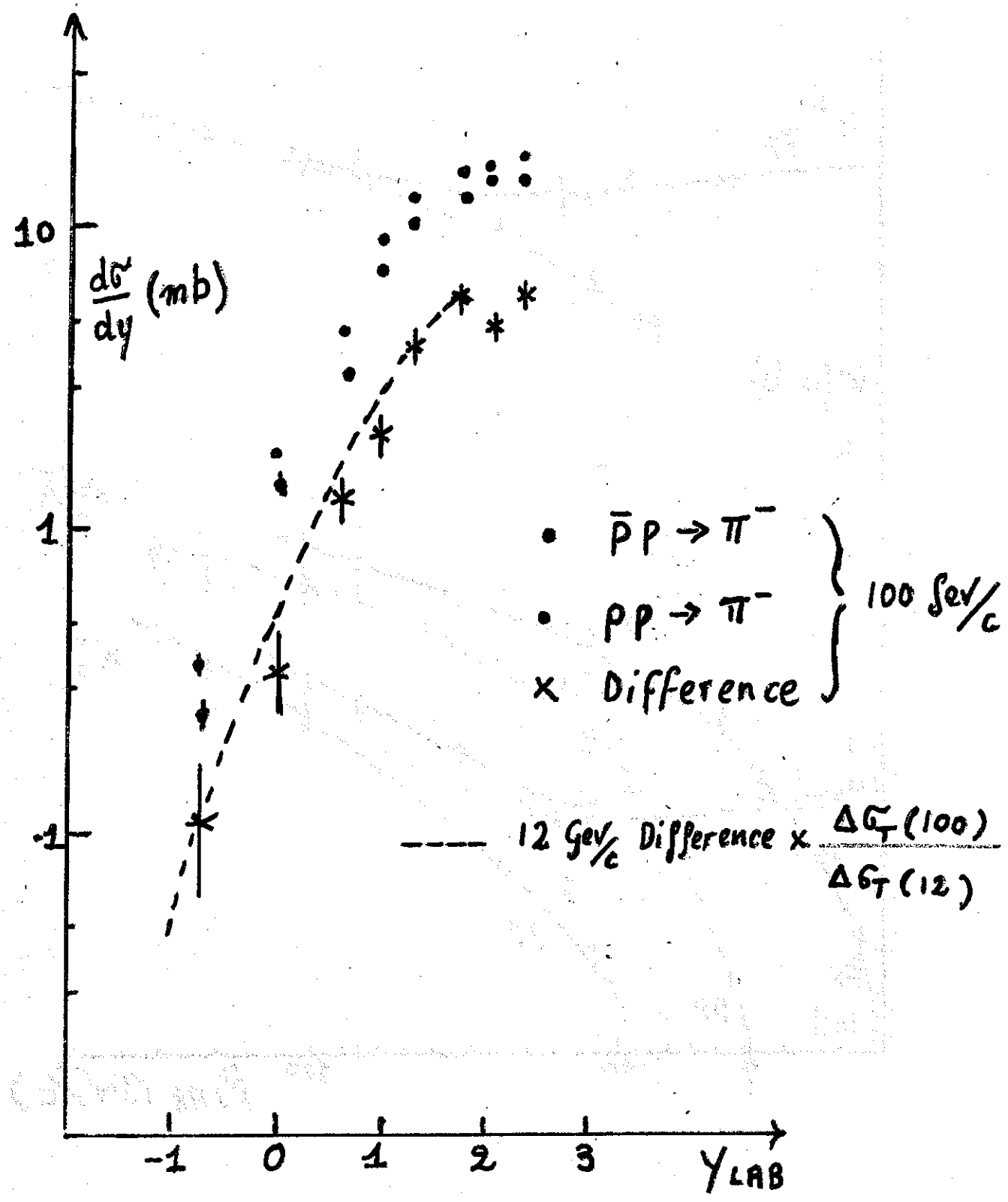

Figure 8 : Rapidity distributions for π^- in $p\bar{p}$ and pp induced reactions

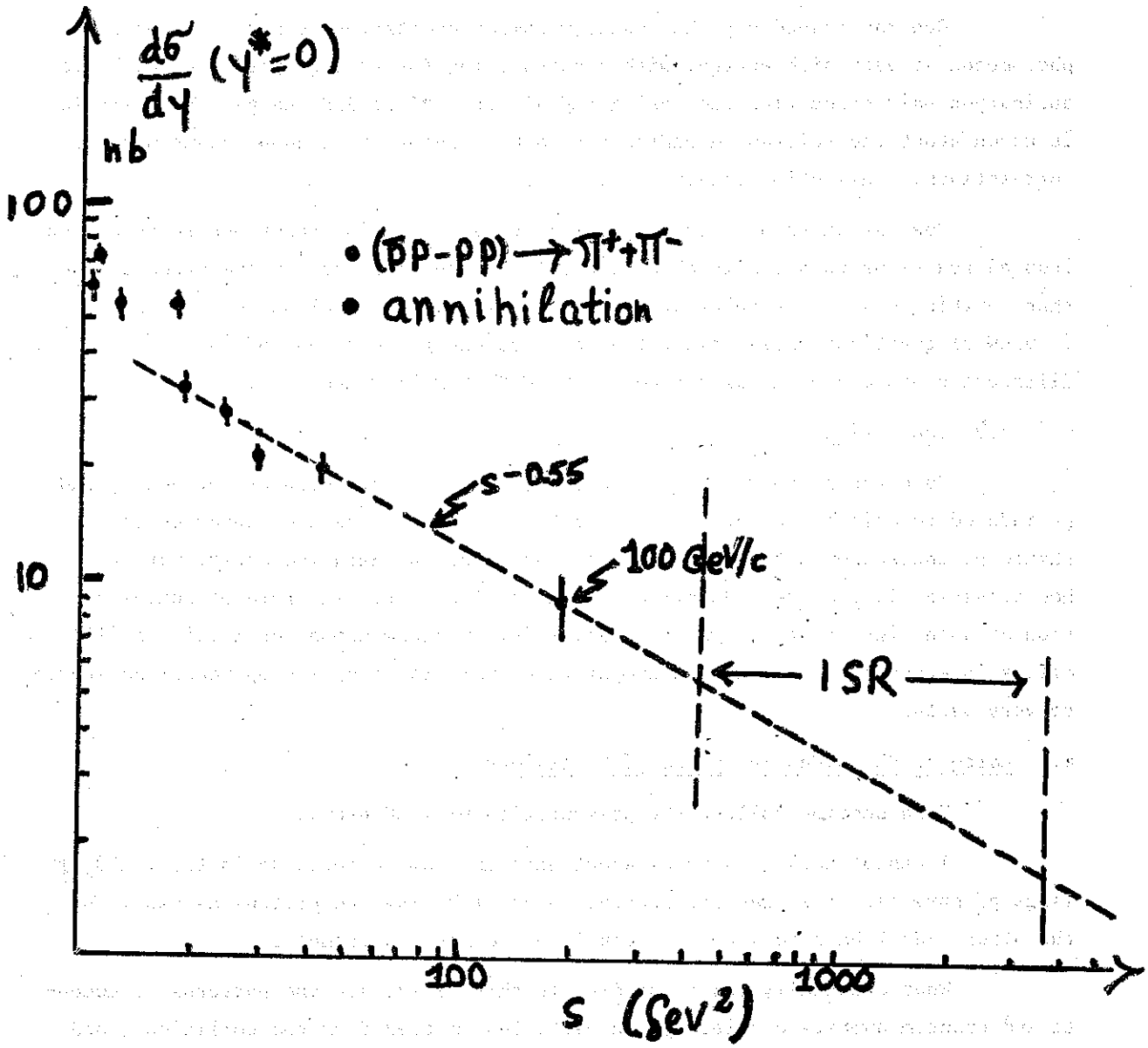

Figure 9 : Energy dependence of the difference in pion yield at wide angle in $p\bar{p}$ and pp reactions

Improvement in detectors (in particular the upgraded split field magnet) should allow for some quantum number identification over a wide angular range. One could also think of Λ and K distributions as determined by V^o's. Comparison between pp and $p\bar{p}$ induced reactions would then be very useful at analyzing quantum number correlations.

One may indeed say that quantum number excitation is a very important phenomenon at very high energy, with cross-section for strange particle and baryon-antibaryon pair production increasing rapidly from PS to SPS energy. Yet, little is known about the relevant dynamics for lack of information about quantum number correlations. This still deserves much effort.

One may think of comparing diffractive excitation reactions in pp and $p\bar{p}$ induced reactions to actually check the diffractive character of the process more than anything else. The relevant information would nevertheless be very useful in view of questions raised about the detailed energy behaviour of inelastic diffractive processes, as discussed in ISR WORKSHOP/2-10 and 2-17.

5.3 Conclusion

Even though no drastic effects are expected, differences between $p\bar{p}$ and pp induced reactions are large enough to be measured. Expected convergences should be checked even though one may not hope for any detailed determination of how cross-sections merge. Surprises could still be met. The rôle of annihilation at such high energy is worth an analysis. Quantum number excitation still offers interesting questions. A comparative analysis of $p\bar{p}$ and pp reactions should be very useful.

6. Large p_t Phenomena in pp and $p\bar{p}$ Collisions

This section follows the presentation by K. Hansen.

I cannot talk in general about what and how we could do in the field of large p_t physics, if we had antiprotons in one ISR ring and protons as usual in the other. So I have to keep to a couple of points and examples.

What eventually can be studied in this field, are the patterns of momenta and quantum numbers carried by the particles emitted from the collisions, and in particular as stressed by Donnachie in his presentation comparisons between these patterns from pp and $p\bar{p}$ collisions.

As well the single particle inclusive spectra as the correlations between two or more particles are potential sources for such studies.

What we are after are of course useful landmarks for the possible ideas about the relations between the high p_t phenomena and the quark beams brought in by the colliding hadrons. Discussions of the rôles of possible basic schemes like

$$qq \to qq$$
$$qM \to qM$$
$$q\bar{q} \to MM$$

may serve as examples.

From the field of single particle inclusive spectra we know already interesting quantities like particle ratios, as for example:

$$\frac{d\sigma\ (pp \to K^+ + X)}{d\sigma\ (pp \to K^- + X)}$$

$$\frac{d\sigma\ (pp \to \pi^+ + X)}{d\sigma\ (pp \to \pi^- + X)}$$

as functions of $x_t = p_t/p_{beam}$ at a fixed cms angle, and so-called beam ratios like

$$\frac{d\sigma\ (pp \to \pi^o + X)}{d\sigma\ (\pi^- p \to \pi^o + X)}$$

as functions of x_t and collision energies at a fixed cms angle.

I refer here to the review of this field given by Professor Donnachie.

It is clear that beam ratios like for example

$$\frac{d\sigma\ (p\bar{p} \to K^- + X)}{d\sigma\ (pp \to K^- + X)}$$

will be useful pointers for the ideas trying to connect the large p_t phenomena with the quark beams and their collisions.

Note that all the interesting, useful information from these quantities occur at $x_t \gtrsim 0.1$.

As for the correlations between the quantum numbers carried by the particles in high p_t events I will use our own (BFS) preliminary results from R 413 experiment as an example of the type of phenomena.

In R 413 (British-French-Scandinavian Collaboration) we study pp collisions ($\sqrt{s}$ = 53 GeV), in which a high-p_t charged hadron is emitted at 90° in cms. The triggering high p_t hadron is measured and identified in the momentum range 0.5 - 4.5 GeV/c by use of the old British-Scandinavian spectrometer, WAS (Wide Angle Spectrometer), and the associated particles are studied with the Split Field Magnet and its detector, giving electric charge and momentum vector for about 2/3 of the associated charged particles.

Here we have learned that the general, global features of the events associated to a given type ($\pi^{\pm}$, $K^{\pm}$, $p^{\pm}$) of trigger particle does not depend very much on the trigger type. Over most of phase-space there are only small ($\sim$10%) differences between the particle densities associated to different trigger types, but in specific high-p_t regions we do see some differences, when one type of trigger particle is exchanged with another one.

A particular interesting effect is pointing out K^- and $\bar{p}$ as something special among the six types of trigger particles.

In Figure 1 is shown a comparison between the average number per event of observed particles recoiling on the away side in the region

transverse momentum : $p_t > 1$ GeV/c
rapidity : $|y| < 1$
azimuthal angle : $|\phi| < 30^o$
($\phi = 0^o$ in the beam-trigger plane)

for each of the six trigger types as a function of the trigger momentum. The above-mentioned close similarity between the observed associated particle densities is seen together with an indication of a deviation from the common pattern in the case of K^- and $\bar{p}$ triggers with trigger momentum above 3 GeV/c.

If one goes a step further out in p_t of these recoil particles, to $p_t > 1.5$ GeV/c, we see the picture, shown in Figure 2. It is seen that for $p_{Trig} > 3$ GeV/c the recoil to K^- and $\bar{p}$ contains few negative particles compared with the recoil to π^- triggers, while the content of positive particles is approximately the same.

The p_t dependence of the observations is shown in Figure 3, where it is seen that p_t of the recoil particle must be larger than about 1.5 GeV/c before the effect shows up clearly.

The observed effect is summarized in Figure 4, which for trigger momenta $3 < p_{Trig} < 4.5$ GeV/c gives the average number per event of observed positive and negative particles on the away side in the region

$|y| < 1$
$p_t > 1.5$ GeV/c

for the six different types of trigger particles. The ratio between the observed densities of associated positive particles and associated negative particles is close to 1 except for K^- amd $\bar{p}$ triggers, for which the ratio is close to 2.

The y dependence of the observed associated particle densities is shown in Figure 5.

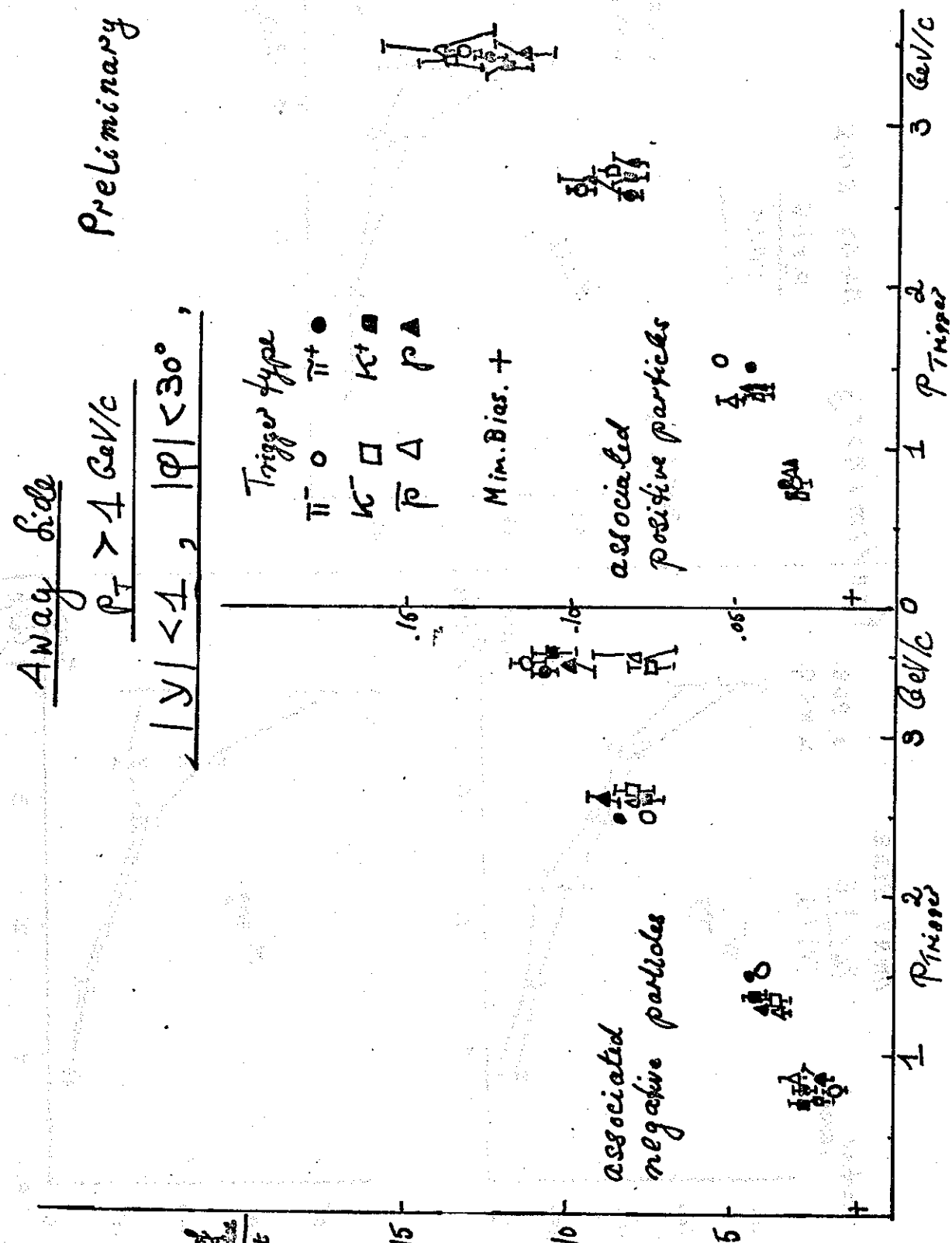
Away side
$p_T > 1$ GeV/c
$|y| < 1$, $|\phi| < 30°$,
Preliminary
Trigger type
π^- o π^+ ●
K^- □ K^+ ■
$\bar{p}$ Δ p ▲
Min. Bias. +
associated
positive particles
associated
negative particles
mu of particles / event
0.15
0.10
.05
.10
.05
0
1
2
3 GeV/c
$p_{Trigger}$
$p_{Trigger}$

Figure 1

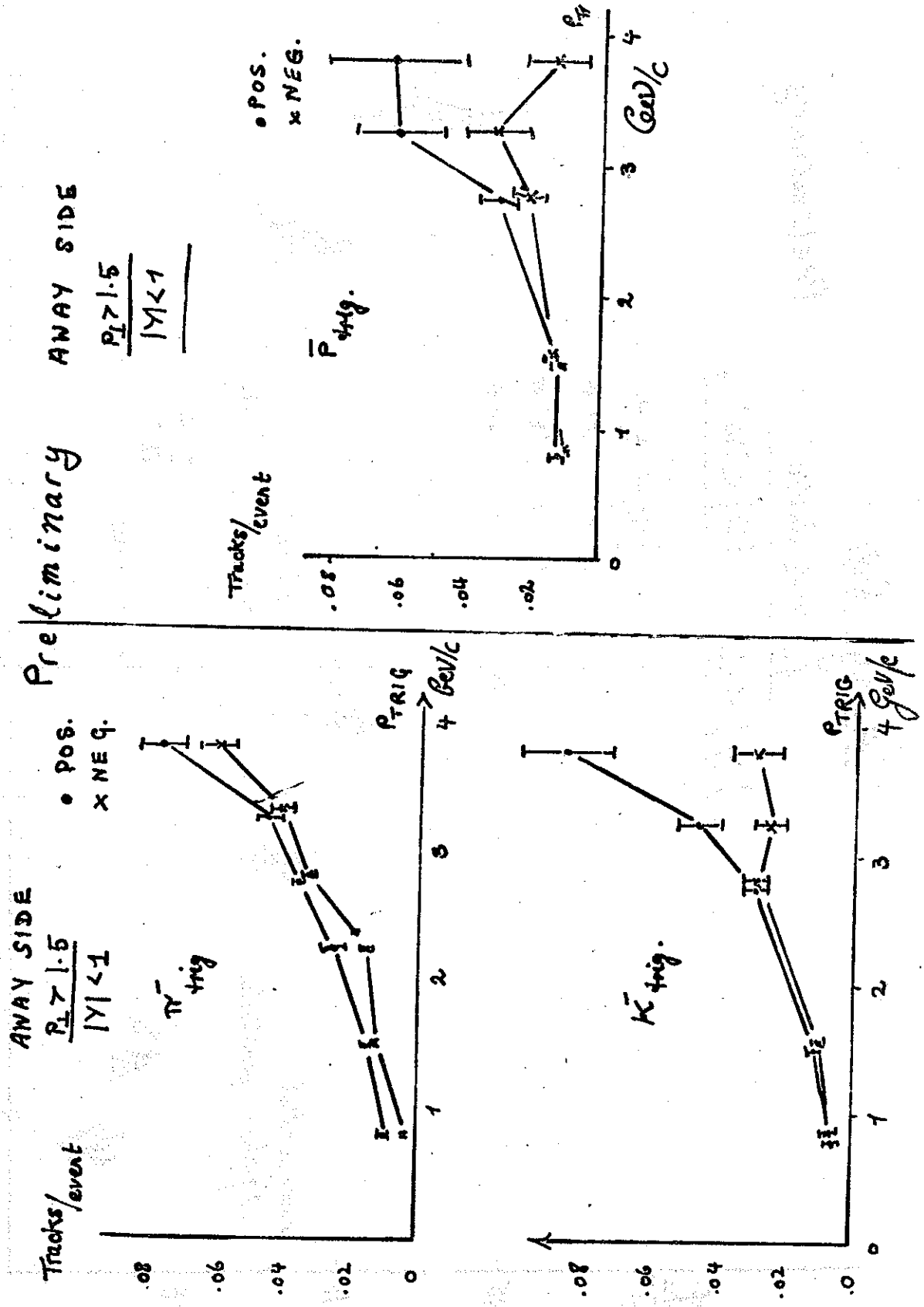
Preliminary
AWAY SIDE
$p_T > 1.5$
$|y| < 1$
• POS.
× NEG.
$\bar{p}_{trig.}$
Tracks/event
p_{TRIG}
GeV/c
AWAY SIDE
$p_T > 1.5$
$|y| < 1$
• POS.
× NEG.
$\pi^-_{trig.}$
$K^-_{trig.}$
Tracks/event
p_{TRIG}
GeV/c

Figure 2

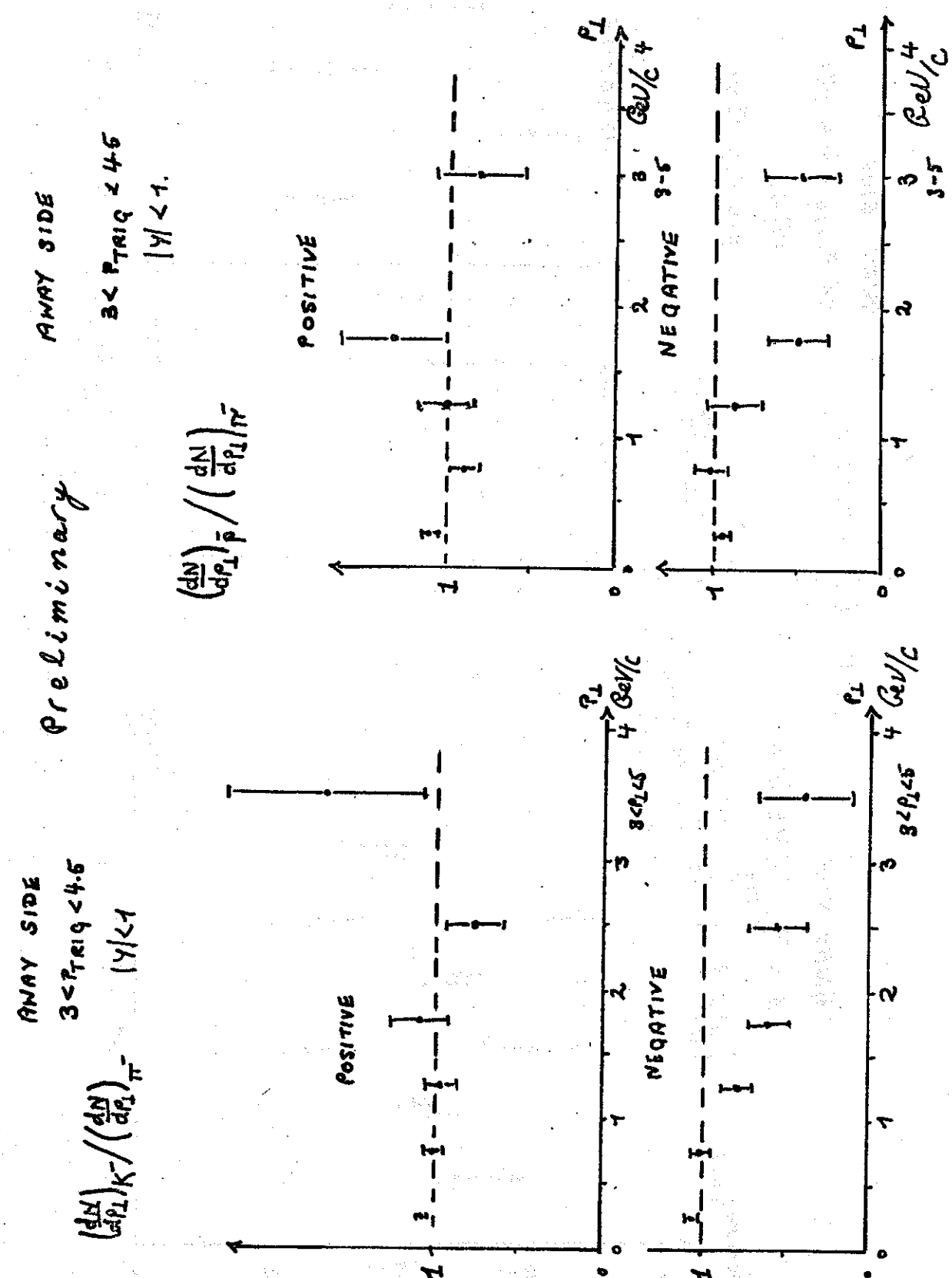
AWAY SIDE
3< P_TRIG < 4.5
|y| < 1.
Preliminary
(dN/dP_T)_p̄ / (dN/dP_T)_π⁻
POSITIVE
NEGATIVE
P_T GeV/c
3-5 GeV/c
AWAY SIDE
3< P_TRIG < 4.5
|y| < 1
(dN/dP_T)_K⁻ / (dN/dP_T)_π⁻
POSITIVE
NEGATIVE
3 < P_T < 4.5 GeV/c

Figure 3

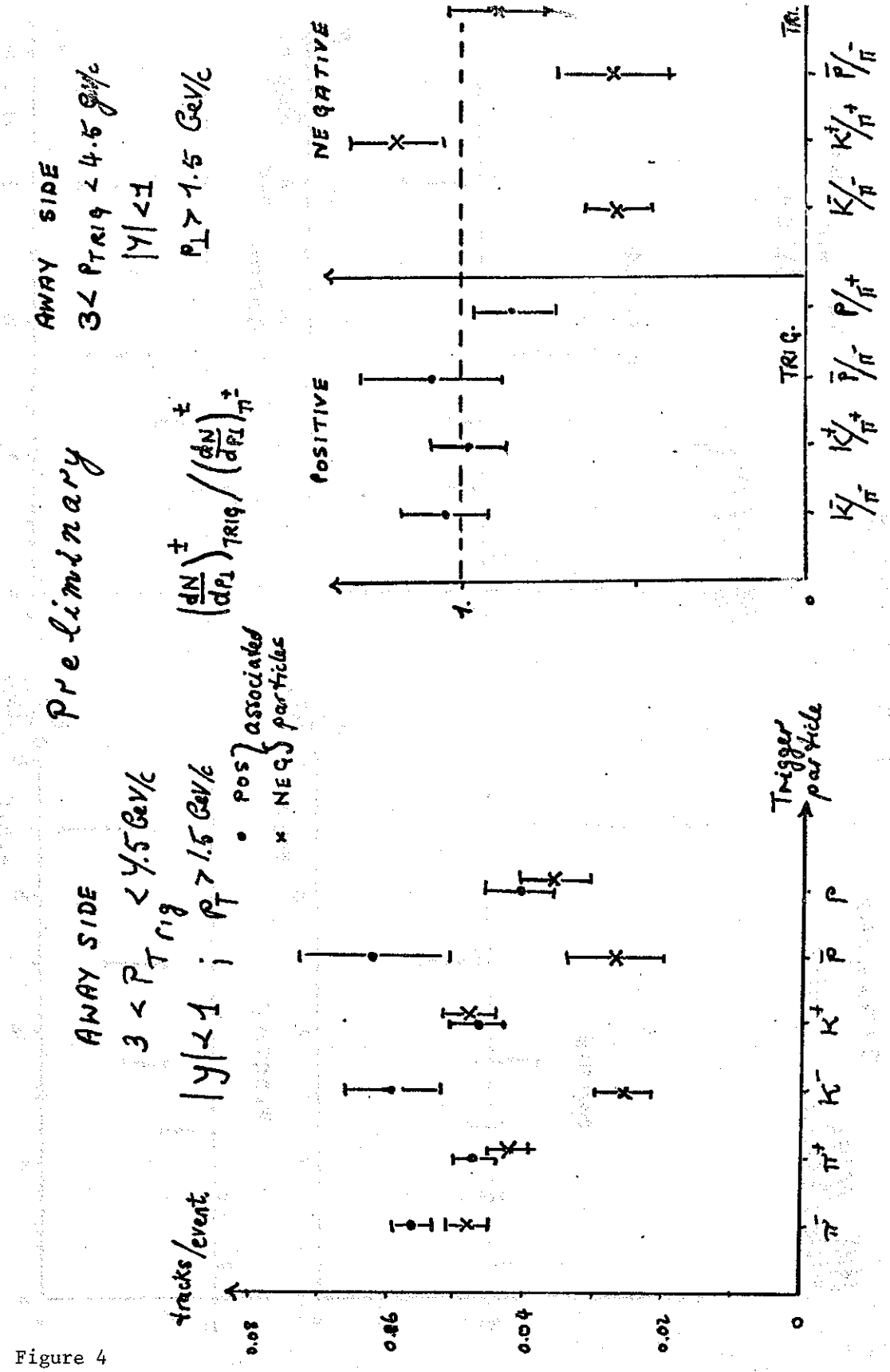
Preliminary
AWAY SIDE
3< PTRIG <4.5 GeV/c
|Y|<1
PL > 1.5 GeV/c
(dN/dPL)± TRIG / (dN/dPL)± π±
NEGATIVE
POSITIVE
1.
0
TRIG.
K⁻/π⁻ K⁺/π⁺ P̄/π⁻ P/π⁺ K⁻/π⁻ K⁺/π⁺ P̄/π⁻
AWAY SIDE
3 < PT TRIG < 4.5 GeV/c
|Y|<1 ; PT > 1.5 GeV/c
• POS } associated
× NEG } particles
tracks/event
0.08
0.06
0.04
0.02
0
Trigger particle
π⁻ π⁺ K⁻ K⁺ P̄ P

Figure 4

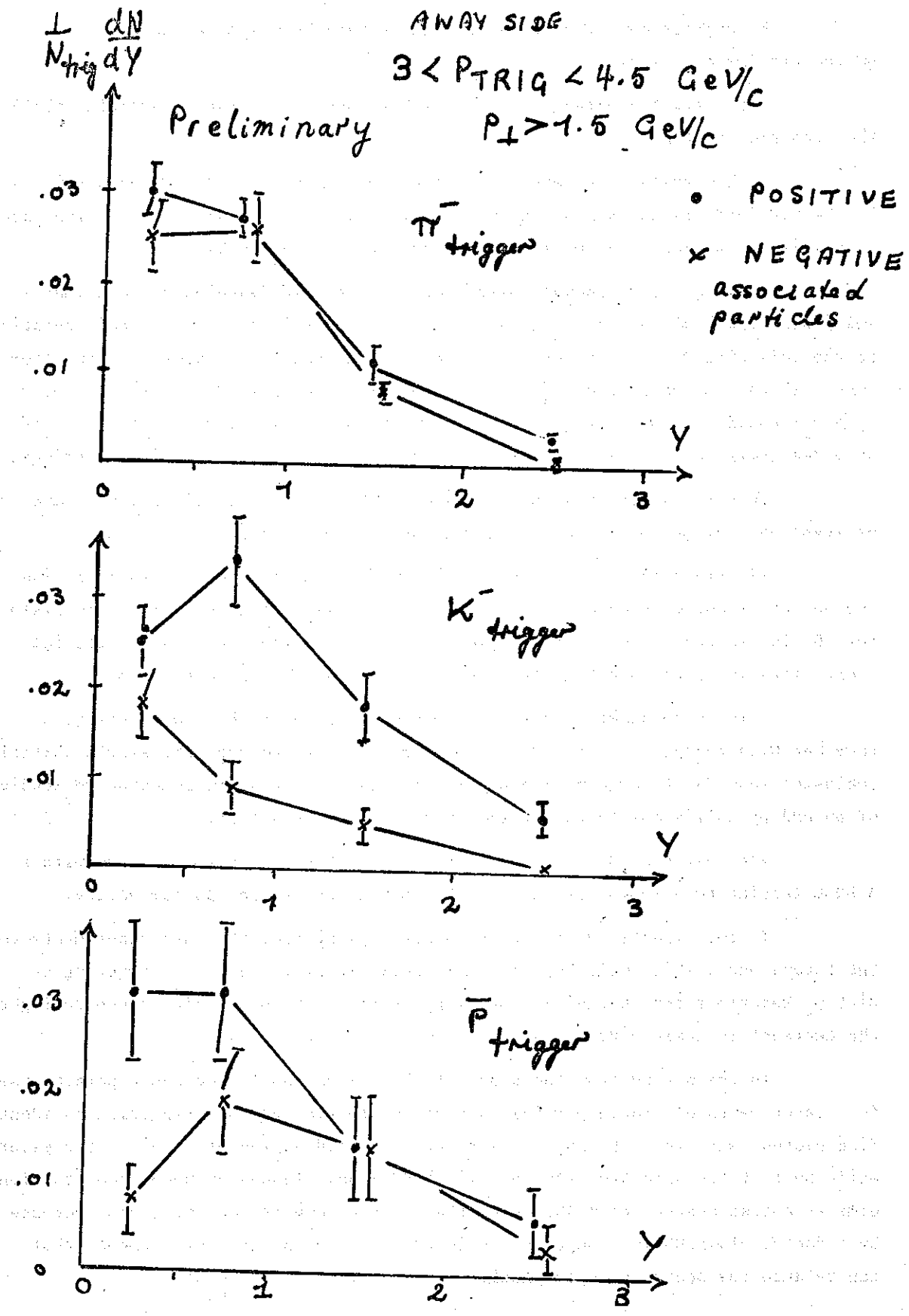
AWAY SIDE
3 < PTRIG < 4.5 GeV/c
P⊥ > 1.5 GeV/c
Preliminary
• POSITIVE
× NEGATIVE associated particles
1/Ntrig dN/dY
π⁻ trigger
K⁻ trigger
P̄ trigger
.03
.02
.01
0
1
2
3
Y

Figure 5

No correction for acceptance effects have been applied to any of the quoted preliminary results.

Note that the effect is only visible, when the trigger particle fulfills the condition $x_t \gtrsim 0.1$.

Such correlations between the quantum numbers of the leading particles in the two jets are not contained in a straight forward picture built on the idea of collisions between the two incoming beams of valence quarks.

Looking for a general reason for the observed features we note that K^- and $\bar{p}$ are distinguished among the six trigger types ($\pi^\pm$, $K^\pm$, $p^\pm$) in their relation to the colliding protons by not having any valence quark in common with the protons. Therefore the particular behaviour of events triggered by a K^- or $\bar{p}$ with $x_t \gtrsim 0.1$ could well be a consequence of a mechanism, which requires a collision of a sea quark and a valence quark in order to give the required K^- or $\bar{p}$ trigger.

This is different in $p\bar{p}$ collisions where all six particle types have at least one valence quark in common with one of the incoming particles.

If this difference in "quark sharing" really is the main thing behind the observations, we should therefore not see the similar effects in $p\bar{p}$ collisions. (At 90^o in cms charge conjugation symmetry will of course give rise to special constraints in $p\bar{p}$ so investigations must be carried out also away from 90^o.)

This is an example of a quantum number correlation effect, which, together with the particle ratios and beam ratios derived from the single particle inclusive spectra, to my mind indicates sufficient interest in comparative studies of pp and $p\bar{p}$ collisions to make them worth while, if possible.

Are they possible, if we can have one ISR proton beam replaced with a $\bar{p}$ beam leading to a luminosity 10^{-3} - 10^{-2} times the present pp luminosity?

In two directions we can see a development from the past experiments to the future ones, which will lead to an increase in efficiency of triggering on high p_t reactions and in analysis power by factors, which are big enough to fight the decrease in luminosity.

In the period from the start of the ISR and up to now the apparatus used for measurements of single particle inclusive spectra and for triggering on identified hadrons with large p_t have had acceptance solid angles of a few to ten mster, while some of the apparatus (for example R 807) now planned or under construction aims at corresponding solid angles of the order of one steradian. This increase by a factor of $\sim$ 100 in acceptance solid angle is one of the developments that can balance the decrease in luminosity.

Another way of increasing the efficiency of triggering on high p_t reactions is the use of a calorimeter trigger as now under way for example in R 807. From the recent calorimeter experiments at FNAL (E 260) and from "charged particle calorimetry" experiments performed by analysis of the Minimum Bias samples studied in R 413 we learn that a "jet-trigger" is more frequent by a large factor ($\sim$100) than a single particle trigger in the p_t range 3-5 GeV/c. So also here is a useful factor available to balance the low luminosity.

So my conclusion is that it is both possible and promising to study high p_t phenomena from $p\bar{p}$ collisions in the ISR, even if the luminosity is as low as 10^{-3}- 10^{-2} times the present one.

Finally I would like to stress that while the region $x_t \gtrsim 0.1$, where the interesting high p_t quantum number effects show up, is accessible for experimental investigations for $p\bar{p}$ collisions at ISR energies, where it is populated by particles with $p_t \gtrsim 3$ GeV/c, it will be extremely difficult to investigate in general for $p\bar{p}$ collisions in the SPS with 2 x 270 GeV/c. But of course the 2 x 270 GeV $p\bar{p}$ in SPS are promising in other respects, as for example a Z^o search.

7. Lepton Production in $p\bar{p}$ at the ISR

This section follows the presentation by F. Vannucci.

It has been proposed to fill one ring of the ISR with an antiproton beam coming from the cooling facility envisaged at CERN. The energies reachable in such a machine would be comparable to the ones achieved now i.e. up to 31 GeV per beam, but the luminosity would be of the order of 10^{29} cm^{-2} s^{-1} while the present pp machine easily reaches a luminosity higher by 2 orders of magnitude.

We study here the interest of such a new machine in the domain of lepton physics.

7.1 Leptons as Probe for New Phenomena

Most if not all of the experiments now running at the ISR are searching for leptons, either in pairs or produced at high transverse momentum. This fashion seems to have been triggered by the discoveries of the past few years and everybody now hopes to see a bump in a dilepton mass distribution or an anomaly in some correlation preferably involving leptons. Historical reasons are not the only ones to explain the present interest in lepton searches, and I see two good reasons to continue lepton hunting in the present and in the near future:

a) new phenomena appearing at one time, always show up with very small cross-sections (otherwise a previous generation of detectors would have detected them). The search for "new physics" in hadronic reactions is then extremely difficult, because of the overwhelming background due to the "old physics". Experimentally

leptons have the advantage of a characteristic signature, and are relatively easy to extract out of an hadronic ocean. Both muons and electrons allow a trigger on rare events and it is tempting to link rare events with rare phenomena.

- Theorists then give arguments to look for leptons : Z^o, W, new $q\bar{q}$ states are predicted to have important branching ratios into purely leptonic decays. Besides this lepton pair production is a priori one of the best tests to study nucleon structure. Lepton pairs are produced, at least for some fraction, through the so-called Drell-Yan mechanism, and testing the predictions of this model gives a good way of observing effects related to particle constituents.

7.2 Advantages of $p\bar{p}$ over pp Reactions

The Drell-Yan process and some of the models trying to explain the new particle production involve an annihilation at the level of the hadron constituents.

Very naively we can picture this process as follows : a quark of momentum $x_1 \frac{\sqrt{s}}{2}$ annihilates with an antiquark of momentum $-x_2 \frac{\sqrt{s}}{2}$ to produce a virtual photon of mass $M^2 = x_1 x_2 s$. In pp reactions we have to have annihilation between one valence quark and a sea antiquark. On the contrary in $p\bar{p}$ the annihilation can take place between a valence quark and a valence antiquark from the $\bar{p}$. In that case $x_2 \sim x_1 \sim \frac{1}{3}$ (?) and one can reach $\frac{M^2}{s}$ fairly high (·1 ?). In the pp case $x_2 \ll x_1$ and $\frac{M^2}{s}$ is expected to be much smaller.

Thus $p\bar{p}$ allows regions of $\frac{M^2}{s}$ much higher than pp, and the difference between $p\bar{p}$ and pp will better reveal itself at large $\frac{M^2}{s}$, that is at high dilepton masses, for similar initial energies.

An interesting experimental result has its place here : the omega spectrometer group at the SPS studied production of J/ψ initiated by beams of p and $\bar{p}$. They found the following ratio between cross-sections :

$$\sigma (p) / \sigma (\bar{p}) = 0.16 \pm 0.08$$

In that experiment $\frac{M^2}{s} \gtrsim 0.1$. This result seems to support the annihilation scheme in the formation of new particles, and at the same time emphasizes the interest of $\bar{p}$ for such productions.

Now for the production of the dilepton continuum, Drell and Yan have suggested that this production is dominated by the elementary process of $q\bar{q}$ annihilation into a time like γ which then converts into a dilepton

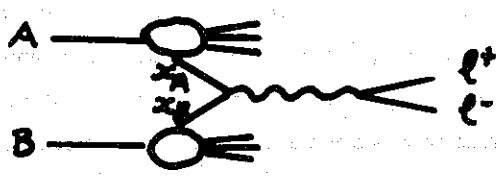

The Drell-Yan mechanism predicts a scaling behaviour :

$$m^3 \frac{d^2\sigma}{dmdx}\Big|_{x = 0} = F\left(\frac{m^2}{s}\right)$$

where $F\left(\frac{m^2}{s}\right) = \sum_k e_k^2 \, q_k^A(x_+) \, q_k^B(x_-)$

$q_k^A(x)$ is the fractional momentum distribution of flavor k in particle A. The sum runs over all quarks and antiquarks. $x \pm = \exp(\pm y) \frac{m}{\sqrt{s}}$. $\sqrt{s}$ is the center of mass energy, y and m the rapidity and mass of the lepton pair.

In pp the main uncertainty comes from the parametrization of the antiquark distribution in the sea. Figure 1 shows various fits to the Fermilab dilepton results with various antiquark distributions. In $p\bar{p}$ the annihilation mainly takes place among valence quarks, and this process is much easier to interpret. By comparing pp and $p\bar{p}$ data, taken in similar conditions, one can estimate the sea quark contribution and in $p\bar{p}$ extract in an easier way the valence quark distribution. This test of comparing pp with $p\bar{p}$ is best done in a region where this difference is large. Again the region of interest is $\frac{M^2}{s} \gtrsim 0{\cdot}1$. This is clear on Figure 1 where a Drell-Yan calculation for $p\bar{p}$ is shown. Practically the machine which is proposed would give beams comparable in energy to the energies obtainable now at the ISR but with a real limitation coming from a luminosity roughly 2 orders of magnitude lower than presently achieved for pp collisions.

We saw that we can expect a gain in cross-section for the production of new particles by using $p\bar{p}$ instead of pp. This gain is at most a factor $\sim$ 100 for $\frac{M^2}{s} \gtrsim {\cdot}1$ and thus just compensates the loss in luminosity for masses around 20 GeV/c^2 if the machine runs at $\sqrt{s}$ up to 60 GeV. For smaller masses the whole luminosity loss directly affects the counting rates. At high masses the cross-sections become very low anyhow and it is fair to say that if no new state is found in pp with the present detectors it is very improbable that $p\bar{p}$ would help us make any discoveries.

On the other hand the study of the continuum must bring some new information about hadron structure. Quark distributions in the hadrons presently come from deep inelastic scattering experiments. The comparison between dilepton mass distributions is most revealing where the difference is largest : at high $\frac{M^2}{s}$. The present ISR produce masses above 15 GeV/c^2 at measurable rates, and so this comparison study seems a realistic enterprise. Actually the ISR are very well suited for this study. Because of the scaling low predicted by the Drell-Yan formula, the cross-section for a fixed mass increases when s increases but the gain levels off. A higher energy machine would have more difficulty to reach the same $\frac{M^2}{s}$ and it seems that the ISR have here a "creneau" to take advantage of. Obviously cross-sections in the region of interest stay extremely small and this entails the use of large acceptance detectors.

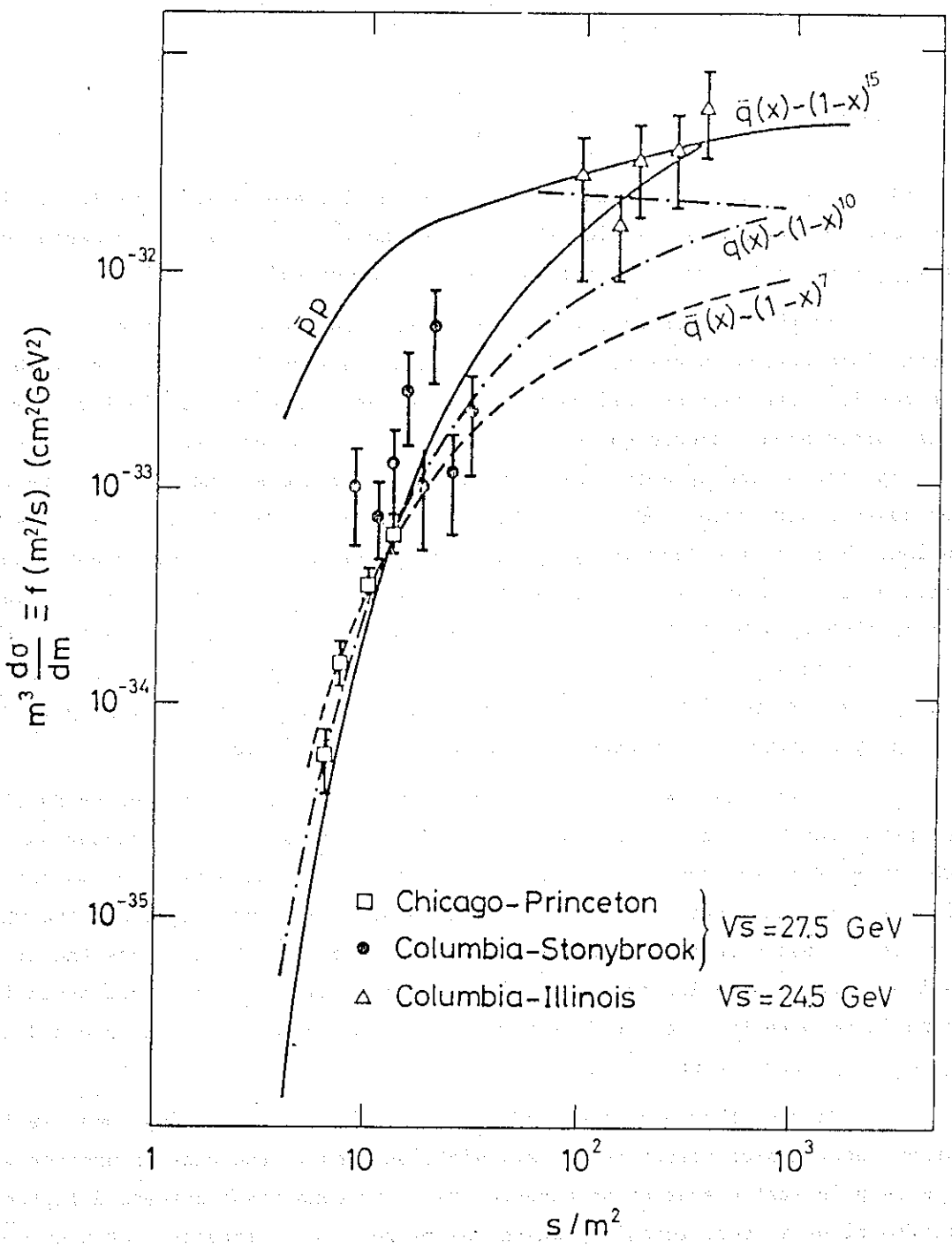
$m^3 \frac{d\sigma}{dm} \equiv f\,(m^2/s)$ (cm²GeV²)
10^{-32}
10^{-33}
10^{-34}
10^{-35}
1
10
10^2
10^3
s / m²
$\bar{q}(x)-(1-x)^{15}$
$\bar{q}(x)-(1-x)^{10}$
$\bar{q}(x)-(1-x)^{7}$
$\bar{p}p$
Chicago-Princeton
Columbia-Stonybrook
Columbia-Illinois
$\sqrt{s}$ = 27.5 GeV
$\sqrt{s}$ = 24.5 GeV

Figure 1

7.3 Lepton detection

a) Muons

Experimentally muons are what is left over when hadrons have been filtered out by shielding. There are two main sorts of background when one is dealing with muon detection : hadron punch through and π or K decays before the absorber. A good muon filter has many collision lengths starting as close as possible to the production vertex. But matter also means multiple scattering and the momentum resolution is relatively poor if the measurement takes place inside or after the magnet.

As an example the present R 209 detector is shown in Figure 2. It is composed of large slabs of magnetized iron which give a minimum of 15 collision lengths on the path of the particles, starting 50 cm from the interaction. Because of its relative simplicity the detector covers about 60% of 4π total angle but the mass resolution for dimuon pairs is not very good : $\frac{\Delta m}{m} \sim 10\%$.

b) Electrons

There are several ways of detecting electrons. One can use gas Cerenkov counters, one can detect the development of the electromagnetic shower in lead-scintillator sandwiches, lead glass counters or liquid argon calorimeter. The rejection against hadrons can be very good if one uses simultaneously different kinds of detectors and checks the compatibility between shower energy measurement and momentum measurement in a spectrometer. Little matter seen by the tracks,, allows very good resolution.

As an example experiment R 806, pictured in Figure 3, uses transition radiation detection and liquid argon calorimetry. The relative complexity of the apparatus and also the necessity of using various cuts to select the wanted signal, limit the acceptance to a few per cent of 4π but the resolution $\Delta m/m \lesssim .10/\sqrt{m}$ can become very good at high masses.

Muon and electron detections represent two very different problems to solve:

Muon detection works well in a hot environment, thus allowing high luminosity and giving high sensitivity. Large acceptance detectors can be built with hadron rejection quite adequate at high momenta. But the limitation remains the poor resolution, due to multiple scattering in the absorber.

On the other hand electron detection allows better hadron rejection, much better resolution but the luminosity cannot be too high.

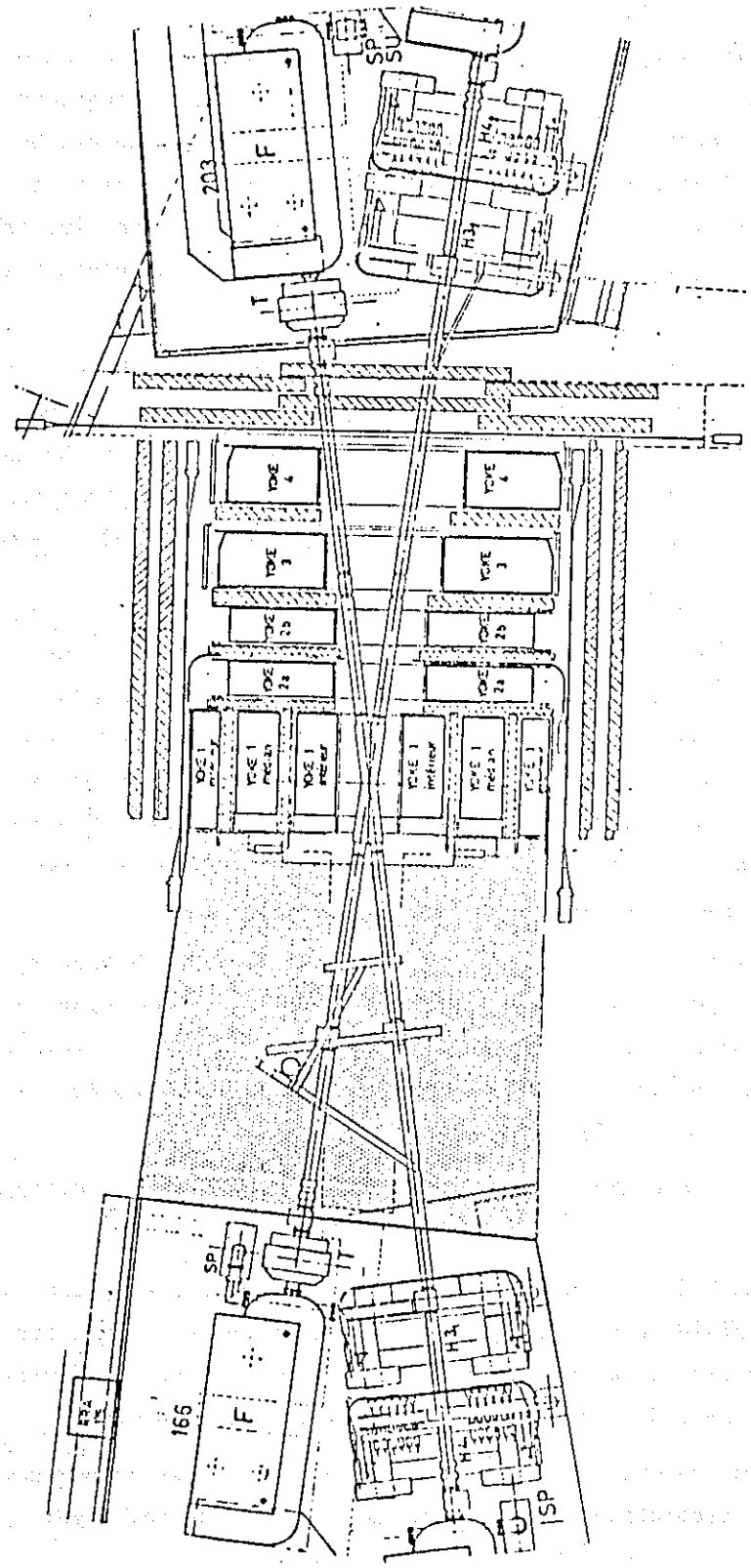

Figure 2

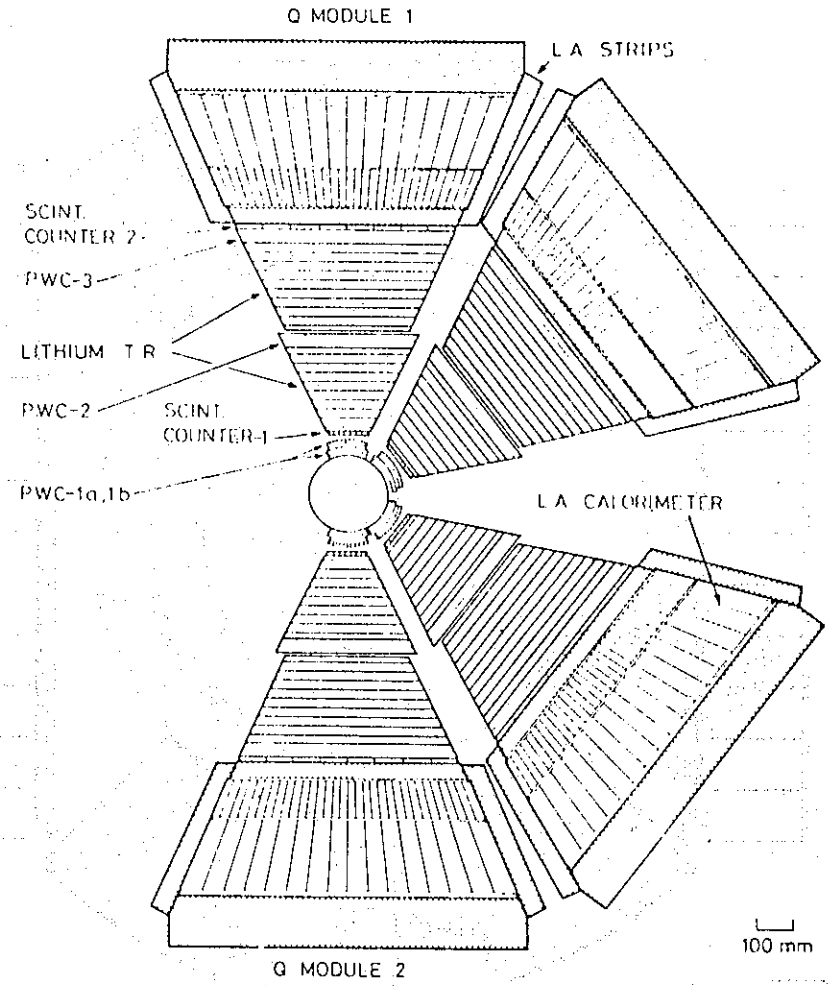
Q MODULE 1
L A STRIPS
SCINT.
COUNTER 2
PWC-3
LITHIUM T R
PWC-2
SCINT.
COUNTER-1
PWC-1a,1b
L A CALORIMETER
100 mm
Q MODULE 2

Figure 3

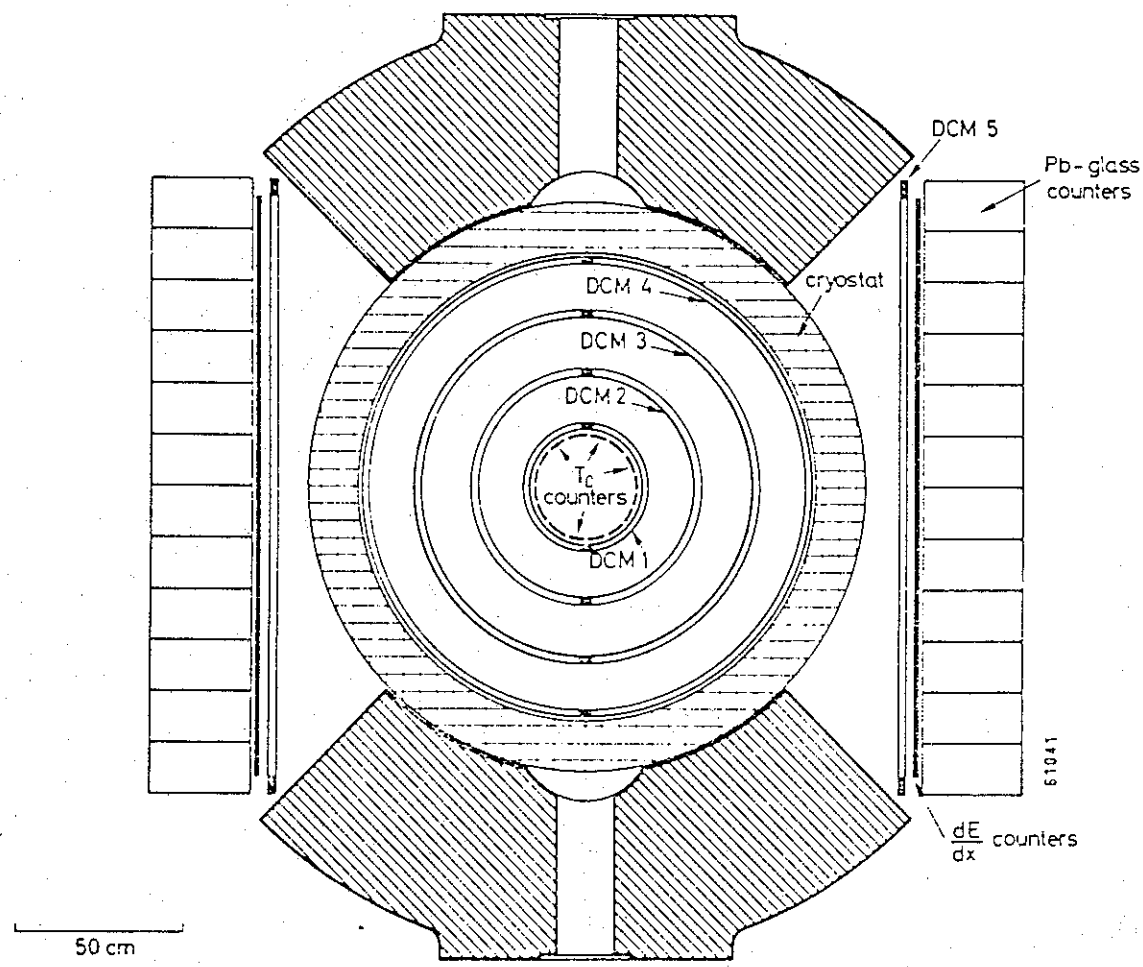
DCM 5
Pb-glass counters
cryostat
DCM 4
DCM 3
DCM 2
T_C counters
DCM 1
$\frac{dE}{dx}$ counters
50 cm
61041

Figure 4

The ISR filled with $\bar{p}$ in one ring will be a low luminosity machine. One does not expect more than 10^4 charged tracks produced per second. This is fully tolerable for good electron detection and the advantage of using muons instead is lost. It seems then reasonable to concentrate on electron physics in this proposed machine, in order to get the best possible precision. If quantity cannot be achieved in any case because of the machine limitation it is certainly wise to try to achieve quality of measurement. This does not exclude some muon detection in conjunction with the electron detection, to study μ, e correlations.

Among the set-ups now running at the ISR, R 108 seems to be the closest to match the above requirements. The detector is shown in Figure 4. Its essential characteristic is the use of a superconducting solenoidal magnet. The solid angle covered for charged tracks is around 60% while lead-glass counters cover 10% of 4π for electron identification. The resolution is $\Delta p/P \approx .07/\sqrt{E}$ in the lead glass array. The weak point of this detector is the relatively small solid angle where electron detection is possible. If no new apparatus specially conceived for $p\bar{p}$ reactions is to be built, it seems that an improved R 108 would be a well suited detector. Improvements could go into two directions: larger solid angle coverage for e identification possibly by detecting electrons inside the magnet, and muon identification outside the magnet, using the return yoke as filter.

Still lepton physics basically is a physics of high luminosity. The machine now envisaged will probably give some interesting results, but the low luminosity will remain its greatest limitation.

8. The Ortho-ISR Scheme for Protonium and Baryonium Spectroscopy in Flight

This section follows the presentation by U. Gastaldi.

8.1 Introduction

Precise and complete experiments on the $p\bar{p}$ system at low energy can provide, in addition to a better understanding of the $p\bar{p}$ interactions, a complementary approach to high energy $p\bar{p}$ experiments for the study of the structure and of the dynamics of the proton and of the antiproton in terms of their internal more elementary constituents. In effect the annihilation, which is distinctive of $p\bar{p}$ interactions when compared to pp interactions, has a cross-section increasing roughly as the inverse of the relative velocity v of the two particles and dominates the other channels at low v: the low kinetic energy region and $p\bar{p}$ bound states are then the most natural places to study this process which is likely to provide a lot of information about the intimate core of the (anti)proton. Moreover the $p\bar{p}$ system has access to a wide variety of J^{PC} states which are expected to form around the two nucleons mass threshold and can be described in terms of the elementary $\bar{p}$ and p constituents. Finally strong interaction effects perturb

the energy levels of the $p\bar{p}$ atom (protonium) and this effect can be used as a sensitive probe of a basic theory of strong interactions.

Paradodoxically the most accurate study of the $p\bar{p}$ system at low energy in the mass centre can be performed if the $p\bar{p}$ system moves at high velocity in the lab[1,2]: this leads naturally to the ortho-ISR scheme and, as a consequence, the storage rings represent the most powerful tool to study both very high and very low energy phenomena. We shall confine to experiments at and below the two nucleons mass threshold where the application of an ortho-ISR scheme to ISR would be optimal.

The following topics will be discussed sequentially:

a) the principle of the measurements,
b) the ortho-ISR scheme,
c) the physics potentialities.

The present experimental and theoretical situations have been recently reviewed by L. Montanet[3] and F. Myhrer[4]. Further new experimental results have been presented at the Budapest[5] and Zurich[6] conferences.

8.2 The Principle of the Measurements

$p\bar{p}$ atoms (protonium) are formed in vacuum in excited n, ℓ levels. The x-ray transitions between $p\bar{p}$ atomic states are detected in coincidence with the γ's emitted in transitions to baryonium levels and/or the annihilation products (Figure 1).

The x-ray signes the quantum numbers (n, ℓ, sometime J) of the initial atomic state formed before the γ transition and/or the annihilation occurred.

The width of the x-ray line provides the total annihilation rate $\Gamma_{n,\ell}$ of the initial state. The shift and width of the atomic levels and the intensity of the x-ray transitions give direct information about the effect of $p\bar{p}$ strong interactions on the $p\bar{p}$ coulomb system.

To perform these measurements two requirements have to be satisfied:

a) form in excited states as many $p\bar{p}$ atoms as possible,
b) get the best energy resolution and the lowest threshold for the detection of x-rays, so as to see as many atomic transitions as possible.

The ortho-ISR method allows to satisfy fairly well point a), and offers a dramatic improvement with respect to point b) when comparing to experiments where $p\bar{p}$ atoms are formed stopping $\bar{p}$'s in fixed targets.

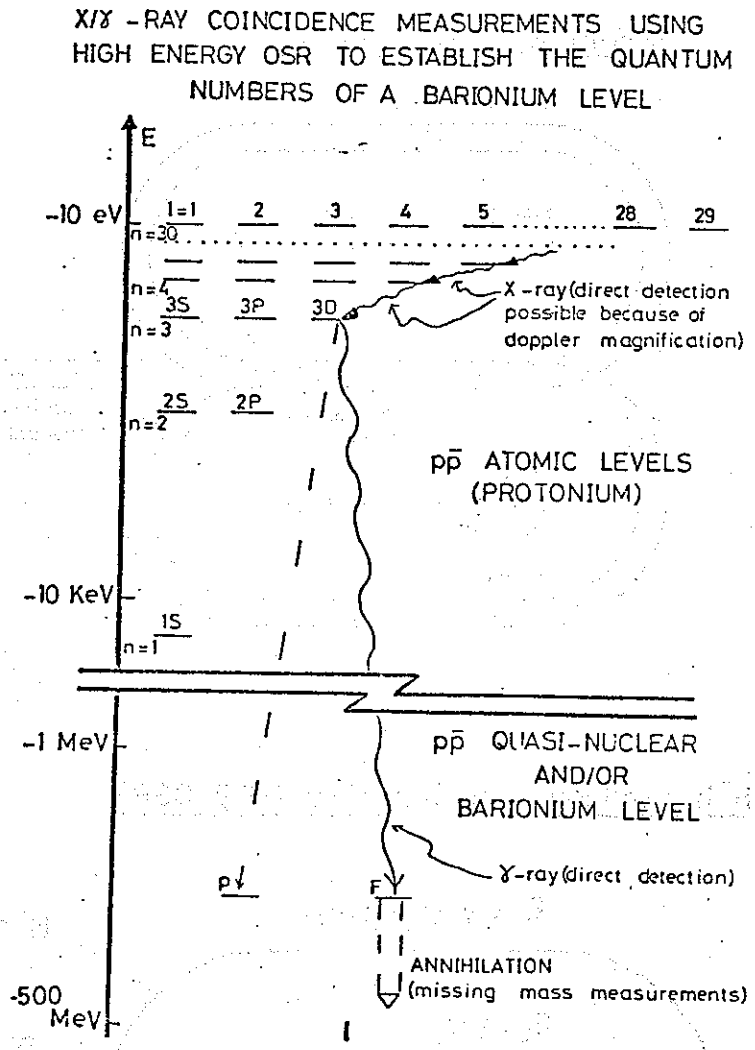
X/γ - RAY COINCIDENCE MEASUREMENTS USING HIGH ENERGY OSR TO ESTABLISH THE QUANTUM NUMBERS OF A BARIONIUM LEVEL
E
-10 eV
1=1
2
3
4
5
28
29
n=30
n=4
3S
3P
3D
n=3
X-ray (direct detection possible because of doppler magnification)
2S
2P
n=2
pp̄ ATOMIC LEVELS (PROTONIUM)
-10 KeV
1S
n=1
-1 MeV
pp̄ QUASI-NUCLEAR AND/OR BARIONIUM LEVEL
γ-ray (direct detection)
p↓
F
ANNIHILATION (missing mass measurements)
-500 MeV

Figure 1

8.3 The Ortho-ISR Scheme

a) The scheme

Two stored beams ($\bar{p}$ and p, or $\bar{p}$ and H^-) circulate in the same direction and with the same average velocity in two separate rings, and the beams overlap in a common straight section (Figures 2 and 3).

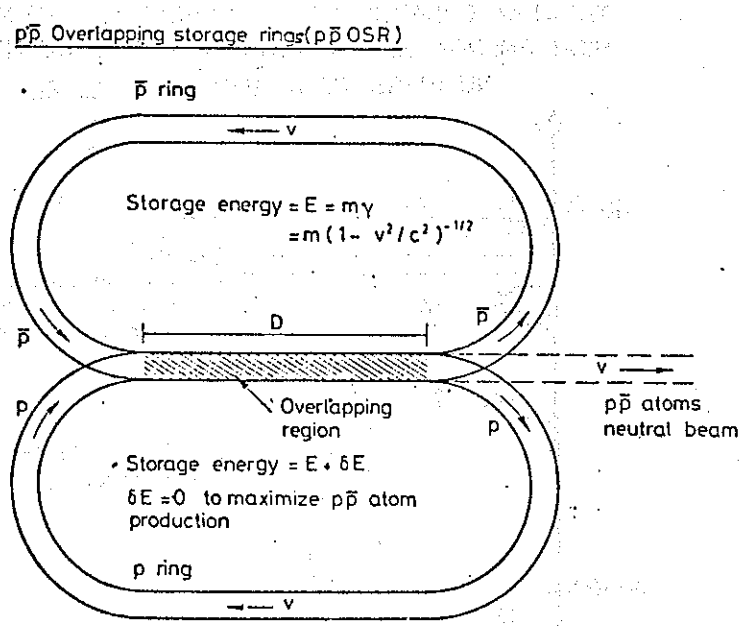

Figure 2

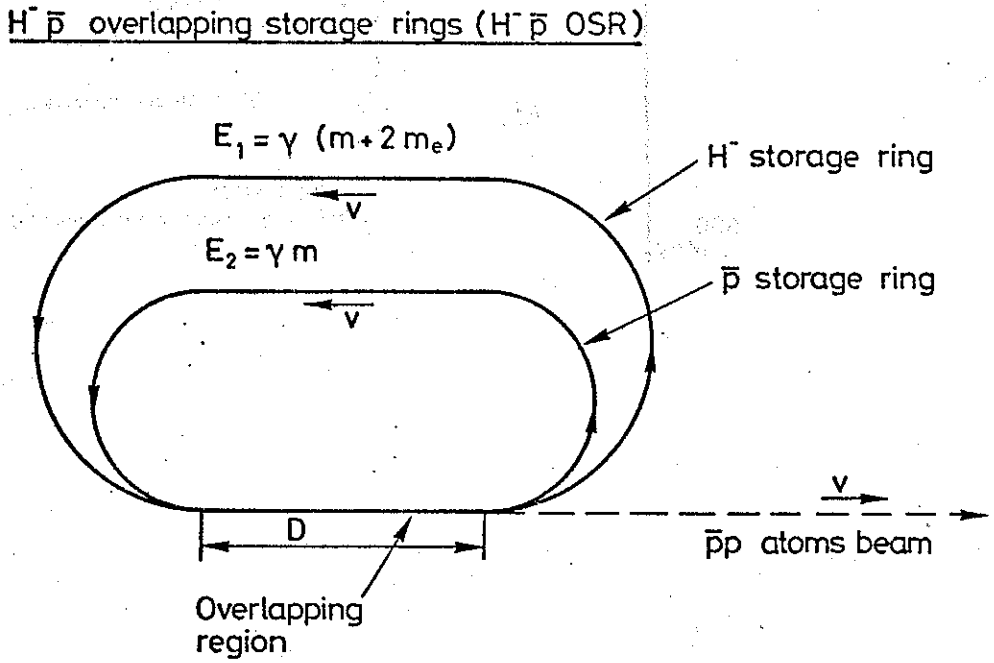

Figure 3

$p\bar{p}$ atoms form in vacuum via radiative capture in the first case (Figure 2) and (mainly) via Auger capture in the second one (Figure 3). The velocity of the $p\bar{p}$ atom is determined by the storage energy in the $\bar{p}$ ring.

By changing independently the storage energies in the two rings so that the beam average velocities remain equal, it is possible to vary continuously the velocity of the $p\bar{p}$ atoms keeping unchanged the probability of formation of the atoms.

This scheme offers many unique advantages for the emission and detection of the $p\bar{p}$ x-rays.

a) The $p\bar{p}$ atoms form and travel in vacuum → the atomic cascade is not influenced by molecular and atomic processes with the surrounding medium and is then determined only by the internal properties of the $p\bar{p}$ system;

b) The angle of emission of x-rays is isotropic in the $p\bar{p}$ c.m. and shrinks forward in the lab so that at higher $p\bar{p}$ velocity a given x-ray detection system covers a bigger solid angle.

$$\theta_{LAB} = \arccos\left(\frac{\cos\theta_{p\bar{p}} + \beta}{1 + \beta\cos\theta_{p\bar{p}}}\right)$$

θ_{LAB} is the angle of emission of the x-ray in the lab. relative to the $p\bar{p}$ atomic beam direction (Figure 4).

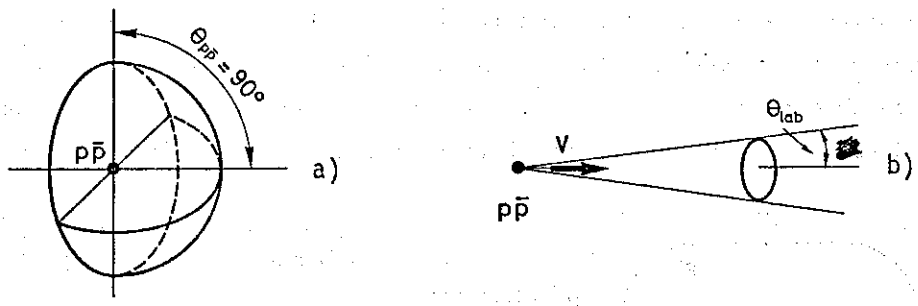

Figure 4 : Angular distribution of x-rays emitted by the $p\bar{p}$ atom in the forward hemisphere

a) in the $p\bar{p}$ rest system
b) in the lab. ($\theta_{LAB} = \arccos \beta$)

c) The energy of the x-rays emitted in the cascade of the $p\bar{p}$ atom to less excited atomic states is magnified in the lab so that more atomic transitions are detectable in the lab. The magnification factor $\delta\ (\theta_{LAB},\ \gamma)$ is given by the relativistic doppler formula

$$E_{LAB} = E_{p\bar{p}}\ \ \delta\ (\theta_{LAB},\ \gamma)$$

$$= E_{p\bar{p}.cm.}\ \ \frac{\sqrt{1-\beta^2}}{1-\beta\cos\theta_{LAB}}$$

Half of the emitted x-rays have an energy magnification ranging from γ to 2γ.

d) The energy of the emitted x-rays can be measured with extraordinary high resolution combining the differential x-ray absorption technique with the possibility of varying continuously in the lab the energy of a given transition (by varying the storage energies of the two beams in parallel).

Many differential absorbers with sharp absorption edges are useable. These absorption edges are known with accuracy better than 10^{-5} so that the limit to the resolution are given by the uncertainty on θ_{LAB} and by the momentum spread Δp of the stored beams.

The error on θ_{LAB} can be minimized by using little x-ray detectors and reconstructing the $p\bar{p}$ annihilation vertex using the charged $p\bar{p}$ annihilation products.

A $\frac{\Delta p}{p} \sim 10^{-3}$ will then provide a $\frac{\Delta E}{E} \sim 10^{-3}$ for all detectable lines independently from their energy: as soon as the doppler magnification is enough to bring the energy of a transition above the threshold of the detector its energy can be measured by looking at which γ it is suppressed by an absorber with absorption edge above the detection threshold (e.g. Al K edge 1.55988KeV, S K edge 2.47048KeV). A simplified scheme of set up is shown in Figure 5.

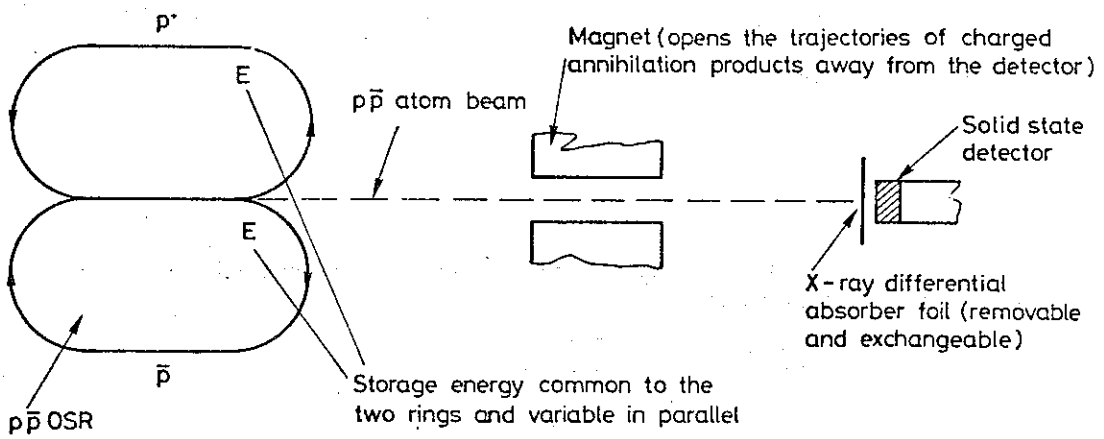

Figure 5 : $p\bar{p}$ ISR with variable storage energy and X-ray differential absorption technique (detection of X-rays from $p\bar{p}$ atoms annihilating with no neutrals)

e) Transitions between $p\bar{p}$ atomic states can be induced using commercial powerful monochromatic (not tuneable) lasers[2,8]. The resonance frequency can be attained simply by varying the velocity of the $p\bar{p}$ atom that sees the laser light doppler shifted in its rest system. The resonance frequency can be detected measuring enhancements or depressions of the yield of x-rays of a given transition. A set-up as sketched in Figure 6 would maximize the density of radiation useful to induce the transitions.

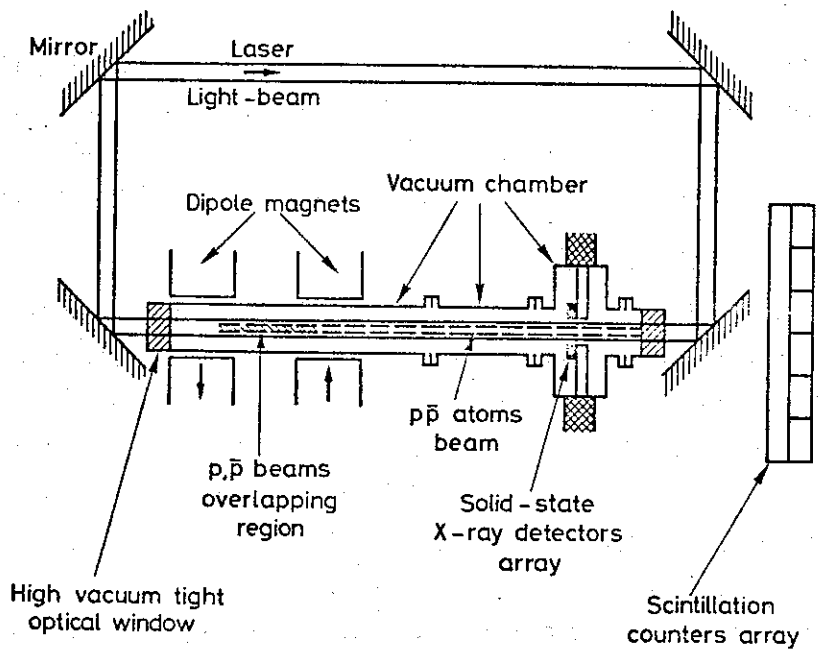

Figure 6

b) Luminosity and formation rates of $p\bar{p}$ atoms

The luminosity L_o for the formation of $p\bar{p}$ atoms in the overlapping region is given, for coasting beams, and assuming a flat transversal spacial distribution, by[3]

$$L_o = N_{\bar{p}} \; N_{p(H^-)} \; \frac{D}{(2\pi r)^2 \gamma S} \; \frac{1}{\gamma} \nu$$

where D = length of the overlapping region

$2\pi r$ = length of the storage rings (10^5 cm for ISR)

S = beam cross-sections in the overlapping region

$N_{\bar{p}}$ = number of stored $\bar{p}$'s

$N_{p(H^-)}$ = number of stored p's (H^-'s)

ν = relative velocities of p's and $\bar{p}$'s in the $p\bar{p}$ mass centre system.

The typical cross-section σ_R for the radiative atomic capture process is $\sigma_R \simeq 10^{-26}$ cm^2 for $v = 10^{-3}$ c ($\bar{p}$ and p beams). The typical cross-section σ_A for Auger capture is $\sigma_A = 10^{-20}$ cm^2 for $v = 10^{-3}$ c ($\bar{p}$ and H^- beams).

Assuming $D = 10^2$ cm, $vS = 1$ cm^2, $N_{\bar{p}} = N_{p(H^-)} = 5 \cdot 10^{11}$, $v \simeq 10^{-3}$ c one gets $L_o \simeq 75\ 10^{21}$ cm^{-2} sec^{-1}.

In the $p\bar{p}$ overlapping mode only few $p\bar{p}$ atoms per hour are formed, while in the $\bar{p}$ H^- overlapping mode the rate R_{H^-} of formation of $p\bar{p}$ atoms is $R_{H^-} \approx \frac{750}{\gamma}$ sec^{-1}.

The advantage of using an H^- beam is evident comparing these two rates. Moreover the Auger capture favours the formation in high n levels, while the radiative capture populates preferentially low n states[2,7]. We shall then restrict the discussion of the ortho-ISR scheme to the case of a $\bar{p}$ H^--Ortho-ISR

c) The $\bar{p}$ H^--ortho-ISR

The handling and the storage of an H^- beam is much more difficult than in the proton case as gas stripping and electromagnetic stripping of the extra electron may cause big beam losses. The gas stripping rate can be estimated using the formula $\sigma_{AIR} \simeq 1.2\ 10^{-18} \frac{1}{\gamma^2 - 1}$ cm^2 which fits nicely the existing experimental data in the energy region 1-500 MeV kinetic energy of the H^- ion[9].

With the typical ISR vacuum of 10^{-12} torr the gas stripping lifetime of H^- ions is $\tau_{GAS} \approx 3000$ sec at $\gamma = 3$. The electromagnetic stripping is due to the fact that in the H^- rest system an electric field $E = \beta\gamma\ 3\ 10^2\ B$ (gauss) V/cm is present when the ion goes through a magnetic field B. This electric field causes stripping of the extra electron (binding energy $W = 0.75$ e) via tunnel effect. The lifetime depends quite critically on the electric field value; for $E = 1$ M V/cm the H^- electromagnetic stripping lifetime τ_E is of the order of many hours, while for $E \simeq 1.2$ M volt/cm $\tau_E \approx 100$ sec.

Considering that the total length of the bending magnets in one ISR ring is ≈ 450 m it turns out that the maximum γ at which the machine can be operated without important electromagnetic stripping is $\gamma_M = 3$[10].

A low momentum spread Δp of both $\bar{p}$ and H^- beams and a perfect matching of the average beam velocities are necessary to get a good rate of $p\bar{p}$ atoms formation and to minimize the background. The importance of having a low $p\bar{p}$ relative velocity v is due to the fact that σ_A increases with decreasing v faster than the cross-section for H^- stripping induced by the $\bar{p}$ beam in the overlapping region. The H^o beam produced by gas and $\bar{p}$ stripping in the overlapping region will presumably represent the bigger source of noise. However, the induced background should be manageable as the annihilation pattern of the $p\bar{p}$ system is quite unique and it is required in coincidence in all the measurements.

The value $\nu \approx 10^{-3}$ c assumed in our luminosity estimation implies a Δp 1 MeV/c and, at $\gamma = 3$, a $\frac{\Delta p}{p} \approx 3\ 10^{-4}$. This should be easily satisfied by the cooled $\bar{p}$ beam, while for the H^- beam a momentum selection of the beam provided by the PS will be probably necessary (the H^- beam cannot be cooled in the cooling ring as the vacuum foreseen is too poor to allow H^- beam survival against gas stripping; in the case of electron cooling additional stripping would be induced by the e^- beam; H^- stochastic cooling in the H^- ring could be considered. The general scheme of the $\bar{p}$ H^--ortho-ISR facility could be as indicated in Figure 7.

Every hour a fresh filling of H^- ion could be obtained running for short time the PS with inversed polarity and using as a source the second Linac. The $\bar{p}$ filling would be the standard one.

The H^- beam would circulate on one modified ISR ring. The modification would affect 1/4 of the ring and would consist in any external by-pass long-circuiting 2 normal interaction points and overlapping the second ring in one region of maximum bending.

The extra magnets necessary to provide the external by-pass would be cheaper than the present ones as they should operate at a maximum field $B_M < 1000$ Gauss as all the other magnets in the machine ($\gamma < \gamma_M = 3$). The total ISR power consumption in the $\bar{p}$ H^- overlapping mode would be then reduced by a factor ~ 100.

The $p\bar{p}$ beam will come out tangent to the external wall of the tunnel. By-passing interaction regions 1 and 2 the exterior of the I-1 hall could be used as an experimental area. The ideal experimental area should be quite long (250 m) as the $p\bar{p}$ atom lifetime when formed in high n states (as it occurs when the formation process is Auger capture) can be longer than one microsecond in the lab.

The experimental apparatus should consist of 3 main parts:

a) an x-ray detector array with cylindrical symmetry along the $p\bar{p}$ atom beam installed inside the vacuum chamber and movable along the beam,

b) a spectrometer, with magnet located upstream and chambers and scintillation counters upstream and aside of the x-ray detector, to localize the annihilation vertex and measure the momentum of the charged products of the $p\bar{p}$ annihilation,

c) a detector of neutrals installed behind the x-ray detectors.

A short dipole with very high magnetic field installed upstream could be used to eliminate, via stripping and sweeping of the p^+ and e^-, the H^0 atoms coming along the beamline which otherwise would reach the X and γ detectors.

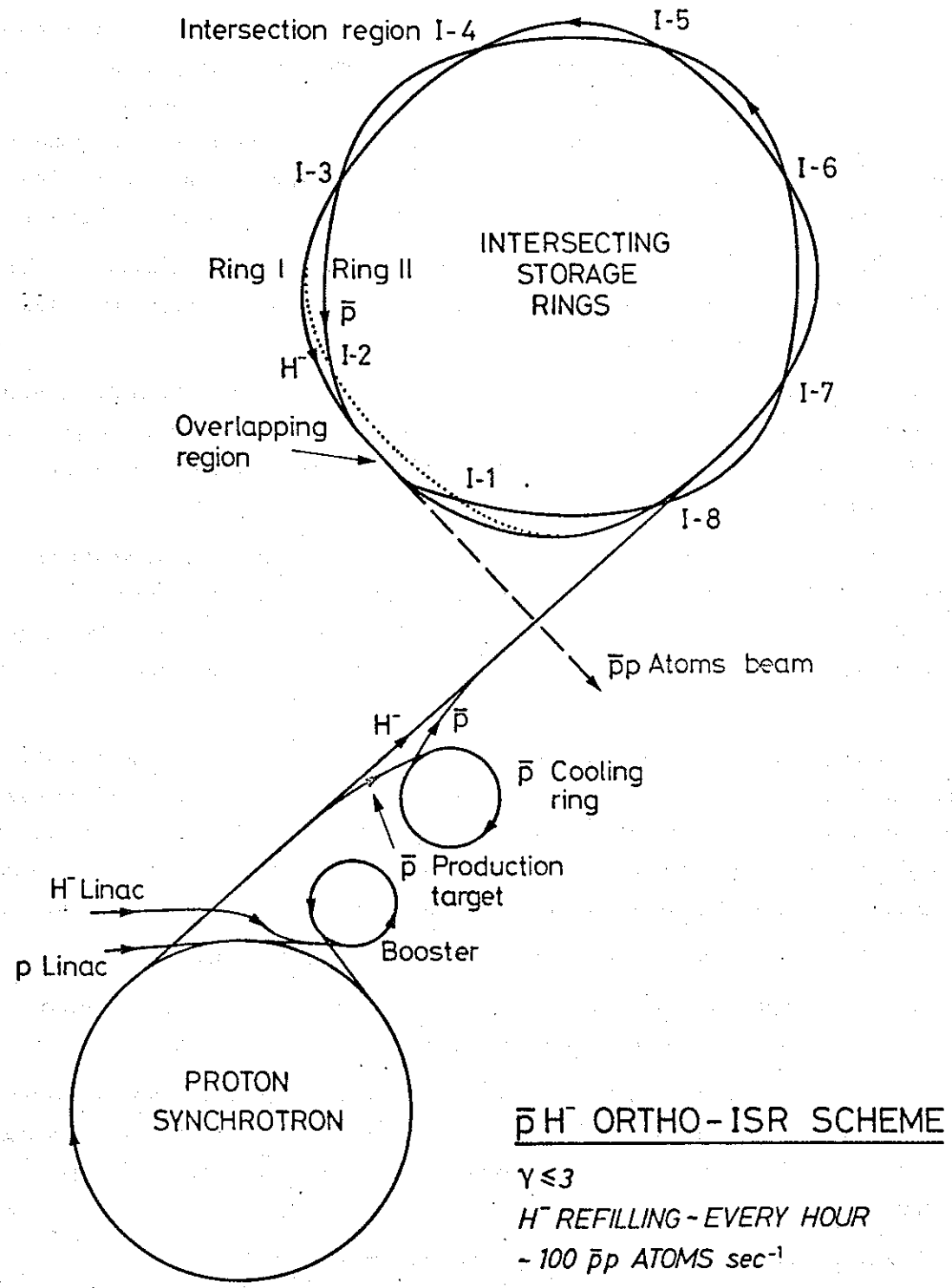
Intersection region I-4
I-5
I-6
I-7
I-8
I-3
I-2
I-1
Ring I
Ring II
INTERSECTING
STORAGE
RINGS
p̄
H⁻
Overlapping
region
p̄p Atoms beam
H⁻
p̄
p̄ Cooling
ring
p̄ Production
target
H⁻ Linac
p Linac
Booster
PROTON
SYNCHROTRON
p̄ H⁻ ORTHO-ISR SCHEME
γ ≤ 3
H⁻ REFILLING - EVERY HOUR
~ 100 p̄p ATOMS sec⁻¹

Figure 7

The dipole magnets aligned on the $p\bar{p}$ atom beam line can be used to perturb the $p\bar{p}$ atom cascade via the electric field induced in the $p\bar{p}$ c.m. rest system (stark mixing of atomic levels).

8.4 Physics potentialities

Working around $\gamma = 3$ and using solid state detectors mounted inside the vacuum chamber without mechanical protection window, so as to have a detection threshold below 2 KeV, it would be possible to detect all the transition to the levels n = 1, 2, 3 and 4 (the $p\bar{p}$ Rydberg is 12.5 KeV).

This means in particular that the population of the levels 1S, 2P, 3D and 4F could be monitored event by event.

Moreover for $\gamma \leq 3$ using commercial lasers (CO_2, CO, Nd, Ruby, Auger) transitions between levels separated up to 15 eV can be induced with high transition probability.

Within this frame the following physics would be feasible:

1) Study of the $p\bar{p}$ annihilation from signed S, P, D, F atomic states (of known energy) (branching ratios; conservation laws, rare channels, total annihilation rate provided by width of atomic line).

2) Study the spectroscopy (energy levels, quantum numbers) and of the annihilation of the baryonium states with $M < 2m_p$ populated via γ transitions from initial atomic states of known quantum numbers.

3) Emission and induced spectroscopy of the $p\bar{p}$ atom. With a $\frac{\Delta p}{p} \sim 10^{-4}$, which seems a reasonable assumption in the data taking phase, measurements of strong interaction effects (line width, shift) with relative accuracy from 10^{-3} (emission spectroscopy) to 10^{-4} (induced spectroscopy) will be feasible. This could represent the transposition of the lamb shift measurements in the domain of electro-dynamics to the strong interaction field.

   The mass and the magnetic moment of the antiproton would be measured with the same kind of precision.

4) Finally the unique facility of a beam of insulated $p\bar{p}$ atoms travelling at high speed in vacuum and a detection system capable of revealing each single cascade process would be available and could be used for basic experiments.

All this represents quite an extended and exciting research programme which could motivate the important transformations necessary to provide ISR with the H^- source, the by-pass and the overlapping region. This facility could maintain a leading rôle for ISR when the normal ISR $p\bar{p}$ programme will arrive at its ebb and ISABELLE will polarize the interest for high energy frontal collisions.

References for section 8

1) T.E. Kalogeropoulos, "Intersecting Storage Rings for Studying Interactions at Very Low Energies", CRISP 72-11, ISABELLE Project (1972)

2) U. Gastaldi, "A Possible New Experimental Approach to the Study of the $p\bar{p}$ System at Low Energies", 1st International School on Exotic Atoms and Related Topics, ERICE 1977, to be published, see CERN/$p\bar{p}$ note 13 (1977)

3) L. Montanet, "Experimental Review on the Baryon-Antibaryon Interaction", in 5th International Conference on Experimental Meson Spectroscopy, Boston 1977, to be published, see CERN/EP/PHYS 77-22 (1977)

4) F. Myhrer, "Low Energy Nucleon-Antinucleon Interaction" in 2nd International Conference on NN Interactions, Vancouver, July 1977, to be published, see CERN/TH 2348 (1977)

5) European Conference on Particle Physics, Budapest, July 1977

6) 7th International Conference on High Energy Physics and Nuclear Structure, Zurich, August 1977

7) U. Gastaldi, "A Scheme to Maximize the $p\bar{p}$ Atom Formation Note in Flight and the Production of High Angular Momentum Baryonium States", CERN/$p\bar{p}$ note 30 (1977)

8) U. Gastaldi, "LAMB-SHIFT-TYPE Experiments on Protonium ($p\bar{p}$ atom)" CERN/EP 76-23 (1976)

9) See R. Richardson, "The Status of TRIUMF" in the Proceedings of the 7th International Conference on Cyclotrons and their Applications, Zurich (1975) (ed. W. Joho, Birkhäser Verlag, Basel and Stuttgart

10) U. Gastaldi, "Estimate of the Lifetime of H^- Ions in $\bar{p}$ H^- Overlapping Storage Rings", CERN/$p\bar{p}$ note 32